Understanding morphological development at the Hoornse Oeverdijk

Insights from a one-year monitoring period of a sandy nourishment in a low-energy lake environment

P. (Puck) van de Ven

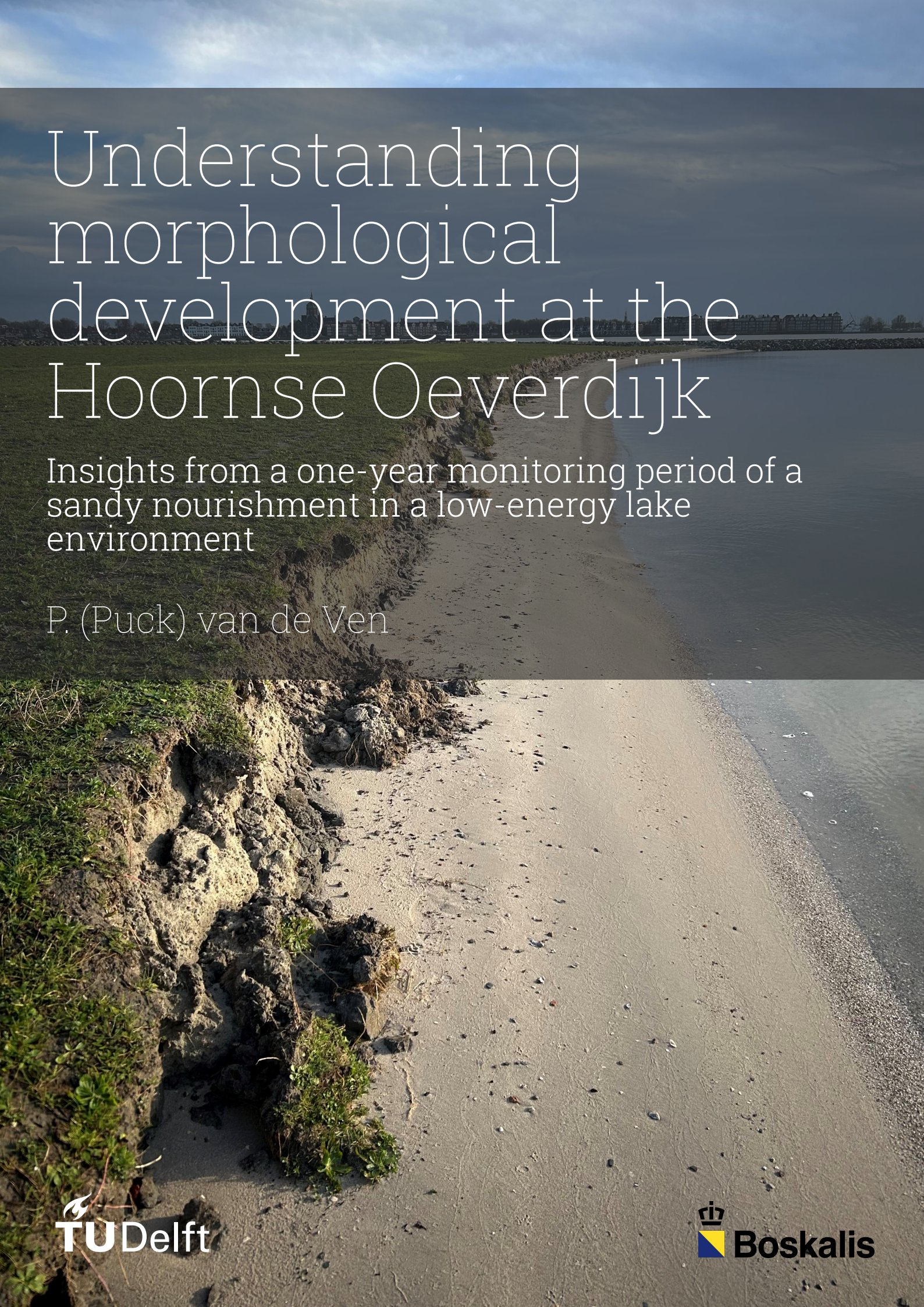

TU Delft

Boskalis

Understanding morphological development at the Hoornse Oeverdijk

Insights from a one-year monitoring period of a sandy nourishment in a low-energy lake environment

by

P. (Puck) van de Ven

In partial fulfilment of the requirements for the degree of
Master of Science in Civil Engineering
at Delft University of Technology

Student number:		4861914
Supervisors:	Dr. ir. M. A. de Schipper (Chair)	TU Delft
	ir. M. A. van der Lugt	TU Delft
	Dr. ir. J. K. Vonkeman	Boskalis
	Dr. ing. M. Z. Voorendt	TU Delft
Faculty:	Faculty of Civil Engineering and Geo-sciences, TU Delft	

TU Delft

Boskalis

Preface

Before you lies the final step to obtaining my Master of Science in Civil Engineering, specialised in Hydraulic Engineering, at Delft University of Technology. Finalising this thesis marks the end of my time as a student in Delft. Deciding to study Civil Engineering was actually a bit of a spontaneous choice, but it worked out in all the best ways. I discovered that it offered me the perfect balance of theory and practical application, in a broad range of directions for further study. I found a specialisation that kept me both interested and challenged: Hydraulic (and within that, Coastal) Engineering. My interest in studying something that is both practical and relevant within this sector led me to the topic of this thesis, looking at the development of an unusual type of coastline.

The process of writing this thesis would have been a lot less smooth without the help of many people, to whom I would like to say thank you! First of all my thanks go out to Boskalis, for providing me with the opportunity to work on this project. I am grateful to have been able to get to know the company and Hydronamic colleagues through this thesis. Specifically I would like to thank Jeanine, you always made time to help me despite your own busy agenda and your help to get me to look at things from the 'sometimes morphology is an art, not a science' perspective, is much appreciated. A thank you also goes out to Jerker, I asked you a hundred random questions and you always made time to get me a useful answer! I also had a lot of help from my TU supervisors. Matthieu and Mark, your help to always have me think twice about what point I'm trying to make, and how to communicate that clearly, is much appreciated. Marlies, during our weekly meetings you listened to all my thoughts and struggles and shared your expertise and insights. Thank you for always making the time for me, I look forward to hearing about your future work! Also, thank you for introducing me to some of your Deltares colleagues, who were happy to think along with me about this research. Finally, I would like to say a thank you to my friends and family. Friends- I am so thankful to have met you all during my time in Delft, you made studying so much more than studying. A special mention to my roommates, who have never complained about having to listen to me talk about this thesis nearly every day over the past 20 weeks. Family- thank you for always supporting me and still being excited about the weekends I come home!

P. (Puck) van de Ven
Delft, July 2025

Abstract

Low-energy, non-tidal coastal environments remain under-represented in coastal morphodynamic research and modelling, despite their growing relevance for (nature-based) shoreline protection. The Hoornse Oeverdijk, a sandy nourishment located along Lake Markermeer in the Netherlands, offers a unique opportunity to study morphological evolution in a low-energy, non-tidal setting. Constructed as a soft engineering alternative to conventional dike reinforcement, the Oeverdijk was designed to maintain a functional profile after natural redistribution of sediment, with minimal post-construction maintenance. However, the processes governing its development remain poorly understood, largely due to the absence of validated models and limited empirical data for such environments.

In this report, we present the first comprehensive field-based and model-supported investigation of the Oeverdijk's morphological and hydrodynamic evolution over a one-year period (January 2024 to March 2025). Using ten high-resolution topographic and bathymetric surveys, combined with local wave, wind, and current measurements, we quantify sediment redistribution and identify dominant transport patterns. Morphological analysis reveals a consistent cross-shore signal of erosion at the waterline and deposition offshore, forming a steep waterline slope (1:10) and a submerged platform (roughly around the depth of closure, at NAP -1 m), that is already between 20 and 40m wide. This is behaviour that is typical of low-energy systems suspected of approaching equilibrium. Long-shore variation is more complex, with observed sediment gain and loss zones likely shaped by wave directionality, wind exposure, and the spatial configuration of breakwaters. Hydrodynamic drivers are characterised by wind-generated waves, with storm events significantly impacting sediment transport, especially in the absence of tidal forcing. The local wind climate is an important driver of sediment transport, as wind and lake geometry drive wave height and direction. Those characteristics are determining factors for relative longshore (wave incidence) and cross-shore (wave height) sediment transport. Delft3D model simulations help contextualise nearshore hydrodynamics, in the absence of field-data, to identify zones for potential sediment transport. This confirms the importance of the local wind climate, in determining the strength and direction of observed bed shear stress, in turn helping to explain long-shore erosional patterns. Model resolution and simplifications limit explanatory power.

By linking morphological change to site-specific hydrodynamic conditions, this study confirms that low-energy beach systems, though often considered morphologically stable, can experience rapid and structured sediment transport and losses. The Oeverdijk experiences transport rates that led to coastline retreat of over 15m/year in some locations, in addition to a net sediment loss of roughly 12000m^3 per stretch of beach (1.4 and 2 km long). Our findings highlight the importance of local wind climate and design choices in shaping sediment dynamics, in addition to showing the added worth of a (thorough) modelling campaign to identify erosive zones and potential for sediment sinks. Moreover, the emergence of consistent profile types across sheltered beaches suggests a large wear-layer volume on a single-slope profile may not be the most material-efficient approach for a sustainable sandy nourishment design. Instead, this research suggests generalising a low-energy (non-tidal) profile, and provides an empirical foundation for implementing it in design approaches for similar settings.

Contents

Preface i

Abstract ii

Nomenclature v

1 Introduction 1
- 1.1 Research context . . . 1
- 1.2 Research problem . . . 1
- 1.3 Research aim and questions . . . 2
- 1.4 Approach and reading guide . . . 2

2 Literature research 4
- 2.1 Sediment transport . . . 4
- 2.2 Hydrodynamics . . . 8
- 2.3 Morphology and profile classification . . . 9
- 2.4 Low-energy lake environments . . . 10
  - 2.4.1 In general . . . 10
  - 2.4.2 Markermeer . . . 11

3 Case study 12
- 3.1 Nourishment site and history . . . 12
- 3.2 Nourishment design and construction . . . 12
- 3.3 Available data overview . . . 14

4 Methodology 16
- 4.1 Site visit . . . 16
- 4.2 Selection of considered period of time . . . 16
- 4.3 Morphology: Data processing . . . 16
- 4.4 Morphology: Location selection . . . 17
- 4.5 Hydrodynamics: Data processing . . . 17
- 4.6 Hydrodynamics: Wind station selection . . . 17
- 4.7 Hydrodynamics: Generating nearshore data with Delft3D model . . . 18
  - 4.7.1 Reason for modelling . . . 18
  - 4.7.2 Model set-up . . . 19
  - 4.7.3 Model validation . . . 19

5 Results: Morphologic and hydrodynamic analysis 22
- 5.1 Morphology: General observations . . . 22
  - 5.1.1 Elevation change . . . 22
  - 5.1.2 Volume change: Total . . . 25
- 5.2 Morphology: Cross-shore observations . . . 25
  - 5.2.1 Profile development . . . 25
  - 5.2.2 Volume change: Cross-shore split . . . 28
- 5.3 Morphology: Long-shore observations . . . 31
  - 5.3.1 Erosion and sedimentation patterns . . . 31
  - 5.3.2 Volume change: Long-shore split . . . 32
- 5.4 Morphology: Connection to site visit observations . . . 34
- 5.5 Morphology: Concluding remarks and next steps . . . 34
- 5.6 Hydrodynamics: General data analysis . . . 34
  - 5.6.1 Wind . . . 35
  - 5.6.2 Water level variation . . . 36
  - 5.6.3 Waves . . . 37
- 5.7 Hydrodynamic variation in time . . . 38
- 5.8 Hydrodynamics: Delft3D modelling output analysis . . . 39

5.9 Hydrodynamics: Concluding remarks . . . 40

6 Link: Coupling morphology to hydrodynamics 42
6.1 Combined data analysis: Cross-shore . . . 42
6.1.1 Forcing and normalised volume changes on (interval) time series . . . 42
6.1.2 Correlation calculations between forcing and volume change . . . 44
6.2 Extended data analysis: Long-shore . . . 45
6.2.1 Theoretical sediment transport: CERC formula . . . 45
6.2.2 General long-shore signals: what do we (not) know . . . 46
6.2.3 Modelling long-shore sediment transport (Delft3D) . . . 47
6.3 Concluding remarks . . . 52

7 Interpretation: a concept system 53
7.1 Cross-shore . . . 53
7.1.1 Profile development . . . 53
7.1.2 Equilibrium profile: generalisation potential . . . 53
7.2 Long-shore . . . 55
7.2.1 Scenario identification . . . 55
7.2.2 Conceptualised system: Scenario 1 . . . 56
7.2.3 Conceptualised system: Scenario 2 . . . 56
7.2.4 Conceptualised system: Transition zones . . . 58

8 Design comparison 59
8.1 Similar system: Marker Wadden and Houtribdijk . . . 59
8.1.1 Morphology: cross-shore profile characteristics . . . 59
8.1.2 Morphology: volume changes . . . 60
8.1.3 Hydrodynamics: water level set-up and set-down . . . 62
8.2 Original design . . . 63
8.2.1 Cross-shore development . . . 63
8.2.2 Long-shore erosion patterns . . . 64
8.2.3 Possibility for unforeseen erosion . . . 65

9 Discussion 67
9.1 Data quality and statistical likelihood of results . . . 67
9.2 Hydrodynamic drivers . . . 70
9.3 Model limitations . . . 71
9.4 Likelihood of conceptualised system description . . . 72
9.4.1 Over-simplification . . . 72
9.4.2 Generalised cross-shore profile . . . 72
9.4.3 Long-shore erosion pattern explanation in perspective . . . 73
9.4.4 Upper losses: aeolian transport and settlement . . . 74

10 Conclusions and recommendations 75
10.1 Conclusions . . . 75
10.2 Recommendations . . . 76

References 78

A Longshore sections volume splits 81

B CERC wave climate 84

C Design profiles 85

D Model validation 88

E Correlations 89

F Storm peak wave height calculation 92

G Bed shear stress modelling 93

Nomenclature

List of abbreviations

Abbreviation	Meaning
ADCP	Acoustic Doppler Current Profiler
AWAC	Acoustic Wave and Current profiler
DoC	Depth of Closure
D3D	Delft3D
CERC	Coastal Engineering Research Centre
GPS	Global Positioning System
KNMI	Royal Netherlands Meteorological Institute
Lidar	Light Detection and Ranging
MHW	Mean High Water
MLW	Mean Low Water
NAP	Normaal Amsterdams Peil (Dutch reference datum)
PoT	Peak-over-Threshold
PCC	Pearson Correlation Coefficient
RMSE	Root Mean Square Error
RQ	Research Question SCC
Spearman Correlation Coefficient	
TI BSS	Time Integrated Bed Shear Stress

List of terms

Term	Definition
Oeverdijk	Sandy nourishment fronting the existing dike at Hoorn, acting as a nature-based flood defence
Wear layer	Additional dynamic sand layer designed to erode without compromising dike safety
Cross-shore transport	Sediment movement perpendicular to the shoreline
Long-shore transport	Sediment movement parallel to the shoreline
Depth of Closure	Lakeward depth beyond which no significant morphological change occurs
Morphological development	Evolution of the coastal profile over time
Markermeer	Shallow freshwater lake in the Netherlands
Delft3D	Process-based hydrodynamic and morphodynamic modelling suite developed by Deltares
Breakwater	Coastal structure reducing energy from waves or currents at the shore
Fetch	Length of water over which wind blows
Equilibrium profile	A stable beach profile shape representing a long-term balance in between sediment transport and driving forces
Sediment budget	The balance of sediment entering and leaving a coastal cell or profile
Non-tidal environment	Waterbody without (significant) tidal ranges
Significant wave height	Average height of the highest one-third of waves in a record
Hydro-morphodynamics	Coupled processes of hydrodynamics and morphology
Storm peak event	A short-term period of elevated wave heights exceeding a defined threshold, often driving significant sediment transport
Concept system	A simplified schematic of how driving forces, sediment transport pathways, and profile changes interact
Sediment sink	A location where sediment is effectively removed from active beach exchange, for example due to offshore currents.
Subaqueous platform	A gently sloped underwater sand platform developing offshore from the beach toe in low-energy systems
Sediment bypassing	The process by which sediment moves around a hard structure to continue alongshore transport pathways
Python	Programming language for scientific computing and data analysis
P-value	Probability measure for statistical significance testing
R^2 value	Indicator of how well a regression model fits observed data

List of symbols

Symbol	Unit	Description
θ_{cr}	[-]	Critical Shields parameter
τ_b	N/m^2	Bed shear stress
ρ	kg/m^3	Water density
ρ_s	kg/m^3	Sediment density
d_{50}	m	Median sediment diameter
H_s	m	Significant wave height
H_{m0}	m	Significant wave height
T_s	s	Associated wave period
α	[-]	Beach slope
c_{br}	m/s	Wave phase celerity at breaker line
S	m^3/s	Longshore sediment transport rate
E	J/m^2	Wave energy density
P	W/m	Wave power
$h(y)$	m	Equilibrium profile bed level
y	m	Distance offshore from mean water line
A	m$^{1/3}$	Profile shape factor
γ	[-]	Breaker index
ν	m^2/s	Kinematic viscosity
η	m	Water surface elevation
q_b	kg/s	Bed load transport rate
u_*	m/s	Shear velocity
u	m/s	Depth-averaged flow velocity
V	m/s	Local instantaneous fluid velocity
C	kg/m^3	Local instantaneous fluid concentration
p	[-]	Porosity
s	[-]	Relative sediment density
ϕ_b	$^\circ$	Wave approach angle at breaker line
Im	kg/s	Immersed mass transport
ds	m	Depth of closure
ϵ	W/m^3	Energy dissipation

1 Introduction

1.1. Research context

The Netherlands is a low-laying country, experiencing the threat of rising sea-level. This means building and maintaining flood defences are a national topic of high priority. A national flood defence assessment revealed that sections of the Markermeer dikes between Hoorn and Amsterdam no longer met the legal standard (Raad van State, 2021). In a dynamic natural world, solutions to threats for society require innovation. The 'Hoornse Oeverdijk' project became one of those innovations, aiming to improve the coastal defence strategy for the northernmost section of the dike at Hoorn. This oeverdijk (bank dike) is a large sandy nourishment, forming a sandy strip in front of the existing dike. This oeverdijk replaces functions of the original dike regarding dampening of wave energy and protecting hinterland against high(er) water levels. The design was realised in October of 2023.

Other nourishments in the area, including the Markerwadden, have already been thoroughly analysed (Ton, 2023). This research aims to be the first to analyse and explain the morphological development of the Hoornse Oeverdijk.

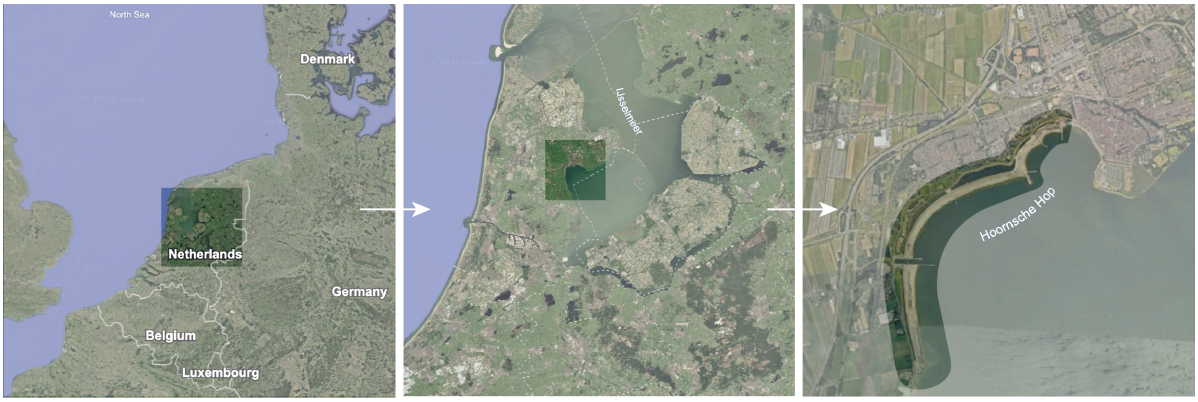

Figure 1.1: Location Hoornse Oeverdijk

1.2. Research problem

The sandy nourishment of the Oeverdijk is located in the Markermeer, a non-tidal lake environment with low-energy hydrodynamic forcing, predominantly under the influence of wind-generated waves. Over time, parts of the nourished sediment will be transported. This will impact local beach profiles, and with that, the effectiveness of the Oeverdijk as a coastal defence mechanism. However, there is limited global experience with the morphological development of large-scale sandy nourishments in such low-energy environments, so developments and consequences are uncertain.

The nourishment design is based on dune erosion as the leading failure mechanism for the outer slope of the dike. Subsequently, the water retention safety requirements are met on the basis of the stability of the remaining beach profile after normative dune erosion. This aligns with the way coastal dunes function. To ensure the required profile is preserved, with minimal maintenance, the dike design encompasses a 'wear layer'. This is an extra layer of sediment on the outer slope of the dike, that can erode without the minimally required volume of sediment becoming endangered. The size of this layer was determined using the process-based morphological models of Delft3D and XBeach, "originally developed to simulate hydrodynamic and morphodynamic processes on sandy coasts, on the time scale of storms" (Deltares, n.d.). The model outcome cannot be validated using a reference

situation, meaning it must be approached with some caution (Alliantie Markermeerdijken, 2017). Now, roughly 1.5 years after completion of the nourishment, data is available on the initial development of the beach profile. This can be used to quantify sediment transport, and evaluate profile evolution and design assumptions.

In existing literature, coastal regions are generally densely populated and heavily analysed. However, where population density does not necessarily differentiate between open coasts and sheltered coasts, such as along bays or lakes, literature does. Very little research exists to explain the behaviour of low-energy beaches compared to exposed coastal beaches (Ton et al., 2021). Few detailed studies of hydrodynamic processes at sheltered beaches have been done (Vila-Concejo et al., 2020), but some generalisations do exist. For example, large morphologic changes at these beaches are mostly associated to high-energy events (Freire et al., 2009), and the profiles tend to develop low-gradient, sub-aqueous platforms (Ton et al., 2021).

Models (originally) developed for open-ocean coasts often form the basis for design and management of protected coasts (Vila-Concejo et al., 2020), of which the use of XBeach for the Hoornse Oeverdijk is a prime example. Amongst others, Freire et al. (2009) have already stated a fetch-limited beach (often coinciding with low-energy), experiences very different beach morphodynamics than established open-ocean models assume. This creates realiability issues regarding model output, and difficulties in the design process of sandy nourishments. Hence, in practice, the morphological development of the northern section of the Oeverdijk, 'Stadstrand Hoorn' was never even modelled, as it is so sheltered the XBeach predictions were already deemed unusable prior to the modelling phase.

It is deemed effective to compare the morphological development of this case study to existing literary theories and modelling assumptions, to gain more insight into the development of low-energy beaches in non-tidal environments such as the Hoornse Oeverdijk.

1.3. Research aim and questions

This research aims to understand the morphological developments and their relation to hydrodynamic forcing of the Hoornse Oeverdijk since its completion, by gaining insight into sediment transport, profile evolution and design assumptions. To this end, the following research questions have been defined.

Main research question:
How do local hydrodynamics shape the morphological evolution of the Hoornse Oeverdijk beach?

Sub-questions:

1. **Research Question** What patterns and quantities of erosion and deposition can be observed at the Hoornse Oeverdijk beach?
2. **Research Question** What local hydrodynamic forcing yields sediment transport at the Hoornse Oeverdijk?
3. **Research Question** How do the morphological developments of the Oeverdijk compare to other sandy coasts in the Markermeer, and to the original design profile and expectations?

1.4. Approach and reading guide

This report is split into chapters that each provide information on a different part of this research. This guide highlights the content of each of these chapters, that follow after the classic introduction, literature research, case study and methodology.

Chapter 2: Literature Research
This chapter investigates existing literature into relevant topics, of which knowledge is required to answer the research questions posed. Specifically, this chapter looks at existing literature on low-energy coastal systems, (requirements for) sediment transport and the development of cross-shore profiles in low-energy environments.

Chapters 3 and 4: Case study & Methodology
These chapters provide some background to form the base of further research. In Chapter 3, relevant information on the case study of this research, the Oeverdijk, is provided. This includes information

on the design profile in which the dike was constructed, expected settlement, but also what data is available for analysis. Chapter 4 explains the way in which this data is selected and processed for analysis in this thesis, in addition to an explanation of the modelling approach to generate nearshore current data.

Chapter 5: Results - Morphology and hydrodynamics
Here, the results of the morphological and hydrodynamic data analysis of the Oeverdijk are presented. In terms of morphology, this includes results on cross-shore profile development, long-shore sediment transport signals and an analysis of volume changes. The essence here is to get a feeling of where sediment is moving to and from, at the Oeverdijk. This answers the first research sub-question. Regarding hydrodynamics, this chapter primarily presents the results of the analysis of wind and wave field-data, in addition to model generated current data near the Oeverdijk. This aims to provide the reader with an indication of the major driving forces behind local morphological change.

Chapter 6: Link - Coupling morphology and hydrodynamics
This chapter combines the morphological and hydrodynamic results presented earlier. Those results are combined both visually and analytically to analyse the way in which hydrodynamic forcing can be used to explain the observed morphological change, or support theories presented in literature. This chapter answers the second research sub-question.

Chapter 7: Interpretation: Creating a concept system
Following the relationships between forcing and morphology that arise in the linking chapter, this chapter comes up with a concept system description. Essentially, a generalised view on the cross-shore and long-shore morphological developments is presented here. This section combines gathered knowledge to answer the main research question, aiming to break down the morphological development of the Oeverdijk by its driving force: wind.

Chapter 8: Comparison
Here, the findings at the Oeverdijk are put into perspective by comparing the observed developments to similar sandy environments in the Markermeer: the Marker Wadden and the Houtribdijk. Additionally, the observed morphological change at the Oeverdijk is compared to the original design, in addition to the modelling-based predictions that were part of the original design process. This answers the third research sub-question.

Chapter 9: Discussion
This chapter takes a broad look at the data analysis and the generated conceptual system descriptions, to reflect on how likely these results or concepts are. This includes a statistical trend analysis, and discusses model limitation. Discussing the possibilities and limitations of this research helps put into perspective how much weight can be given to the conclusions drawn here.

Chapter 10: Conclusions and Recommendations
Finally, the last part of this research draws conclusions to answer the originally posed research questions, and comes back on some critical remarks. Furthermore, this chapter contains recommendations for further development of low-energy beaches, and future research in this area of interest.

2

Literature research

This chapter presents literature research on relevant nearshore morphological processes and sediment transport, in addition to research on what is known regarding the development of low-energy (non-tidal) beaches. This knowledge forms the base of answering the first research question, in addition to providing context surrounding the data analysis and interpretation that follows, for example by providing a base for selecting areas where sediment transport is expected as a result of local forcing.

2.1. Sediment transport

Understanding and explaining morphological change in a specific environment often starts at sediment transport. The morphological development of a beach is the result of spatial gradients in the rates of (net) sediment transport. Sediment transport can be defined as the movement of sediment particles through a well-defined plane over a certain period of time (Bosboom et al., 2021). Particle movement will occur when the instantaneous fluid force on a particle is larger than the resisting force. In literature this is often described through the definition of 'initiation (or threshold) of motion', occurring when the dimensionless bed shear stress (θ) is larger than the threshold value (θ_{cr}) (van Rijn, 2007). Threshold of motion plays an important role in calculation of sediment transport rates both within and outside of the surf zone (Soulsby, 1997). Many experiments have attempted to determine the value of this threshold, yielding a large variety of ways to calculate sediment transport.

In both literature and practical research, bed shear stress is often discussed alongside shear velocity (u_*). Bed shear stress is proportional to this velocity squared, multiplied by the water density; a relationship that follows from an analysis of force balance (gravity and lift) on a sediment particle at rest, in a flow (2021). The work of Shields (1936) combined sediment and flow characteristics in the Shields parameter (θ_{cr}). A relation to the Reynolds number lies at the base of this formulation, with C needing to be determined through experiment measurements:

$$\theta_{cr} = \frac{\tau_{b,cr}}{(\rho_s - \rho)gD} = C \tag{2.1}$$

Where:

θ_{cr}	critical Shields parameter	[N/m^2]
τ_{bcr}	critical bed shear stress	[N/m^2]
ρ_s	sediment density	[kg/m^3]
rho	water density	[kg/m^3]
D	sediment diameter	[m]

All the interdependent contributors to this critical Shields parameter can make application difficult. An attempt to simplify this is the Shields curve, as shown in figure 2.1. From there, sediment or flow requirements for sediment transport can be extracted. However, this Shields formulation holds for uniform flow over a flat bed and must therefore be used with caution when analysing more complex, natural situations.

Bed load and suspended load transport

Generally, sediment transport distinguishes between bed-load and suspended sediment transport. When looking at bed-load transport, Ribberink (1998) assumed that the sand transport rate relates to the difference between the actual time-dependent non-dimensional bed shear stress and the critical bed shear stress. The difficulty in this formulation is that it requires instantaneous dimensionless bed shear stress,

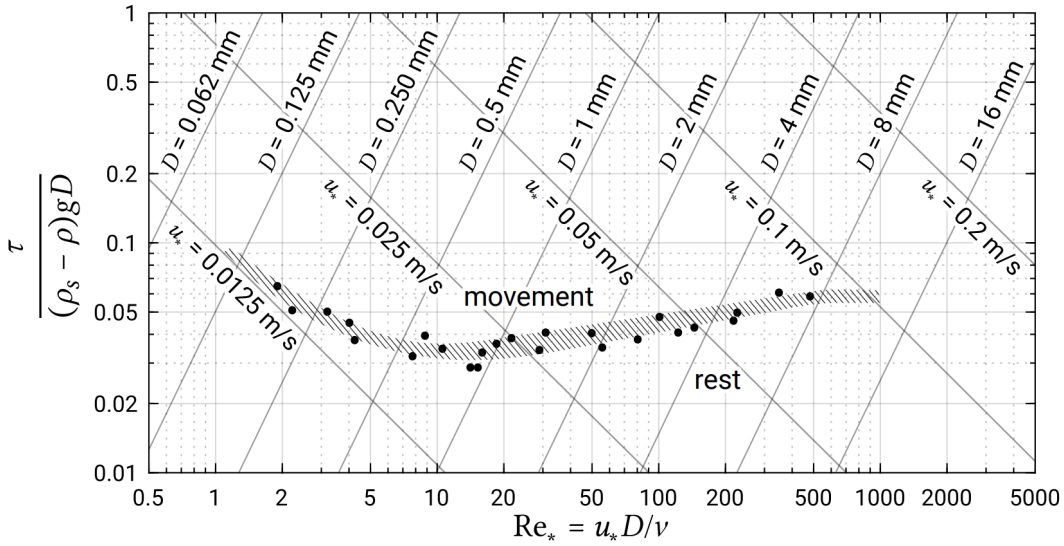

Figure 2.1: Shields curve (Shields, 1936), taken from Bosboom et al. (2021). The lines of constant D and u_* do not originate from Shields and hold for constant density ρ_s = 2650 kg/m^3 and kinematic viscosity $\nu = 1.25106m^2$/s at a water temperature of 12 °C.

which is computationally difficult. Van Rijn later (2007) developed a simplified bed load-load transport formula for steady flow, TR2004, (with or without waves):

$$q_b = 0.015\rho_s uh(d_{50}/h)^{1.2}M_e^{1.5} \tag{2.2}$$

Where:

M_e	mobility parameter	[-]
u_e	effective velocity	[m/s]
u	depth-averaged flow velocity	[m/s]
d_{50}	median particle size	[m]
h	water depth	[m]
ρ_s	sediment density	[kg/m^3]

The model shows relative agreement with experimental data from both lab and field collection, specifically for sediment in the range of 200 - 1000μm. Direction of transport aligns with direction of effective and depth-averaged velocity, determined by current and wave-induces flows. It must be noted the comparison of calculated to measured coastal sediment transport rates was carried out only for the field data collected by Hoekstra et al. (2001), reliable data of bed-load transport in coastal conditions is very rare (van Rijn, 2007). Lack of reliable data sets to calibrate transport formulations remains an important reason behind uncertainty surrounding attempts to model coastal sediment transport. Furthermore, Van Rijn (2007) stated that for computations of cross-shore bed-load transport in the surf and swash zone, this computation is not sufficient.

Suspended sediment transport rate, concerning transport of sediment that is suspended in the water column, is the product of concentration over the vertical, and the velocity over the vertical of the water column. A main requirement for this type of sediment transport is that the transported sediment has a diameter and density combination that allow it to stay suspended whilst being transported.

$$q_s = \int_a^{h+\eta} VC\,dz \tag{2.3}$$

Where:

a	thickness of bed load layer	[m]
η	water surface elevation	[m/s]
V	local instantaneous fluid velocity at height z above bed	[m/s]
C	local instantaneous fluid concentration at height z above bed	[kg/m^3]

Although formulations above can provide an indication, there is often a large difference between the existing sediment transport formulas and their results, in addition to differences between those results and measurements. Therefore, confidence in a (bed load) sediment transport formula would require thorough calibration, and preferably validation using locally collected data. When that is not necessarily possible, a more general relationship between sediment transport and flow velocity can be derived (2021): $\langle S \rangle \propto \langle u\,|u|^{n-1} \rangle$, with n = 3 to 4. This (time-averaged) relationship relies on the quadratic relationship between shear stress and velocity, and the returning relationship of sediment transport and shear stress with varying powers between 1.5 and 2 for different bed load formulations.

Cross-shore transport

Two directions of coastal sediment transport are commonly distinguished: cross-shore and long-shore. Cross-shore transport refers to the cumulative movement of sediment perpendicular to the shoreline, as a result of currents generated by tides, wind and/or waves (Seymour, 2005). Cross-shore sediment transport enables a redistribution of sediment over the beach face, upper shoreface, and lower shoreface, until the Depth of Closure (DoC). This DoC is a parameter that is defined, for a given time interval, as "the most landward depth seaward of which there is no significant change in bottom elevation and no significant net sediment transport between the nearshore and the offshore" (Kraus et al., 1998). However, it is not impossible for cross-shore sediment transport to occur across this depth boundary, for example during high-energy events such as storms. The parameter does not define an absolute transport limit (Stive et al., 1995), and attempts to calculate it have used many different methods based on data ranging from extreme wave conditions to depth variations (Aragonés et al., 2019). As a result, this boundary can be interpreted at different locations depending on the method of calculation. The relevance of the transport boundary formed at the DoC lies in the fact it is closely related to required volumes of nourishment sediment in coastal protection schemes (Aragonés et al., 2019). In literature, sediment transported beyond DoC is often considered a 'loss' to the sediment budget of the coastal system (Guillén et al., 2024).

Most literature still uses the calculation for the depth of closure as defined by Hallermeier (1980), with the following formula:

$$d_s = 2.28H_s - 68.5\frac{H_s^2}{gT_s^2} \tag{2.4}$$

Where:

d_s	depth of closure	[m]
H_s	significant wave height	[m]
T_s	associated wave period	[s]

Generally, storm events yield sediment erosion in offshore direction of a profile, with risk of this 'permanent' sediment loss over the DoC. This is due to the dominance of undertow, an offshore directed current, during these conditions. Beach profiles also undergo natural post-storm recovery, through onshore sediment transport as a result of wave skewness in calmer conditions. This onshore transport occurs over weeks to months and is, in coastal environments, reasoned to be caused by the non-breaking wave action associated with swell waves (Guillén et al., 2024). Recent research by Harley et al. (2022) even observes large net positive sediment gains over the upper shore face in the period after extreme storm events, indicating that under the right conditions, more sediment can return to beach sections than initially eroded. There is little definitive knowledge about the characteristics or processes that define the strength of this recovery process, but an analysis of two micro-tidal coastal environments has shown nearshore morphological recovery time scales positively correlate with averaged longshore current in the days after a storm (Ranasinghe et al., 2012).

Long-shore transport

The second governing transport direction when analysing sediment budget is directed along the shoreline. This, long-shore sediment transport, requires the stirring of sediment at a given location, most often done by waves, and a longshore current to transport sediment parallel to the coastline. In the absence of a tidal current, non-perpendicular incoming waves or large scale lake circulations can still generate a longshore current. Longshore gradients in this transport can result in shoreline retreat or advance. According to Nutz et al. (2018), a lake classification of 'wind-driven waterbodies' exists. In their case, large circulation patterns arise as a result of wind action, "producing alongshore drift along the shores running parallel to the wind direction". These circulation can form the basis for a long-shore sediment transport stream, even in the absence of tides.

To quantify long-shore sediment transport, bulk longshore transportation formulations exist. They calculate transport over the entire littoral zone width, but do not yield a distribution over the cross-shore surf zone . One widely used bulk transport formula is the CERC formula, which can be written in many forms, one simplified version of which is the following (Bosboom et al., 2021):

$$S = \frac{K}{32(s-1)(1-p)}\, c_{\text{br}}\, H_0^2\, \sin(2\theta_0) \tag{2.5}$$

Where:

S	longshore transport	[m^3/s]
K	calibrated parameter = 0.42	[-]
p	porosity = 0.4	[-]
s	relative density of the sediment = 2.65	[-]
c_{br}	phase celerity at breaker line = $\sqrt{g h_{br}}$	[m/s]
H_0	offshore significant wave height	[m]
θ_0	incidence wave angle at breaker line relative to shore normal	[°]

This formulation is based on longshore sediment transport as a result of the action of waves approaching the coast at an angle. This explains wave height and wave angle as controlling factor of the formulation. Tidal influences are not considered, or assumed negligible, making the formulation more suitable for non-tidal environments. However, other influential factors such as sediment characteristics and slopes are also neglected, despite their (potentially significant) influence on sediment transport capacity.

Kamphuis (1991) derived an alternative bulk longshore transport formulation, aiming to include grain size, beach slope and wave steepness. In this formulation, the influence of wave angle now seems rather weak, similar to the grain-size. This research was largely based on laboratory experimental data. The formulation is cited by Bosboom and Stive (2021), as:

$$I_m = 2.27 H_{\text{sig,br}}^2 T_p^{1.5} (\tan\alpha_{\text{br}})^{0.75} D_{50}^{-0.25} (\sin 2\phi_b)^{0.6} \tag{2.6}$$

Where:

I_m	immersed mass of transported sediment	[kg s^{-1}]
T_p	peak wave period	[s]
$\tan\alpha_{\text{br}}$	profile slope at breaker point	[−]
D_{50}	median grain size	[m]
ϕ_b	wave angle at breaker line	[°]

More recent research by Mil-Homens et al. (2013), has evaluated both formulations above, with an extensive dataset of long-shore sediment transport. They conclude that, using their calibrated coefficients, the Kamphuis formulation performs best. However, roughly 40% of all predictions, also using the improved formula, still deviate more than a factor 2 with respect to the observations. Additionally,

a difficulty in use is that the Kamphuis formula requires a profile slope that is not always known in a morphologically dynamic area, in addition to it changing both in time and space.

2.2. Hydrodynamics

Hydrodynamics are the primary source of energy, required for sediment transport, in any coastal system. The amount of energy available in a system can allow for classification, one of the distinguished types being a (non-tidal) low-energy beach. Although the definition of these beaches varies in literature, the main hydrodynamic processes that play a role at there are wind waves and water level fluctuations. The origin of these fluctuations can vary (Jackson et al., 2002; Nordstrom et al., 2012).

Even in non-tidal environments, variations in water level still occur. According to Nordstrom and Jackson (2012), this can be due to various causes such as rainfall, storm surges and tides, and strong onshore winds. Equilibrium beach profiles evolve around a water level and a beach profile will reconfigure, relative to a new water level, through shoreline recession or advancement (Dean, 1991). Although water level fluctuations often occur on a smaller time scale than a new equilibrium is reached, processes of erosion and deposition set in motion by the change still occur. Furthermore, higher water levels allow surface waves to reach higher sections of the beach profile. Elevated water levels in lake beach environments have been found to result in beach erosion, especially in combination with wind-generated waves (Kirk et al., 2000). Variations in water level over time are often on a much smaller scale in non-tidal compared to tidal environments.

When wind is the main energy source of a lake system, locally generated wind waves are present to drive sediment transport. Waves can play a big role both in stirring up sediment for transport, and in generating currents to transport stirred sediment. Many models work on the assumption that sediment is mobilised by the orbital velocities related to incident waves, making waves an important driver in sediment transport (Davidson-Arnott et al., 1989). The length of open water over which the wind can generate these waves, called fetch, is important to determine how much energy they have (Nordstrom et al., 2012). Increased wave energy results in higher potential sediment suspension and transport. Fetch differs depending on the wind direction and the orientation of the beach (section) considered.

The direction of local wind waves is of high importance for the dynamics in both bays (Cooper et al., 2004) and at low-energy beaches (Jackson et al., 2002). Fetch-limited wind waves often have short wave lengths, therefore experiencing limited refraction before reaching the shoreline (Nordstrom et al., 2012). Predominantly oblique wave action emphasises the role of longshore sediment transport and consequential erosion patterns (Shipman, 2010). Considerable difference in orientation along a coastal stretch can result in significantly varying impact of wave action on sediment transport.

Considering waves as a source of energy for sediment transport, insight into available wave energy and wave power can be relevant. These quantities can provide insight into the maximum amount of energy that may be available to generate sediment transport, and the rate at which this is available. For that, general formulations include:

$$E = \frac{1}{8}\rho g H_{rms}^2 \tag{2.7}$$

$$P = Ec_g = \frac{\rho g^2 H_{m0}^2 T_{m02}}{64\pi} \tag{2.8}$$

Where:

E	wave energy density	[J/m^2]
P	wave power	[W/m]
H_{m0}	significant wave height	[m]
T_{m02}	mean wave period	[s]

Wave power can be analysed both as cross-shore and long-shore component by multiplying P by $sin^2(\theta)$ and $cos^2(\theta)$ respectively, where θ is the relative wave approach angle to the shoreline [°].

2.3. Morphology and profile classification

Hydrodynamic forcing exceeding conditions required to transport sediment, yields sediment transport. A strong indicator of morphological development is the beach profile. This profile can also be an indicator of the combination of hydrodynamic conditions and sediment characteristics that have shaped it. The morphological change that a sandy coast experiences under variable forcing is confined to a steady envelope, within which all the variable profiles lie. The mean or this envelope is defined as the dynamic equilibrium profile. Dean (1991) concluded that Bruun (1954) introduced a "reasonable approximate and useful form" for this equilibrium profile, extending to the depth of closure, when described through:

$$h(y) = Ay^{\frac{2}{3}} \tag{2.9}$$

Where:

h	bed level	[m]
y	offshore distance from mean water line	[m]
A	shape factor	[$m^{1/3}$]

The theoretical definition and definitive calculation of A, the controlling shape factor in this equation, appears unclear (Bosboom et al., 2021) and the value that provides a best correlation fit differs per coast. Furthermore, the extensions of this profile to the depth of closure means the offshore 'endpoint' of the profile can vary, depending on the method of calculation for this depth. A is given by:

$$A = \left(\frac{24\epsilon(D_{50})}{5\rho g^{\frac{3}{2}}\gamma^2})\right)^{\frac{2}{3}} \tag{2.10}$$

Where:

ϵ	energy disspation	[W/m^3]
D_{50}	grain size	[m]
γ	breaker index = $H_{sig,br}/h_{br}$	[-]

In practice, the value of A has been determined empirically too, in which a least-squares fit is seen to result in values for A ranging from 0.079 to 0.398 for various profiles on the US coast (Robert G. Dean, 1977), and between 0.055 and 0.093 for analysed Dutch coasts (Bosboom et al., 2021). It should be noted that using this equation to determine a beach profile, regardless of the determined value for A, yields a gradual profile, without predicting any kind of step or sudden slope change.

Despite Dean's equilibrium profile suggesting a gradually changing profile, available research suggests coastlines experiencing various levels of hydrodynamic forcing can display more variable cross-shore profiles. Jackson (2002) gathered that for sandy, low-energy, tidal beaches, research shows the observed profile often consists of a narrow, steep foreshore, no backshore, and a gently sloping platform seaward that is often referred to as a "low tide terrace". Four study sites in lake Markermeer (low-energy, sandy beaches located in a non-tidal environment), also share the 'commonly found steep foreshore and low-gradient platform' (Ton, 2023).

In a few cases globally, field measurements allowed for the classification of low-energy beach morphotypes. Hegge et al. (1996) classified 52 beach profiles from sheltered beach sites on the south-western Australian coast into 4 low-energy categories: concave, moderately concave, stepped and moderately steep, seen in Figure 2.2. The morphotypes were primarily distinguished by dimensions, slope and curvature. Analysis revealed that sediment characteristics had a close correlation to the classification, but were not always defining.

Travers (2007) investigated very low energy beaches (where wave heights can be < 0.15m under non-storm conditions), looking at profiles in a fetch-limited, low-energy basin in southwestern Australia. The analysed profiles were grouped into four morphotypes, visible in figure 2.2. In addition to concluding that

low-energy beach morphologies should become subject of much more research, Travers also found a simple exposure factor (Ef = log(Fl / Ms), with Fl as fetch length and Ms as marginal shoal width), to be useful in characterising profiles.

Makaske and Augustinus (1998) analysed a beach face on the shoreline of the Rhone-Delta, protected against strong wave action by a nearshore bar. Profiles were measured during a single spring-neap tide cycle. Three morphological states were found: straight, concave and convex. All profiles were roughly concave, but distinguished by their lower beach face slopes, as seen in Figure 2.2 where a comparison with various research outcomes is made.

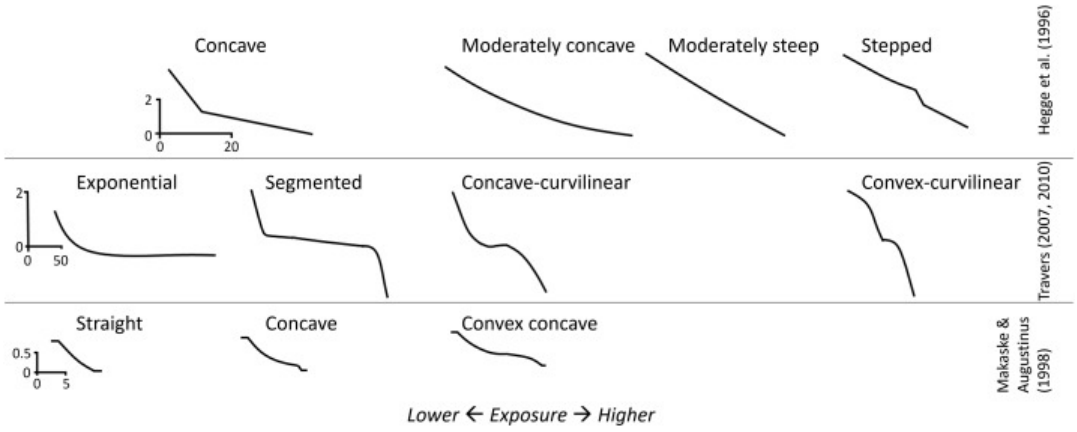

Figure 2.2: Low-energy cross-shore beach morphotypes by and adjusted from Hegge et al. (1996), Travers (2007) and Makaske and Augustinus (1998), combined by Ton (2021)

Most of the examples above consider tidal beach environments. Tidal range is known to slow surf zone processes and cyclically shift the position of the swash, surf and shoaling zone (Masselink et al., 1993). This allows for the possibility that specific profile characteristics may become more pronounced when the tidal shift doesn't smooth them over. Limited literature is available on beach profile classification in low-energy non-tidal (lake) environments, so the extent to which low-energy beach profiles observed in tidal environments are an indication of what can be expected in non-tidal environments is unclear.

2.4. Low-energy lake environments

2.4.1. In general

Globally, implementing "soft" solutions in hydraulic engineering, such as sandy beach nourishments instead of concrete revetments, is becoming increasingly popular, slowly showing signs of an international movement towards a Building with Nature approach (De Vriend et al., 2015). This can result in hydraulic solutions being realised in a location where the interaction of solution and surrounding is still unknown. Sometimes, this means a sandy nourishment is realised as a soft solution, to provide coastal protection in a low-energy lake environment; a combination that has little relevant research explaining the resulting physical processes and morphodynamics (Ton, Anne et al., 2020; Vila-Concejo, 2024). Generally, high-energy beaches have their connection to open water (with tides) as an energy source, in addition to deep waters and long fetch. In the case of low-energy lake systems, this connection is absent.

In descriptions of beaches, 'low-energy' is a term used for a broad variety of conditions and environments, but often poorly defined. In literature, 'low-energy' is also referred to as 'sheltered' or 'protected' and often coincides with 'fetch-limited' (Jackson et al., 2002). The main aspect of a beach being fetch-limited, and not sheltered, is that only locally generated wind waves form a source of energy in the system. The magnitude of these waves is dependent on the strength and origin of the source that formed them, coming down to wind speed, duration, fetch-distance and basin dimensions. Over vast basins, such as oceans or the North Sea, wind duration is often a limiting factor. In the case of smaller basins, as lakes or estuaries, fetch distance gains importance. Hence, certain low-energy environments can gain the name of a fetch-limited system (Jackson et al., 2002). The impact of strong winds can become limited by the alignment of wind and fetch.

Fetch-limited systems are often characterised by short, smaller-amplitude waves and by beach morphologies that are strongly shaped by high-energy events (Freire et al., 2009)). This aligns with other common low-energy environment characteristics in existing literature: short wave periods, low wave heights and short beach lengths (Jackson et al., 2002). Despite the existence of significant variation in all those characteristics across research, low-energy beaches are generally described to experience significant wave heights of < 1.0m, coming down to as low as < 0.15m, even during strong onshore winds (Jackson et al., 2002).

2.4.2. Markermeer

Lake Markermeer is a shallow, fresh water lake located in the Netherlands. The lake is partially bordered by the Houtribdijk, a dam that separates the lake from Lake IJsselmeer. It is a non-tidal environment, with regulated summer and winter water levels. The lake has a significant wave height that does not exceed 1.5, making it a good candidate for a low-energy, non-tidal coastal system by most literary standards (Ton et al., 2021). The system only experiences locally generated waves, mostly by the common southwestern winds, and sees a positive correlation between wave height and wind set-up (Steezel, 2017) in aligning direction.

The lake houses several sandy solutions, including the pilot study at the Houtribdijk into dike foreshore reinforcement using sandy foreshores (Penning et al., 2015), and the artificial archipelago of the Marker Wadden, using locally extracted sediment to create marshland in the lake (Steezel, 2017). Extensive monitoring and research has been done into the development of both of these projects, primarily by Ton et al. (2021), amongst others. Their morphological analysis of four analysed beaches showed rapid changes in profile after completion, with the important conclusion that the beach profiles were evolving towards a profile with a low-gradient platform near Hallermeier's (1978) depth of closure, but taking at least 4 years to reach equilibrium. Furthermore, cross-shore erosion as a result of storm events was significant. In addition to the relevance of storm-events, a closer look into lake-scale circulation patterns also proved relevant, showing nearshore flow direction to be as, if not more important than assumed flow direction as a result of incoming wave angle.

3

Case study

This research is centred around the analysis of data collected at a specific sandy nourishment site: the Oeverdijk in Hoorn. This chapter gives insight into the site, the design and realisation of the nourishment, and the collected data that is available for this research.

3.1. Nourishment site and history

The discussed nourishment site is the 'Hoornse Oeverdijk', located in Hoorn, the Netherlands, as depicted in 1.1. The Oeverdijk is a nourishment located on the lake-side of the 'West Frisian Circular Dike', the original dike in place to keep Hoorn, and other surrounding settlements, dry. This original dike used to separate Hoorn from the Zuiderzee, a water body with an open connection to see. However, over the course of multiple land reclamation trajectories by the Dutch government, the Zuiderzee has become the lake 'Markermeer', covering roughly 700 km^2. This lake is a non-tidal environment, with wind as the only major hydrodynamic forcing. The Oeverdijk nourishment was constructed in the Markermeer, in front of the existing dike, not on top of it.

This adjustment was required because the existing dike no longer met legal safety requirements. In 2006, a series of tests already revealed multiple parts of the dike section along the Markermeer, between Hoorn and Amsterdam, no longer met that standard. Of he total stretch of 47km, a significant 33km was rejected, often on the basis of 'height' and 'stability' (Alliantie Markermeerdijken, 2018b). The waterboard Hoogheemraadschap Hollands Noorderkwartier, responsible for dike maintenance, has entered into a public-private collaboration with Boskalis and Volkerwessels (collectively 'Alliantie Markermeerdijken') to realise the required reinforcements over those 33km. This stretch has been split into 16 modules, of which the Oeverdijk design covers the first 3.

3.2. Nourishment design and construction

The starting point of the design for the Oeverdijk is that it is a sandy dike, physically and functionally separated from the existing dike, incorporated in a "soft" engineering solution (Alliantie Markermeerdijken, 2017). In designing the (workings of the) Oeverdijk, parallels to the functionality of coastal dunes, a natural form of coastal protection, were drawn where possible. This means that the Oeverdijk's primary functionality is based on dune erosion as failure mechanism for the outer slope. Additionally, similar to coastal dunes, the water retaining function of the dike is guaranteed by a minimally required sand volume remaining in the dike, the 'limit profile', after passing of a normative storm.

Mathematical model tests, primarily using XBeach and DurasTA revealed a 1:40 slope to yield a roughly maintenance free design under 'standard' circumstances. Therefore, that slope was chosen for the final design. However, the Houtribdijk, a sandy nourishment on the other side of the Markermeer, revealed that it is likely a steeper slope (1:10) will quickly develop around the waterline, with a very gradual slope slightly underwater. It was debated to incorporate this profile shape into the original design, but too little was known about the forcing mechanisms that trigger this profile development. If this 'Houtribdijk' profile were to be constructed initially, further development could lead to too little sediment volume remaining in the dike. Therefore, the design will keep in mind the possible loss of sediment around the waterline, specifically between NAP -1.0m and NAP +0.5m, as a result of the development of this profile, but will not actively construct it that way to begin with (Alliantie Markermeerdijken, 2018a).

Part of using a sandy solution for a coastal problem, is that mobile sediment is placed under the influence of wind and waves. This makes the outer slope of the Oeverdijk dynamic. To allow this dynamic behaviour of (part of) the Oeverdijk without it endangering the required limit profile, a 'wear layer' has been designed on top of the required safety profile. This wear layer is an extra volume of sediment,

added between NAP +0.5m and NAP -1.0m at a slope of 1:25, with occasional additions to match the wear layer to the profile beneath.

Practically speaking, the three modules of the Oeverdijk stretch over 1.4km (south), 2.0km (middle) and 0.9km (north) lengthwise, with a rough cross-shore length of 200m. Each module construction was tested according to the minimum volume required in profiles, at 199 m^3/m (south), 211.9 m^3/m (middle) and 211.9 m^3/m (north), between the top of the dike and NAP -2 m. The design is based on a grain size diameter (D_50) of 200 µm. A clear condition or safety requirement to test the Oeverdijk profiles or volumes after the initial morphological developments has not been set.

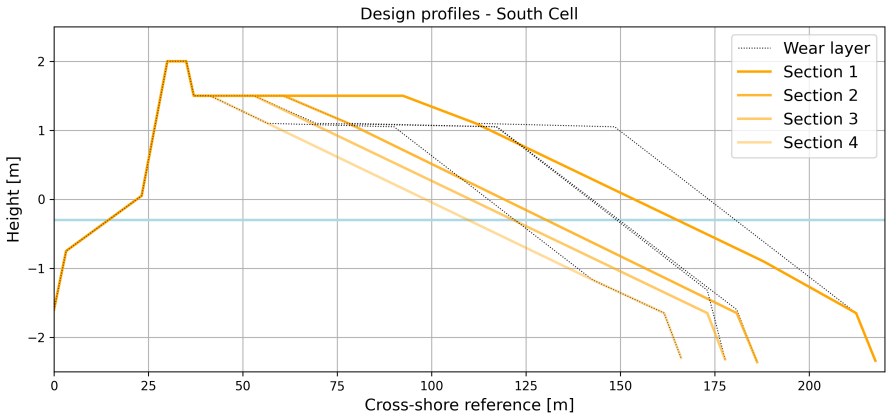

Figure 3.1: Design profiles different sections in the southern stretch of the Oeverdijk. The main slope is 1:40 for all profiles, additional wear layer is depicted by the dotted black line. For spatial reference of these cells, see 4.1

Settlement was a thoroughly considered aspect of design engineering in this project. Based on methods by Yin and Graham (1989) settlement predictions were made for during the construction of the Oeverdijk, and afterwards. This is visualised in settlement prediction curves that were made for various locations, an example is provided in figure 3.2. Settlement beacons were placed at the prediction locations to measure settlement over the course of construction (starting September 2019) (Alliantie Markermeerdijken, 2022). The (slope of the) settlement prediction graphs for all beacon locations are very comparable for 1000 days after start of construction onwards, all showing the same straight settlement line. It is important to note that the analysed period in this report falls after the plotted time period (Febuary 2025 is more than 1500 days after September 2019), but visual analysis of the graph at 1500 days suggests no more than 0.04m of settlement over a year (1/5th of the grid cell height). Tables in the full settlement documents (Alliantie Markermeerdijken, 2022) also print expected settlement values for 10, 30 and 50 years after construction. These range from 0.02m, 0.04m and 0.08m (relative to completion respectively), to 0.08m, 0.11m and 0.13m depending on which beacon location is analysed. The design demands stated residual setting must be limited to 0.5m, 50 years post-completion. Completion dates range between winter of 2022 and summer of 2023.

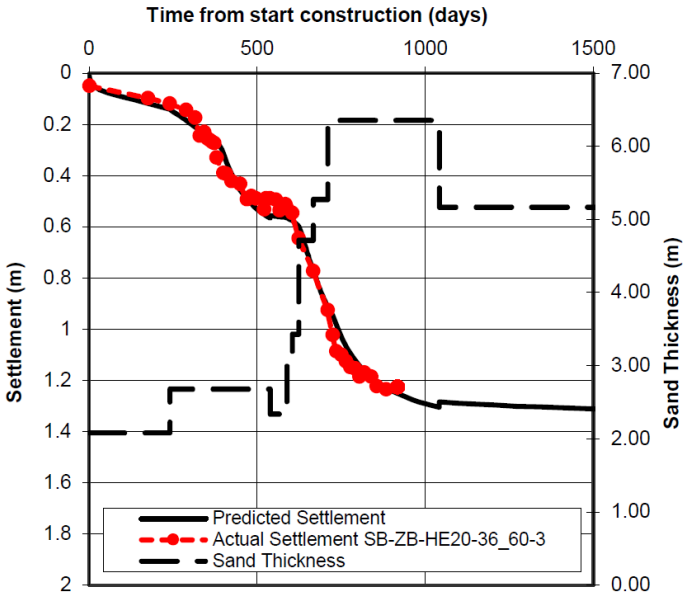

Figure 3.2: Example of a settlement prediction curve, part of the design process. This is the prediction curve validated against measurements at beacon SB-ZB-HE20-36-60-3, located at the top of the Oeverdijk in the middle of the middle beach cell (Alliantie Markermeerdijken, 2022). The considered period in this research lies beyond this graph (starting roughly 2000 days after construction).

3.3. Available data overview

Following the construction of the Oeverdijk, monthly surveying campaigns were carried out. Each measuring campaign covered a few days. For the sake of this analysis, the spatial data collected over these days is combined into a single elevation file. The following data was collected:

- Topography data: collected by a drone with Lidar technology (equipment accuracy theoretically +/- 3cm). This data covers the dry section of the Oeverdijk, sometimes including the original dike behind, the breakwaters and other surrounding structures. Intrinsic resolution is 50 x 50 cm.
- Bathymetry data: collected using a multibeam echosounder on a boat (equipment accuracy theoretically +/- 2cm). This covers the underwater area, starting slightly further offshore than the waterline as the boat cannot fully reach the coast. This data sometimes covers a larger area of the bay, and sometimes does or does not cover the underwater area in front of either of the northern beaches. Intrinsic resolution is 50x50cm.
- Waterline data: this is data collected by hand, covering the waterline and the shallow area not reachable by boat. This data consists of cross-shore GPS points, collected using a hand-held Trimble GPS (equipment accuracy theoretically +/- 2cm). This method of data collection is most sensitive to human influence and is very scattered, without clear initial resolution. Although the cross-shore points are roughly in a shore-normal line, the number of points per profile varies (usually about 15), in addition to the distance between the walked lines (usually about 20m) and the height contours between which the points lie.

The available data is summarised in table 3.1.

Dataset	Date	Comment
1	2023 week 42/43/44	General: still during a lot of land works
2	2023 week 46	General: limited offshore reach bathymetry. North cell: missing northern beach bathymetry.
3	2023 week 50	North cell: missing northern beach bathymetry.
4	2024 week 04	North cell: missing northern beach bathymetry.
5	2024 week 08	North cell: missing northern beach bathymetry.
6	2024 week 12	North cell: missing northern beach bathymetry.
7	2024 week 16	North cell: missing northern beach bathymetry.
8	2024 week 20	North cell: missing both beaches bathymetry.
9	2024 week 24	–
10	2024 week 28	North cell: missing southern beach bathymetry.
11	2024 week 35	North cell: missing southern beach bathymetry.
12	2024 week 40	North cell: missing southern beach bathymetry and waterline.
13	2025 week 10	–

Table 3.1: Overview available data

A first analysis of the accuracy of the data was carried out to determine if there were any major outliers. As the topography and bathymetry do not cover the same area each time, exact comparisons are difficult. However, average z values of both datafiles reveal the average topography z-value is 1.11m, with individual dataset extremes of 1.07m and 1.15m. For the bathymetry files the average z-value is -2.65m, with individual dataset extremes of -2.52m and -2.70m. Individual outlying values were also analysed. The only impactful numbers were topography values of z > 5m, where a building is being constructed next to the northern cell beaches. The waterline data points are labelled 'waterline' at a single point in each cross-section, allowing for the calculation of the waterline z-value in each data set. This leads to an average waterline z-value of -0.29m, in line with an expected water level when regulated levels of the Markermeer are set at -0.2m and -0.4m. In very few cases, the label 'waterline' is given to a point that does not realistically lie at the water line, or with multiple 'waterline' points in a single cross-section. Those points were not considered.

In addition to collected spatial data, data on wind, current and waves was also collected at KNMI weather stations and a buoy placed in the Hoornse Hop bay. This data will be discussed in the chapter on hydrodynamic results. To provide a spatial indication of where all data was collected, see figure 3.3.

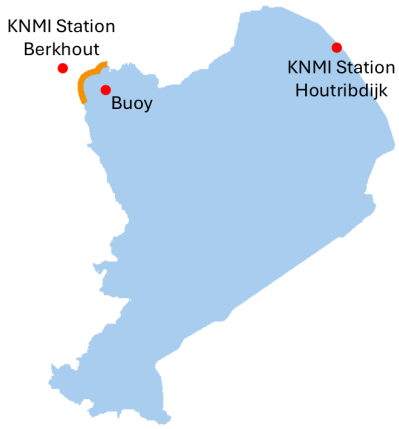

Figure 3.3: Spatial reference for the locations of collected data. Surveying campaigns were carried out at the Oeverdijk (in orange), and hydrodynamic data was collected at the buoy and KNMI wind stations (red markers).

4
Methodology

This chapter discusses the methodology applied to obtain, process and analyse available data, and the methodology applied to generate new data through modelling. Briefly, the site visit are discussed, followed by determination of the time frame within which the available data is analysed. Finally, the method applied to analyse the morphological and hydrodynamic data is discussed. The analysis itself is then performed in Chapters 5, 6 and 7.

4.1. Site visit

A visit to the Oeverdijk was scheduled on January 9th, 2025. The goal of this trip was to gain an impression of the scale and local conditions at the Oeverdijk. During the trip, all three sections of the Oeverdijk were visited on foot. It was a very cold and calm day, with a weak wind of around 3 m/s, primarily from the north-west, and a temperature around 2 degrees celsius. Photos that were taken and other specific observations are discussed later.

4.2. Selection of considered period of time

Initial analysis of the available data (Chapter 3.3), revealed the first three available morphological data sets (weeks 42/43/44, 46 and 50 of 2023) were collected during phases of the project in which bulk sediment transports still occurred, both on land and around the waterline. Amongst other things, this results in patterns of large off-shore deposition, and significantly impacts volume calculations along Oeverdijk sections. Therefore, this analysis will not consider those surveys. All other observations are used, ranging from 2024 week 04 to 2024 week 05 over 10 surveys. The available hydrodynamic data stretches over a much longer time period, with buoy data available from July 2023 onwards, and wind data available from 1999 onwards. For some long-term trend analysis this may be used, but the primary focus of this data analysis is on the period of 1 January 2024 - 13 March 2025.

4.3. Morphology: Data processing

The data available for the morphological analysis is composed of several types of measurements per surveying expedition (Chapter 3.3). The retrieval dates vary, but occur within a week, and spatial availability of that data varies (3.1). The raw data is handled fully through python scripting. First, the data is filtered, after which the raw topography and bathymetry data is gridded (via linear interpolation), onto a common grid with a resolution of 1x1m covering the Oeverdijk. The waterline data points were interpolated along long-shore contour lines (at -1.0, -0.8, -0.6, -0.4, -0.2 and 0m), after which those longshore bands of data points were also gridded onto the same common grid as the topography and bathymetry data. Finally, any gaps that were still present in the data, for example occurring when the bathymetry did not reach the waterline data, were also filled through linear interpolation. For the interpolation, Python's *scipy.interpolate.griddata* function is used. A threshold of 10 meters is applied, meaning interpolated points that are more than 10 meters away from a data point are removed. When combining the gridded bathymetry, topography and GPS data sets some overlap sometimes occurred. In that case, the average value between the two values was used.

The collected GPS points were roughly located along various cross-shore lines, and contained a label of 'WATERLINE' for the data point in each the cross-section that was located at the waterline. The waterline data points from the most dense GPS dataset (collected in 2024 week 08) were used to plot a smoothed waterline curve using Python's *scipy.interpolate.splprep* and *scipy.interpolate.splev*, which was later used for plotting and cell outlining. Cross-section profile data is extracted from the combined elevation data grids, using cross-sections normal to the waterline, and extracting according grid points using Python's *scipy.ndimage.mapcoordinates*.

4.4. Morphology: Location selection

This analysis plots multiple cross-sections during analysis. Additionally, a specific cell outline is selected within which volumes and areas are analysed. Figure 4.1 displays these locations on the Oeverdijk. Three cross sections are selected along each of the longer stretches over Oeverdijk, with a location within range of a breakwater effetcs on either end. A cross-section in the middle of each cell is selected to provide insight into the morphological evolution of exposed stretches of Oeverdijk. The cells have longshore edges parallel to the shoreline. The onshore border aims to include all areas under influence of marine transport but exclude as much of ongoing landworks as possible (for that reason, an upper limit of NAP +0.9m is also applied). The offshore border is 120m lakeward of the waterline, reaching a depth of over 3m in most places. The aim here is to reach well beyond the depth of closure, which only barely reaches a depth beyond 1m during storms. It is assumed that, due to the offshore extent of the cell and the fact that both breakwaters extend beyond that limit, no sediment bypasses the cells and breakwaters into the next longshore cell.

The cross-sections cover a length of 160m, 40m landinwards from the waterline, 120m lakewards. The middle cell covers a longshore length of 2 km, the southern cell covers a longshore length of 1.4 km. The cells share the cross-shore length of the analysed profiles, at 160m. The sections within the cells are not of equal long-shore length, to allow them to be compared to the analysed cells in the design. In the middle cell, sections 1, 2, 3 and 4 have lengths of 523, 570, 527 and 472 m respectively. For the southern cell, this is 343, 357, 344 and 356 m respectively.

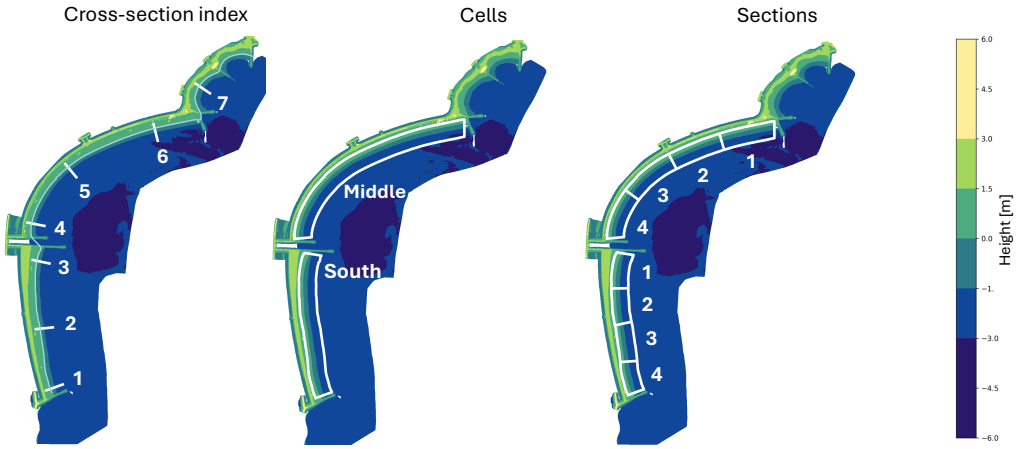

Figure 4.1: Bathymetry of the entire Oeverdijk, with numbered and named cross-sections and cells for spatial reference in further analysis.

4.5. Hydrodynamics: Data processing

The available data for the hydrodynamic analysis is raw data transmitted directly from the measuring buoy, located in the Hoornse Hop bay. Before analysis, this data required filtering to ensure unrealistic values (including wave directions over 360 degrees, negative wave heights, etc.) were all removed.

In some cases, the data was filtered more to extract certain events, peaks or other relevant points in the data. All demands set to these filters, such as thresholds in space or time for different variables, are mentioned accordingly in the analysis chapters.

4.6. Hydrodynamics: Wind station selection

Wind measurements are available from two measuring stations, one located in Berkhout, and one located on the Houtribdijk (see figure 3.3), facilitated by the Royal Netherlands Meteorological Institute (KNMI). Due to the set-up of the station on the dike at the Houtribdijk, this station tends to overestimate wind speeds. Additionally, wind speeds obtained at the Berkhout station correlated more closely to the measured local wave heights, visible in figure 4.2, likely due to the fact this weather station is only located a rough kilometer from the Oeverdijk. Therefore, this specific analysis will consider local 'wind'

as the wind data collected at the Berkhout station.

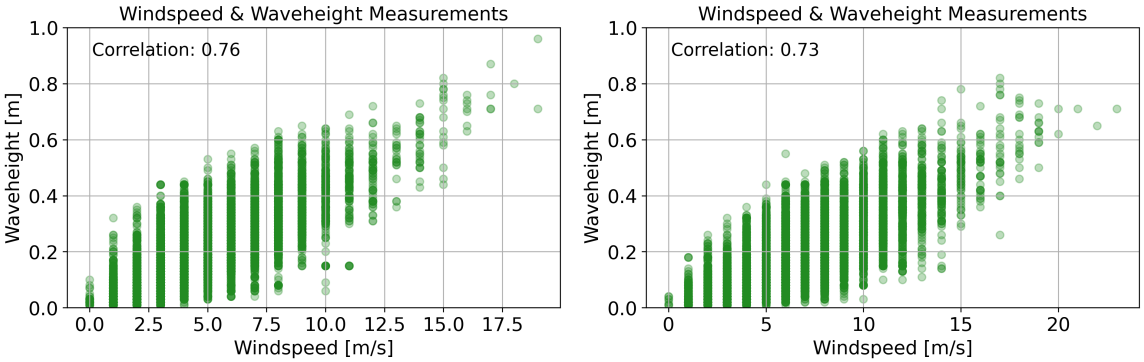

(a) Station Berkhout

(b) Station Houtribdijk

Figure 4.2: Correlations between measured wave heights at the buoy, against measured wind speeds at the KNMI stations of Berkhout and the Houtribdijk. Under the assumption that wind is the single driving force for the local wave climate, this correlation is used as indicator for which station is best suited to analyse local hydro- and morphodynamics.

4.7. Hydrodynamics: Generating nearshore data with Delft3D model

This thesis uses the Delft3D (D3D) Markermeer model to investigate hydrodynamics near the Oeverdijk at Hoorn. Delft3D software simulates free surface flows based on numerical computations, and can be used to simulate interactions of water, sediment, ecology and more, in space and time. In this case, the focus lies on water flow only, and will use the Delft3D-FLOW and Delft3D-WAVE components in the Delft3D 4.05.01 version.

4.7.1. Reason for modelling

The acoustic doppler current profiler (ADCP) that measures current offshore of the Oeverdijk (see figure 3.3 for the location), does this at three points in the water column, roughly between 120 cm above the bed, and the water surface. This means virtually no information of current at depth is available, visualised in figure 4.3. Considering the shape of the bay in which the buoy is located, the low velocity measurements could be a result of a circulation cell around the buoy. In that case, velocities closer to shore could deviate significantly from the measurements at the buoy. Additionally, no information on longshore variation in hydrodynamic forcing is available through this method of measurement. Therefore, Delft3D modelling is used to gain a general insight into the influence of wind speeds and directions on the development of longshore flow patterns near the Oeverdijk. As extensive modelling is beyond the scope of this research, certain assumptions and simplifications will be made throughout this process.

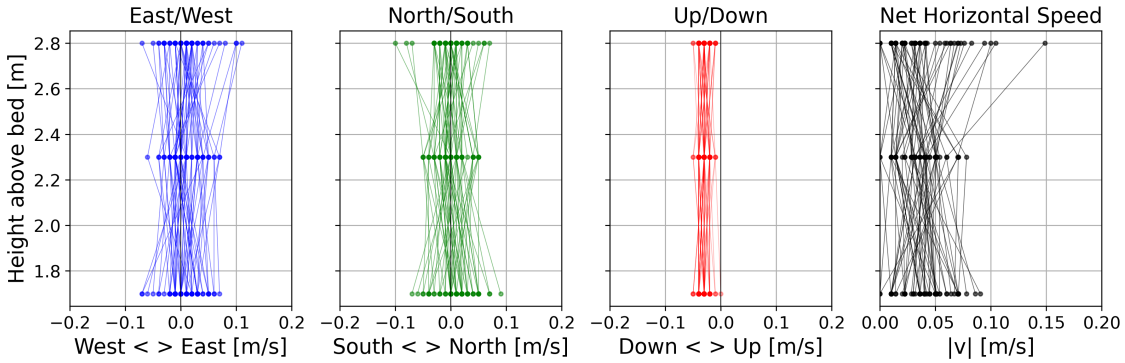

Figure 4.3: Current measurements from the ADCP. The first three graphs are the seperate measurement outputs, the net horizontal speed plot is calculated from the Easting and Northing currrents.

4.7.2. Model set-up

The model used to investigate flows at the Oeverdijk consists of two models: the larger total Markermeer model, and the nested (coupled) Hoornse Hop model. The resolution of the Hoornse Hop model is smaller, meaning local interactions between bathymetry and flow can be analysed at a more detailed scale, with the trade-off of higher computational time.

Table 4.1: Differences between *Total model* and *Nested model*

Comparison	Total model	Nested model
Grid points in M direction	197	371
Grid points in N direction	206	191
Average gridsize at Oeverdijk	150 m $\times$ 225 m	15 m $\times$ 25 m
Time step	2.5 min	1.0 min

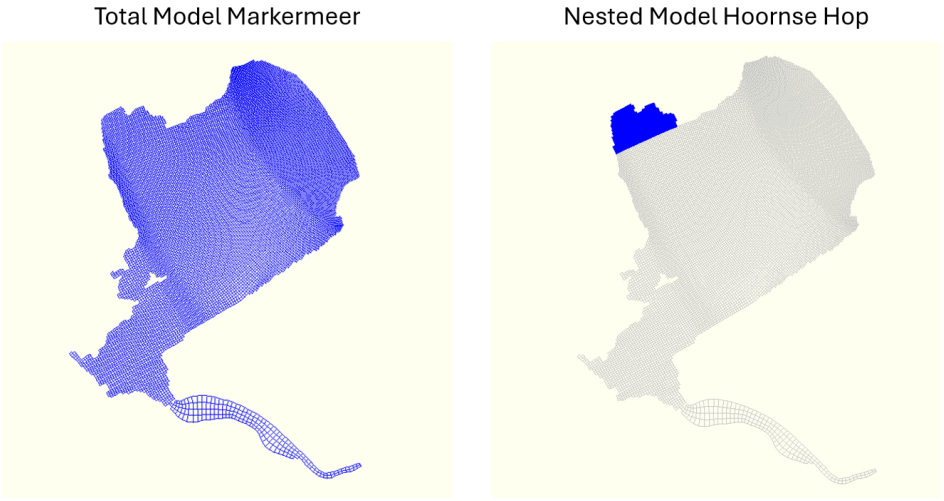

Figure 4.4: Computational grid of total model and nested model within, at Hoornse Hop.

This process of nesting essentially means that the total model is run first (left of figure 4.4), writing model output on water level to observation points at the boundary between the total model and the nested model via the Nesting(1) tool of Delft3D. After that, the Nesting(2) tool can be used to translate the output of the total to input for the nested model, which then has to run on its own. This nested model has a finer grid, and can therefore also have a finer bathymetry, shown in figure 4.5 below. Within the nested model, thin dams are placed at the locations of the breakwaters in the Oeverdijk design, to ensure no water flow can be computed 'through' these grid cell boundaries, to mimic the effect of the breakwater on real life flow. For the full-year runs, it was too time consuming to run both models consecutively. Therefore, those runs were done through on-line coupling, where data is exchanged between the models as they run simultaneously.

4.7.3. Model validation

An existing Delft3D model of the Markermeer system forms the base of this section of research, developed by Deltares. As stated in Chapter 4, a finer grid on a recent bathymetry of the Oeverdijk is used for analysis. Before building on the model output of this nest, a validation is carried out to the extent that is possible considering limited available measurements. This validation uses KNMI wind measurements during a stormy week of January 2024 as input for the nested model, and compares the output at the location of the ADCP buoy to the actual measurements of that buoy over the relevant time period. A storm period is used here as it is assumed that high-energy events primarily shape low-energy beach morphology (Freire et al., 2009), but a low-energy period comparison is also available in Appendix D. Here, figure 4.6 plots the calculated significant wave height, direction and period over time, against the values that were measured during that same stormy period. The plotted wind speed and direction are

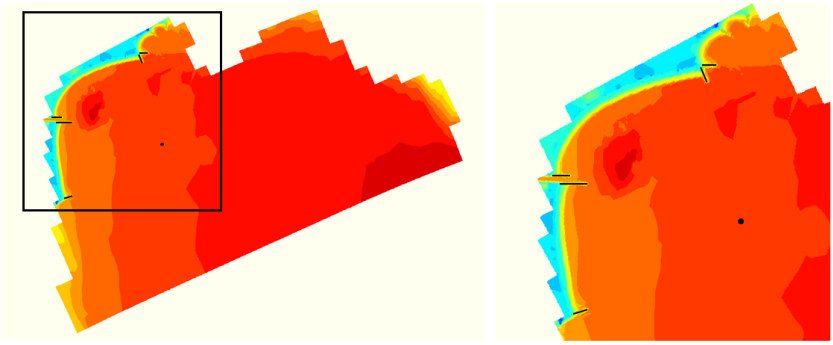

Figure 4.5: Bathymetry of the nested model at Hoornse Hop, black lines indicate flow-blocking thin dams in the model, and a black dot at the location of the buoy. An observation point is modelled there, to collect output data.

the input for the model over the same time period.

The top panel of figure 4.6 shows that the calculated wave height is slightly lower than the observed wave height, specifically during peaks. However, the calculated peaks occur at the same time, and at the same relative scale as the measured peaks. For the three measured peaks during this storm, the calculated significant wave height lies about 0.2 m lower. This effect is not constant, and virtually non-existent during calm periods between peaks. For the Delft3D online coupled output, this effect is slightly smaller, especially during the first peak, but still doesn't reach measured peaks. For data interpretation, it is therefore important to keep in mind that measured nearshore quantities such as velocities or bed shear stress (both related to wave height), may be larger in real life than in model output.

Furthermore, it is observed that the wave direction lies closer to the input wind direction than to the observed wave direction, but all three lines follow a similar trend. Generally, the measured wave and wind direction are more aligned for higher wind speeds, so all three lines are relatively close in those periods. This makes it more likely for modelled nearshore flow directions to be nearer to the 'true' direction during high energy situations. An exception is observed during the aftermath of the second peak, in which wind and wave direction temporarily differ by over 70 degrees. This visual analysis suggests this may also be the result of slight erroneous wave direction measurements. During calmer periods, the difference between modelled and measured wave direction barely reaches above 30 degrees. Delft3D output for online and offline calculations yield relatively similar output.

Finally, the wave period of the measured and modelled waves is compared in the lower panel. Here, a clear trend is visible in which the peaks in wave period of the actual waves are reflected in peaks of the modelled waves. However, the peak wave period of the modelled waves remains lower than the measured waves. Lower wave periods generally indicate shorter waves, with a lower wave energy flux. Similar to the two upper panels, the alignment between measured and modelled data for wave period improves during periods of lower wind speeds. Here, the difference between the offline and online coupled D3D output is much more obvious than in the two panels below; the online coupled Delft3D output reflects the measured peak period very well. Although figure 4.6 only plots a few days of a specific storm, a similar model run and graph was produced for a much calmer period in may of 2024, yielding very similar results.

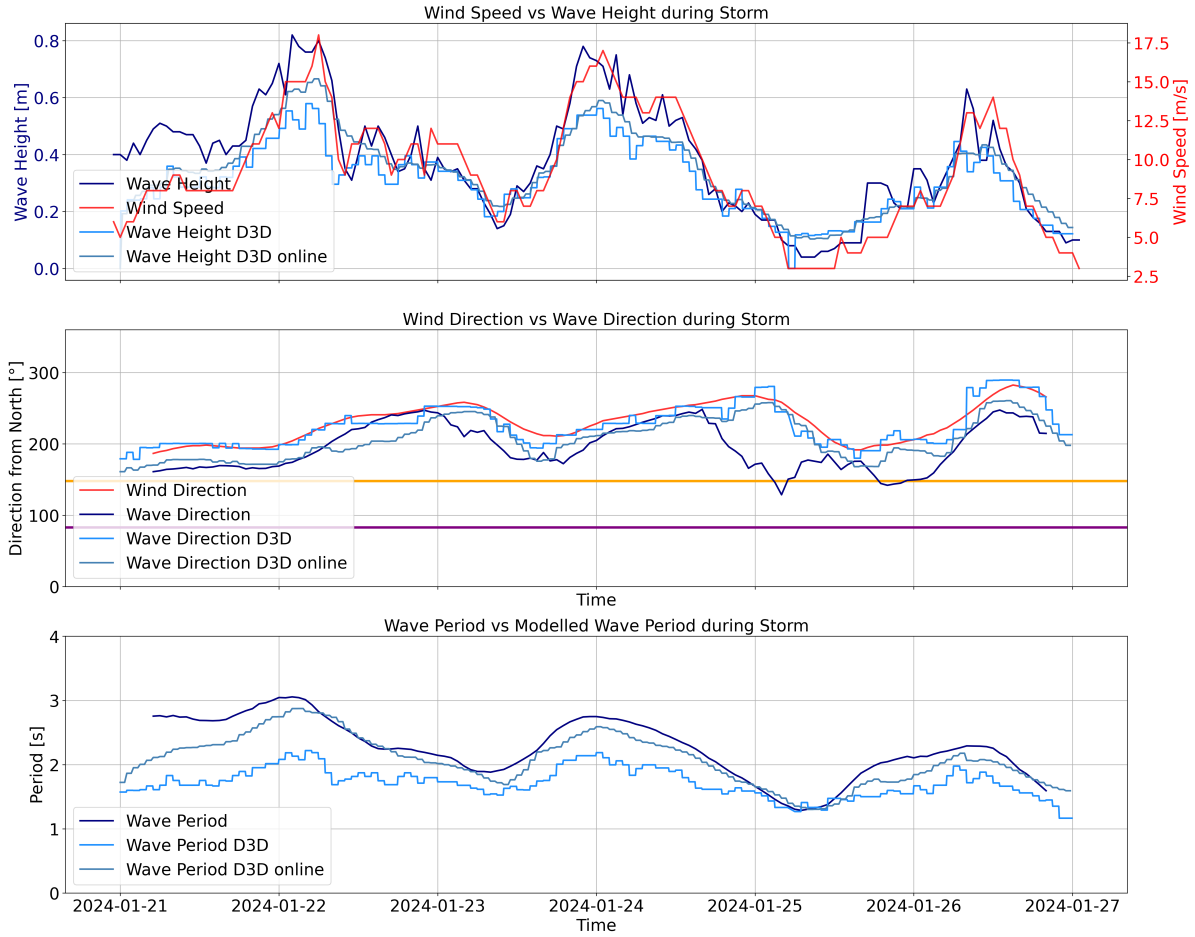

Figure 4.6: Graph to compare measured wind data (KNMI station), measured wave data (buoy) and wave data (Delft3D and Delft3D with online coupling) as a result of measured wind input, during a storm in January of 2024. The Delft3D output is numerical output at an observation point in the location of the buoy, in the Hoornse Hop bay. In the direction plot, the orange line aligns with shore-normal-incidence at the middle cell, the purple line shows this incidence for the south cell.

5

Results: Morphologic and hydrodynamic analysis

In this chapter the morphological and hydrodynamic data concerning the Oeverdijk is analysed. First morphologically, with a general spatial data analysis using elevation difference plots, followed by a first impression of volume analysis. After that, specific morphological observations in cross-shore direction will be analysed, followed by the analysis of long-shore trends. Then a small summary can be found, introducing the relevance for the hydrodynamic data analysis that will follow. The hydrodynamic analysis looks at wind, waves and water level fluctuation, to get a feeling for how the hydrodynamic system at the Oeverdijk works. After that, the relationship between different hydrodynamic variables in time will be analysed. Finally, nearshore hydrodynamic data is generated using a Delft3D model of the Markermeer. Analysing all these aspects of the morphological development and the forcing that causes it, helps form an idea of the full Oeverdijk system dynamics. This forms the basis of creating a conceptual system design by linking forcing to (morphological) change. Those steps follow in the next chapters.

5.1. Morphology: General observations

5.1.1. Elevation change

Elevation difference maps provide a first insight into general patterns of sedimentation and erosion. They are generated by plotting the difference in elevation (Δz) between data sets at two points in time. The difference maps between January 2024 (week 04) and March 2025 (week 10) are shown in figures 5.1, 5.2 and 5.3. This time frame, roughly a year, is deemed representative to extract general, large scale patterns of sedimentation and erosion from, as all major construction works on land were finished by this time, and a full year window means impacts of singular events are generally smoothed over by general trends.

Main observations, across all three figures, include a general trend of erosion around the waterline, and deposition slightly offshore on the underwater slope. This is explicitly obvious in the northern edge of the middle cell (figure 5.2) for example, with a red and blue line at either edge of the forming plateau. These are indications of cross-shore transport, and the development of an underwater platform. This pattern is also seen at the beaches in the northern cell (5.3), with one (likely numerical) defined deposition line. In longshore direction, areas of stronger erosion are seen near the middle of the southern cell (figure 5.1), and the northern edge of the middle cell (figure 5.2). This long-shore gradient in strength of erosion and deposition are characteristics of longshore transport, often expected at beach sections between breakwaters, where a coastline can rotate between hard edges. The on-land area of the Oeverdijk also displays some smaller areas of extreme elevation change where bulk earth movement from construction has occurred.

Furthermore, a general, but very slight, trend of erosion is observed across the majority of the dike body, specifically obvious in the middle cell (figure 5.2). The dike shows one blue area on the southern cell (figure 5.1), a result of landworks. Between weeks 12-16 (April), and 16-20 (May) of 2024, toplayers of soil were added to the middle and southern cell respectively, to encourage plant growth across the dike. Still, an eroding trend is observed, suggesting that even with the addition of this toplayer sediment volume to the dike, sediment is lost from the upper dike body.

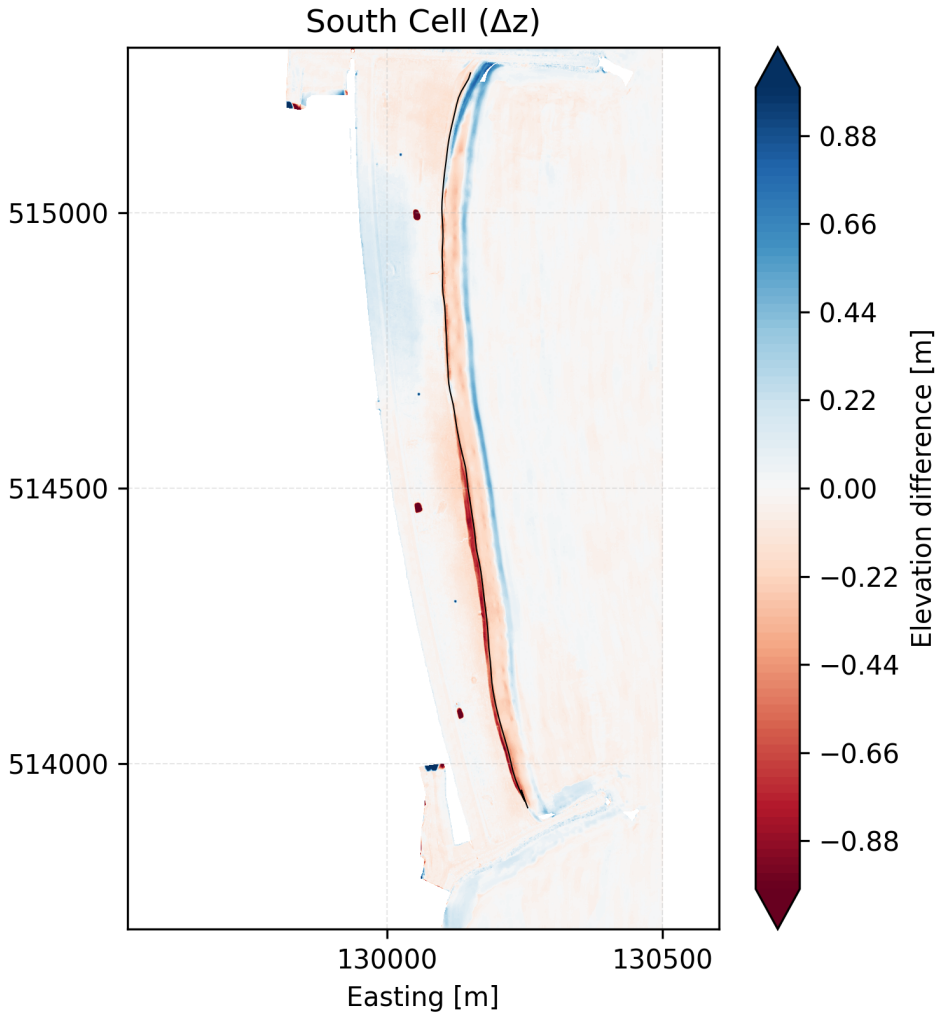

Figure 5.1: Elevation difference between the survey of 2025 week 10 and 2024 week 12, where positive (blue) indicates sedimentation and negative (red) indicates erosion. The black line is the waterline.

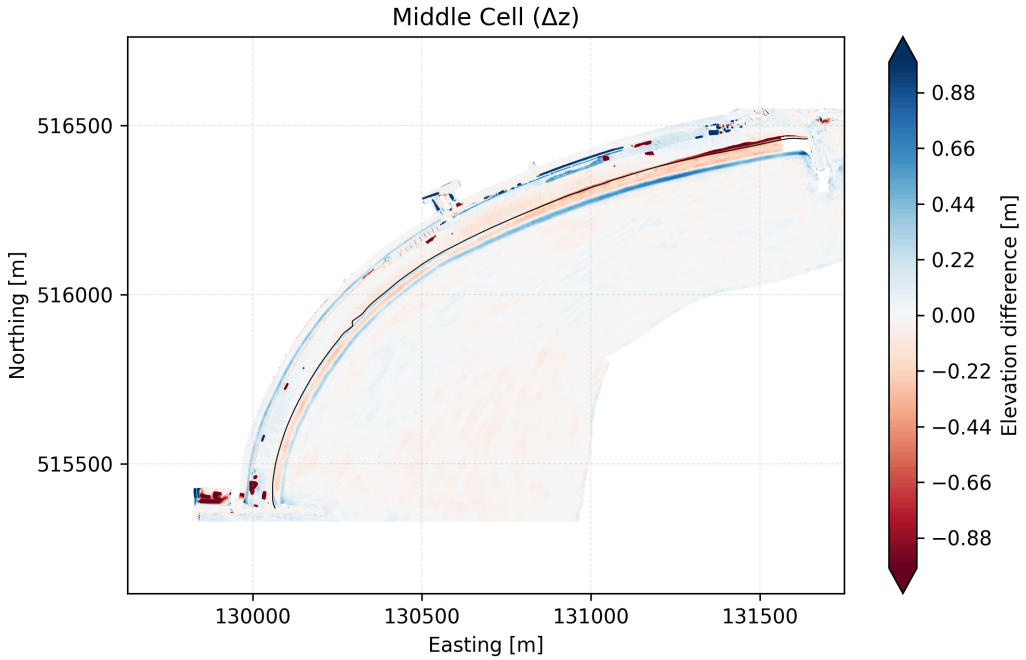

Figure 5.2: Elevation difference between the survey of 2025 week 10 and 2024 week 12, where positive (blue) indicates sedimentation and negative (red) indicates erosion. The black line is the waterline.

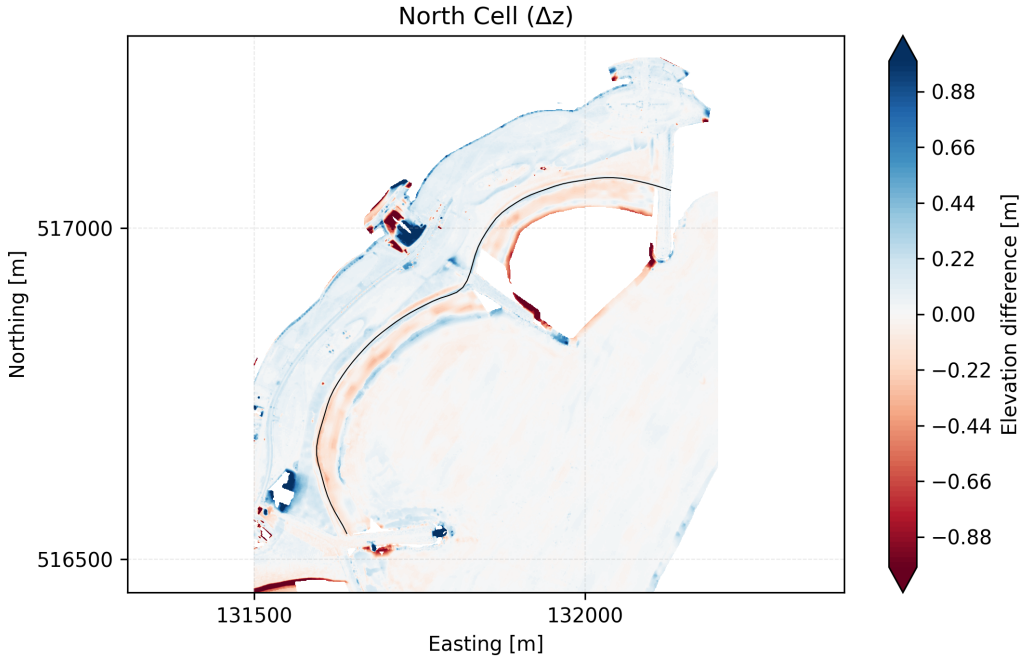

Figure 5.3: Elevation difference between the survey of 2025 week 10 and 2024 week 12, where positive (blue) indicates sedimentation and negative (red) indicates erosion. The black line is the waterline.

5.1.2. Volume change: Total

A volume analysis can help quantify whether sediment is being deposited or eroded across entire areas of interest. Here, this was done for the middle and southern cell of the Oeverdijk in figure 5.4. The northern cell was specifically left out of the scope of this analysis, partially because bathymetry data is missing for this area, making it difficult to get a full grasp on the available sediment. Additionally, the northern cell is so relatively small and sheltered, that significant sediment losses here are deemed unlikely, and siginficant sediment gain, athough also deemed unlikely, is not relevant.

The general volume analysis reveals the total sediment volume decreases over time for both cells, both cells losing roughly 12 000 m^3. The volume of the middle cell appears to have a longer period of staying roughly steady at first, but displays an eroding trend after that. The southern cell also shows clear erosion, reaching a comparable total volume loss that is similar to the middle cell, despite the southern cell covering a smaller long-shore distance. Both cells show a relatively large drop in their volume, in week 16 and 35 for the southern and middle cell respectively, after which a slight recovery can be seen. The general trend for both cells remains erosive.

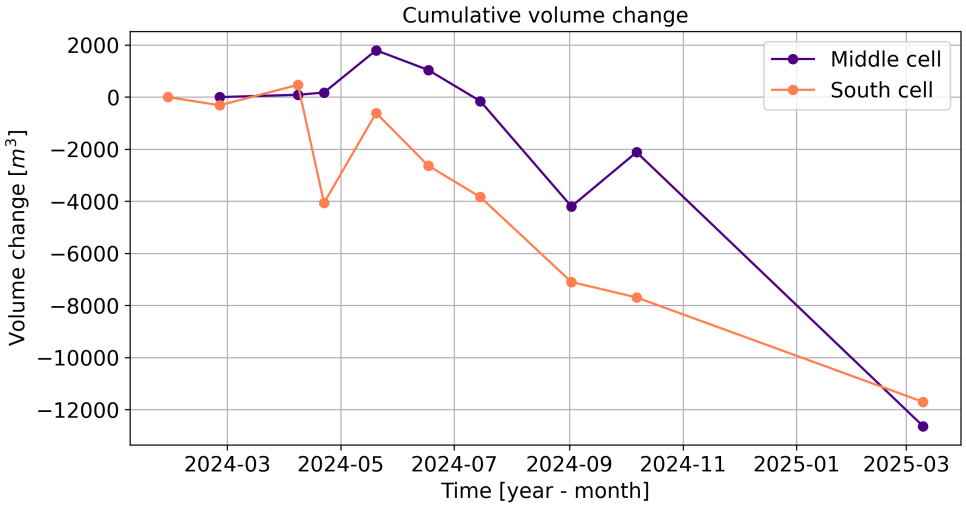

Figure 5.4: Cumulative volume change per cell over time. The first time step, between 2024 week 04 (January) and 2024 week 08 (February) has been removed for the middle cell, as a significant volume was added in that cell as a result of beach face construction works in this time frame. Only volumes below 0.9 m are considered.

Strong relative erosion for both cells occurred in interval 7 (weeks 28 to 35, August, of 2024). The Southern cell experienced the strongest erosion in interval 3, although this may be an anomalous result looking at figure 5.4. Significant deposition occurred for both beaches in interval 4 (weeks 16 to 20, May, in 2024), with another interval of significant deposition for the middle cell in interval 8 between weeks 35 and 40 of 2024.

5.2. Morphology: Cross-shore observations

5.2.1. Profile development

Various locations along the Oeverdijk are analysed to assess the cross-shore morphological evolution, some of which are visualised in figure 4.1. Analyses of these transects support the idea that the beach face is eroding around the water line, whilst (partially) depositing that sediment at the lakeward edge of a submerged platform. This trend is observed across all three cells at the Oeverdijk, as seen in figure 5.5. During a site visit this waterline erosion was easily observed; small sand ridges or mini cliffs of over 50 cm were observed near the waterline (see figure 5.17 for observation photographs), while a shallow plateau could be seen from the beach, reaching into the lake. Figure 5.5 suggests the rate at which the profiles are developing is not necessarily slowing down, which would be indicated by the difference between successive profiles diminishing. This indicates the profiles have not reached an equilibrium state yet. A visual result of the developing trend is steepening of the profile around the waterline, confirmed by the calculation of slopes locally, seen in Table 5.1. This section around the

waterline is developing to become the steepest part of the profile, all along the Oeverdijk.

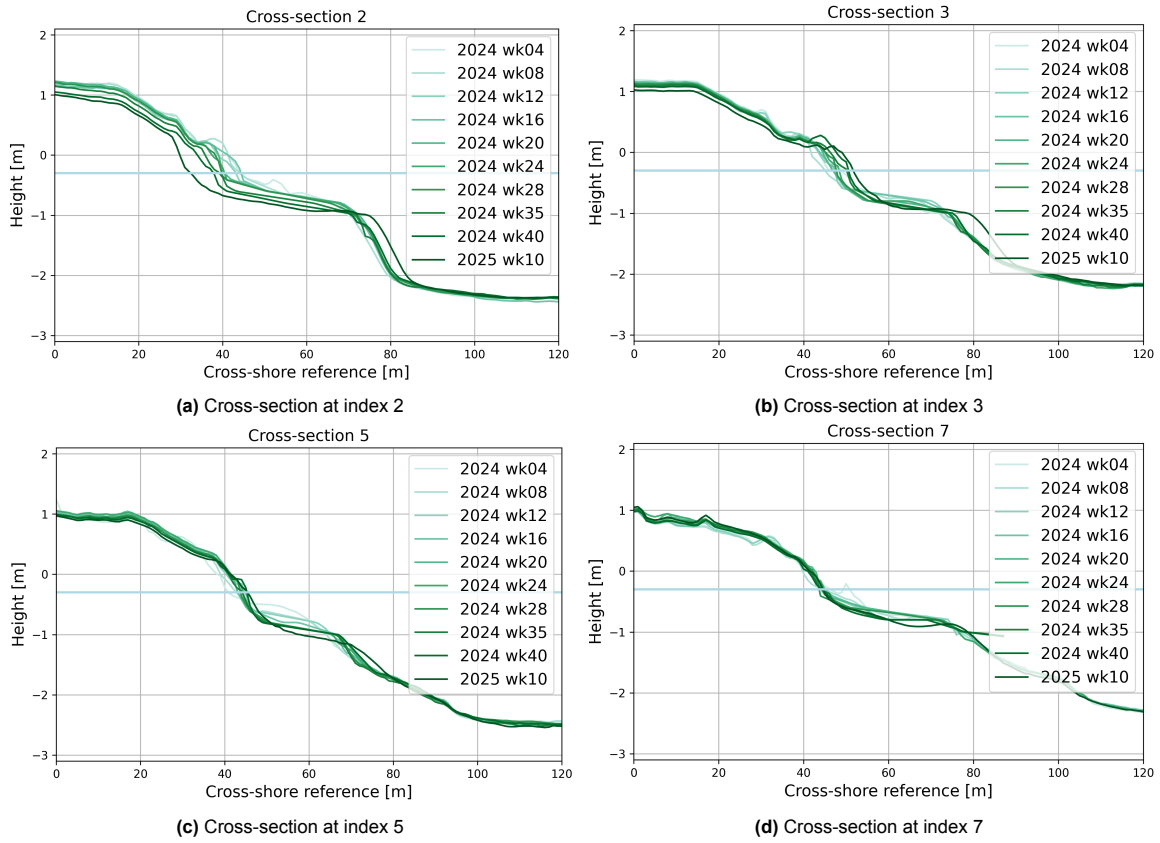

(a) Cross-section at index 2

(b) Cross-section at index 3

(c) Cross-section at index 5

(d) Cross-section at index 7

Figure 5.5: Overview of various cross-section developments in time

Index	Shoreline slope [1:m]		Platform width [m]		Platform slope [1:m]	
	2024 wk04	2025 wk10	2024 wk04	2025 wk10	2024 wk04	2025 wk10
1	1:29	1:12	8.9	27.6	1:18	1:56
2	1:29	1:10	15.8	39.4	1:31	1:77
3	1:18	1:8	20.2	25.3	1:40	1:50
4	1:40	1:9	9.0	23.8	1:18	1:48
5	1:15	1:11	15.1	10.6	1:30	1:21
6	1:24	1:10	10.9	37.6	1:22	1:77
7	1:26	1:8	23.3	31.9	1:48	1:63

Table 5.1: Profile characteristics, calculated between the profile intersections with an elevation of -0.05m and -0.045m for the waterline slope, around the average waterline of -0.3m, and between elevations of -0.5m and -1.0m for platform characteristics. This is done for different cross-shore indices at the start and end of the analysed morphological period.

The eroded sediment is, partially, deposited more on the offshore end of the profile, allowing an underwater platform to grow outwards. This growth is reflected in platform width increasing from anywhere between 8-20m in week 04 2024 (January), to 23-40m in week 10 2025 (March) (see Table 5.1). The platform width decrease for index 5 is due to the platform forming below -1.0 m, visible in figure 5.5. A platform growth is still observed. The pattern of sedimentation also leads to an increasingly mild slope for the platform, see Table 5.1. The average profile slope starts at 1:30, developing to 1:56. The only decreasing slope, of index 5, also comes back to the platform dropping below -1.0 m. The design profiles (figure 3.1) intended a slope of 1:40. Evidently, the first few weeks after construction already lead to a steepening of the slope around the water line, as the average slope waterline in week 04 2024 was already 1:24, increasing to 1:10 in week 10 2025. The strength of the offshore sedimentation effect

differs between sections. However, even where the deposition effect is mild, the combined impact of cross-shore erosion and deposition leads to a more gently sloped terrace forming just underwater. This confirms the theory that low-energy coastal environments, such as Markermeer, develop towards an equilibrium profile with an underwater platform of mild slope.

A cross-section that does not fully follow this trend can be found just south of the breakwater in the southern cell (see index 3, and to a lesser extent index 5, in figure 5.5). Here, deposition is seen along the water line instead of erosion, growing the profile outwards. However, this profile experiences a steepening of the profile around the water line simultaneously, in addition to sedimentation at the offshore end of the underwater platform. Therefore, the profile still develops towards the profile shape of steep slope around the waterline, with a mildly sloped underwater plateau, as seen in other profiles. This, too, was evident during the site visit. Sand ridges were virtually non-existent in the corner behind the breakwater here.

Although this general trend of developments can be observed, the exact profile differs along the Oeverdijk. Figure 5.6 is a good example of this, showing the variety in exact profiles after construction. However, all profiles show a clear development towards a very similar shape over time. The steeper part of the profile that develops around the water line shows varying gradients along the Oeverdijk. The plateau that forms varies in width, but appears to be developing between -0.5m and -1.0m everywhere. On the offshore end of the platform, a connection to the bottom of the lake is made through a sloped section. The step size and gradient of that slope differs, depending on the plateau height, width and the bed level to which the slope connects.

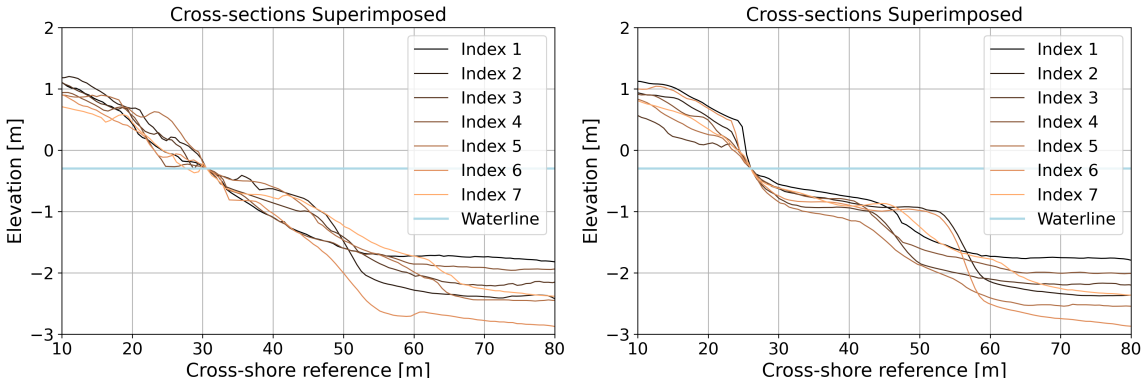

(a) Cross-sections in 2024 week 04

(b) Cross-section in 2025 week 10

Figure 5.6: Overview of the specified cross-section developments in space, by superimposing them at the intersection with a -0.3 m waterline

Table 5.2: Average annual shoreline retreat calculated as distance moved landward (in m) by the point of intersection between the profile and the z = NAP -0.3 m waterline, at the 7 analysed profiles, based on measurements between the survey of 2024 wk04 and 2025 wk10. Negative retreat indicates lakeward movement of the shoreline.

Index	1	2	3	4	5	6	7
Shoreline retreat [m]	15.71	10.60	-2.51	7.70	-4.14	12.13	3.85

In addition to developing profile characteristics, the waterline location of the profiles is also adjusting spatially. Table 5.2 provides an indication of the shoreline retreat for the 7 analysed indices, between the first and last considered survey. Two profiles show lakeward movement of the waterline, due to their location in a longshore location experiencing deposition around the waterline. The other profiles are retreating, at rates between roughly 4 and 15 m / year. For most profiles that is a result of a linear trend, not yet reaching an equilibrium. The design width of the wear layer at the height of the average waterline varies from roughly 15 to 30 m for comparison.

Profile analysis confirms the suggestion of the elevation plots that erosion at the waterline is much more evident than deposition at the offshore end of the platform, not necessarily in distance but in total volume. This suggests sediment loss. Hypsometric curves in figure 5.7 help provide insight into

where eroded sediment is moving in the profile. This type of graphs shows the relative section of area above a certain elevation. A crossing of a 0m elevation with a fraction of 0.6 would mean that 40% of the surface lies at 0m or higher. Therefore, changes in this graph can indicate sediment travelling to further up or down in a profile. Evident in both cells of figure 5.7 is the shift of sediment from the upper beach profile, to a lower, subaqueous platform extension. A smaller cumulative area remains in the higher parts of the profile. In the middle cell, this effect looks relatively balanced: the area gained at the outer platform edge and slightly below, look similar to the area lost around and just below the waterline. In the southern cell this balance is less evident. Clear erosion is seen on top of the dike, and around the beach face and platform, indicating volume loss in those sections. However, the area fraction representative of the deeper offshore area, below -2m, shows little to no increase, indication sediment lost from the profile does not end up in nearshore depth, but is transported further out of the considered cell.

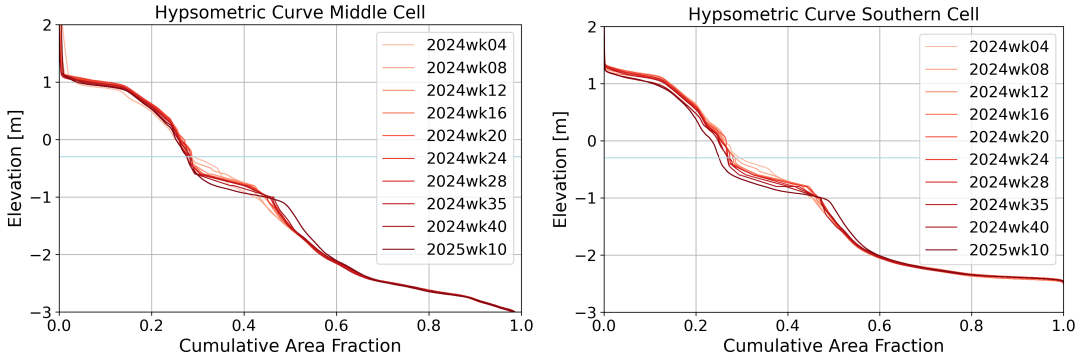

(a) Hypsometric curves of Middle Cell

(b) Hypsometric curves of Southern Cell

Figure 5.7: Hypsometric curve per cell, over time. A hypsometric curve plots the ratio of surface area in a region at a specific elevation, providing an indication of the vertical volume distribution in all profiles within a cell at a time.

5.2.2. Volume change: Cross-shore split

To quantify cross-shore volume changes, the cross-shore profile has been divided into three vertical sections (see figure 5.8), defined by the following elevations:

1. Beach face section [+0.9 m to -0.3 m]
2. Platform section [-0.3 m to -1.5 m]
3. Offshore section [-1.5 m to -3.0 m]

These limits were set for different reasons. The top +0.9 m limit was set to ensure as much of the on-land construction works as possible would be excluded from calculations. The definition of the platform section has been set in line with research and calculations by Ton (2021), to allow for potential comparison of volume changes. The bottom boundary of -3.0m is set to ensure the full lake bed is included in all parts of the cells.

Total Cells - Cumulative volume change

This vertical distribution allows for a next step in the analysis of volume changes in time, seen in figures 5.9 and 5.10. This reveals that the total volume in the beach face decreases over time for both cells. The first increase in beach face volume in the middle cell was the result of final construction works, and has thus been left out of the 'total' calculation for that time step. After that, the middle cell beach face volume shows a decrease (about -3 m^3/m over the surveyed period cumulatively), although less significant than in the southern cell (-5 m^3/m over the surveyed period). The platform section of the middle cell shows a very slight decrease, but not significant. The eroding trend of the south cell platform section is stronger, aligning with the observed beach trend. The offshore section of the middle cell fluctuates around zero over time, compared to slight offshore growth in the southern cell. The local dips in the total volume of both cells show to be linked to a decrease in offshore section volume at that time interval. The total volume in both selected cells shows a net decrease. Although the magnitudes of total volume change are relatively close between cells (-6 m^3/m for the middle cell, -8 m^3/m for the southern), patterns in the vertical sections are much more defined for the southern cell.

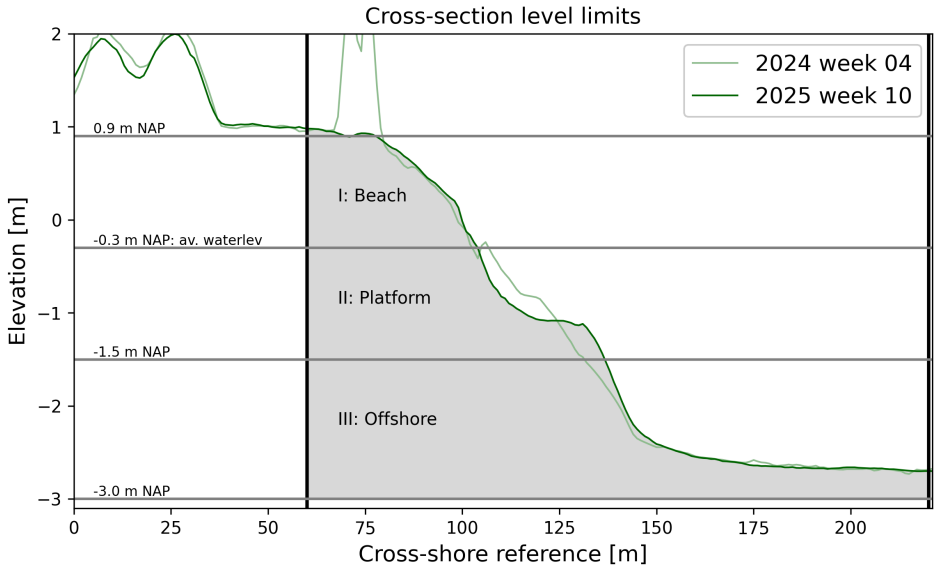

Figure 5.8: Visual representation of the levels at which cross-shore is split in volume calculations.

The only 'known' anomalous result, as mentioned, is the initial beach face increase at the first time step of the middle cell, due to landworks. However, there is also an unusual volume dip in April for the offshore section of the southern cell. This dip has no known physical cause, such as dredging works.

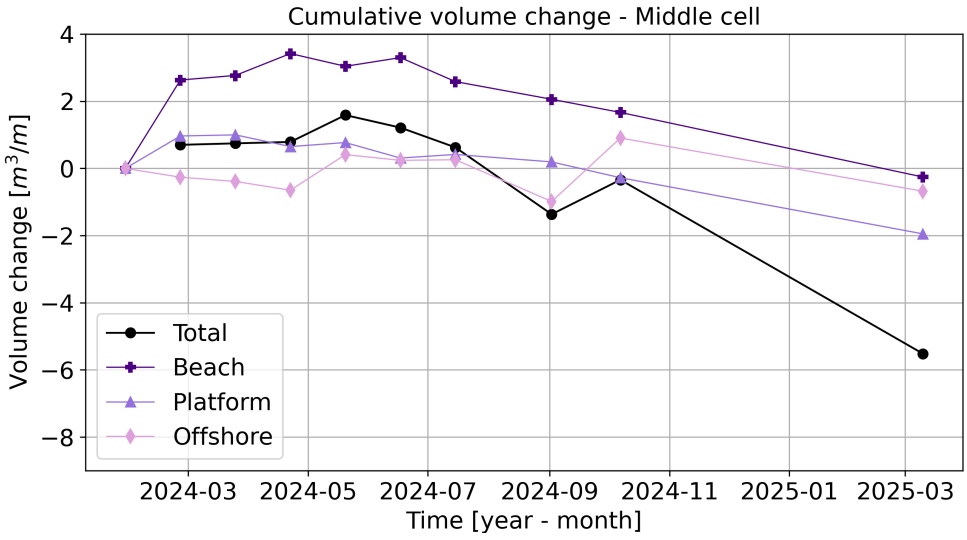

Figure 5.9: Volume change per 1m cross-shore section of the middle cell. Contribution of beach face volume change to total was left out for 2024 week 04 - 08 due to construction work sediment addition

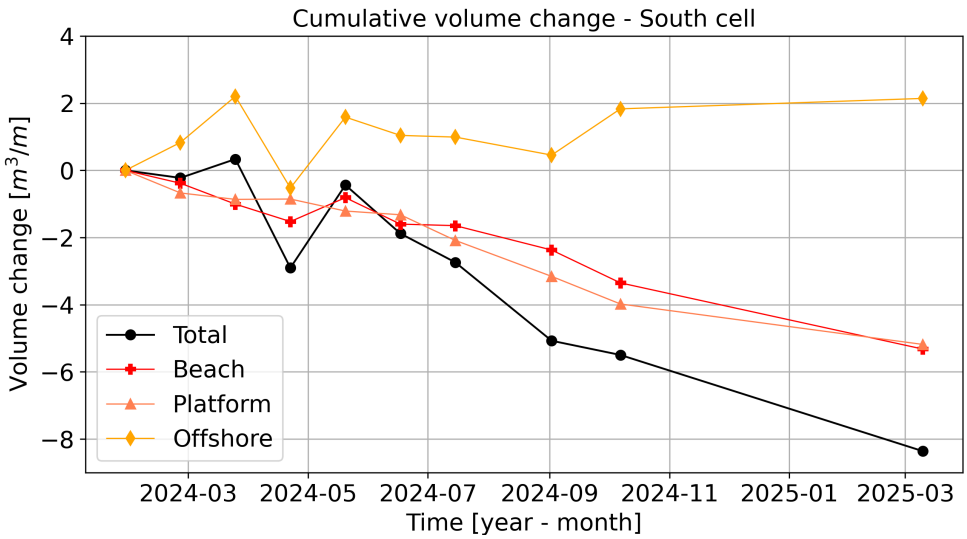

Figure 5.10: Volume change per 1m cross-shore section of the south cell

Total Cells - Normalised volume change

To gain closer insight into the relative volume changes at the Oeverdijk, specifically per interval instead of cumulative change, the normalised relative change per interval and per section is plotted over time in figures 5.11 and 5.12. To filter out (potential) anomalies, the first survey of the middle cell has been ignored, in addition to the fourth survey of the southern cell. At first sight, clear trends are absent. Intervals 5, 6, 7 and 9 display overall erosion in both cells, although rates and splits over the vertical cross-sections differ. Furthermore, interval 8 shows a very similar pattern for both cells, with significant offshore deposition against beach face and platform erosion. On a more general scale, the graphs show that neither cell exceeds volume changes of +/- 0.4 m^3/m/week. Additionally, both graphs show the beach to be the section experiencing erosion the majority of the time. Main differences include that the general trend of net erosion is much more evident in the southern cell, with a clear negative volume change focus. Additionally, the southern cell shows larger volume changes in general, both positive and negatively. From these bar charts, the southern cell appears more dynamic, or atleast experiencing a more singular signal when it comes to sediment transport.

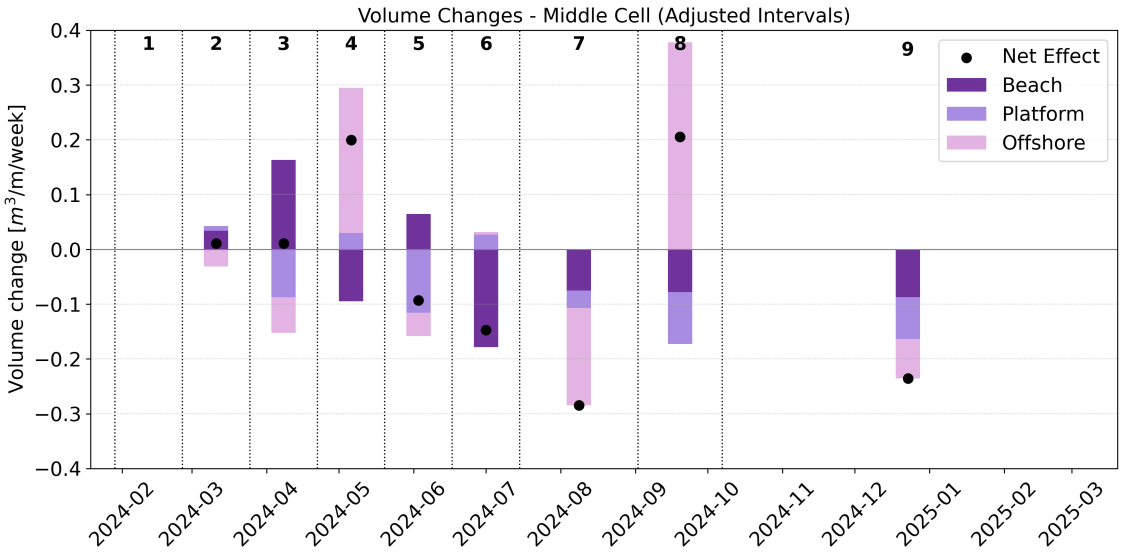

Figure 5.11: Normalised volume change per of the middle cell, as change per meter of coastline, per week, in each interval over time. This is a non-cumulative graph, so looks only at the change in the given interval. Contribution of volume change was left out for 2024 week 04 - 08 due to significant construction work sediment addition.

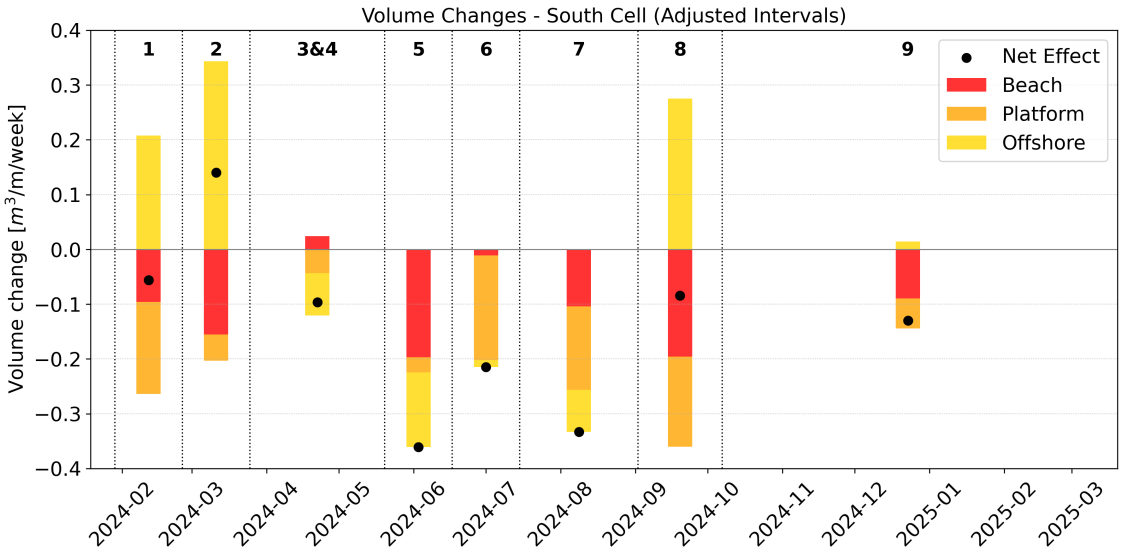

Figure 5.12: Normalised volume change per of the southern cell, as change per meter of coastline, per week, in each interval over time. This is a non-cumulative graph, so looks only at the change in the given interval. Measurements were left out for 2024 week 16 due to significant offshore erosion visible from figure 5.10, indicating a measuring error, so interval 3 and 4 are combined into a single time step.

5.3. Morphology: Long-shore observations

5.3.1. Erosion and sedimentation patterns

As the Oeverdijk is located along a curved stretch of coastline, variations in long-shore morphological development are expected as a result of alongshore variation in wave energy. The elevation differences already suggest this. By projecting net sediment volume change over the longshore distance, longshore transport signals can be distinguished, visible in figures 5.13 and 5.14.

For both cells of the Oeverdijk, a general pattern of erosion over the entire cell can be seen. However, the strength of the erosion and deposition are not uniform over the shoreline, signalling long-shore transport. In the southern cell, significant erosion occurs over the largest part of the shoreline, most

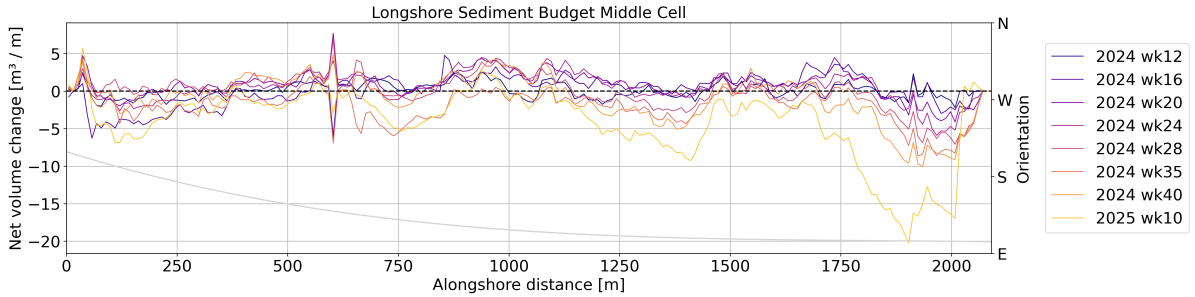

Figure 5.13: Volume change over longshore distance of the Middle cell, referenced to the survey of 2024 week 08. Only volumes below a height of 0.9 m are considered. Light grey line shows coastline orientation over the longshore. Alongshore distance = 0 is located at the southern end of the cell.

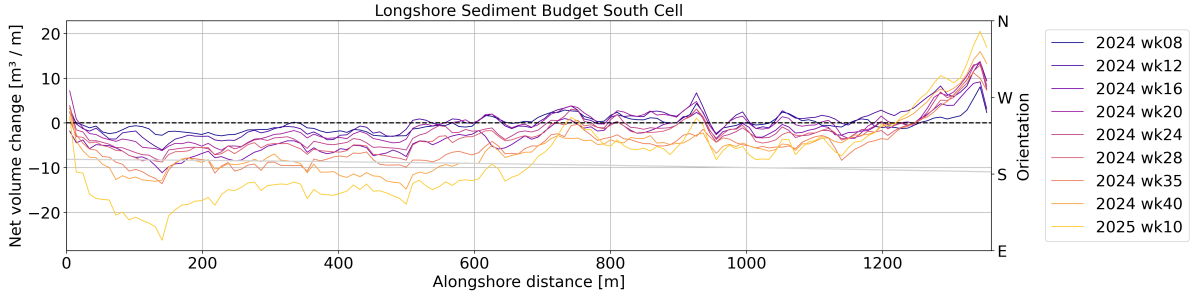

Figure 5.14: Volume change over longshore distance of the South cell, referenced to the survey of 2024 week 04. Only volumes below a height of 0.9 m are considered. Light grey line shows coastline orientation over the longshore. Alongshore distance = 0 is at the southern end of the cell.

evidently between 0 and roughly 700m alongshore. The volume loss decreases slightly during the summer of 2024 (weeks 20-35), specially visible between the longshore distance of 0-400m. This section also shows a relatively large sediment loss between 2024 week 40 and 2025 week 10, through a winter season, suggesting susceptibility to weather conditions. The northern tip of the cell, roughly from 1200m alongshore onwards, shows a growing coastline. This section is located next to a breakwater, suggesting sediment being transported in northward direction is deposited there. The sedimentation rates here (reaching a maximum of 20 m^3/m), do not compensate the total sediment loss (reaching up to 30 m^3/m and over a longer distance). The middle cell of the Oeverdijk shows a very different longshore transport signal. Ignoring the significant erosion peak between 0 and 100m longshore (landworks of sand removal on the beach), this cell remains relatively steady between 0 and 1000m alongshore. Moving northward of the 1000m, a trend of more erosion over the longshore can be recognised between 1000 and 1500m, and more significantly between 1750m and 2000m. Likely, this is related to the rotation of the shoreline over the longshore advancement. In this cell, too, slower rates of erosion are seen in the summer period of 2024, with a significant erosive jump from measurement 2024 week 40 to 2025 week 10, indicative of the storm season in the winter of 2024/2025.

5.3.2. Volume change: Long-shore split

Using the vertical distribution displayed in figure 5.8, and the long shore section split as displayed in figure 4.1, long shore patterns in volume change can be analysed.

A longshore volume analysis of the middle cell shows clear beach face erosion of the northern two sections (1 and 2), when excluding the land works that placed extra sand on the beach of section 2 during the first surveying interval, see figure 5.15. In contrast, section 3 and 4 are relatively stable. The beach development of section 3 does show a slight trend of growth until june, after which erosion sets in, but only for relatively small volume changes. The platform sections show a similar general trend, with relatively neutral sections 3 and 4, and most erosion in section 1 (up to 7.5 m^3/m over the analysed period). The platform of section 2 also shows a relative increase of nearly 3 m^3/m in the first interval, like the beach, possibly related to the land works on that beach too. The volume change of the offshore part of each section in the middle cell is stable, experiencing no significant gain or loss over

the analysed period. Figures for the platform and offshore volume change of middle cell sections can be found in Appendix A.

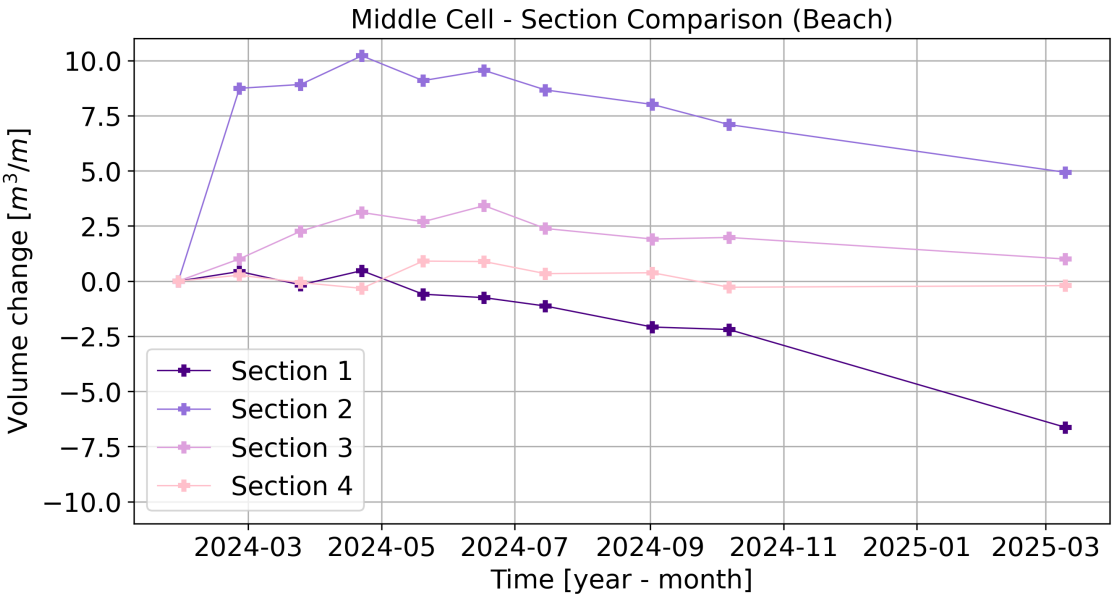

Figure 5.15: Cumulative volume change over longshore distance of the middle cell, split into the four longshore sections.

Figure 5.16 displays this long-shore split of volume change for the beach face of the southern cell. This trend is virtually the same for the platform section (see Appendix A). The beach face of section 1, at the northern end, stays constant. Section 3 displays the highest erosion rate, losing nearly 10 m^3/m over the analysed period. Sections 2 and 4 lie in the middle, indicating a fluctuating pattern of relatively less, more, less and more erosion at the beach face in longshore direction, from north to south. In contrast, a different pattern is observed in the offshore parts of all sections. There, the outer two sections (1 and 4) stay virtually constant over the analyses period, whilst the offshore area of the middle two sections experience mild growth of about 4 m^3/m over the analysed period. These two patterns balance out in such a way that, over the total cell, the more uniform trend displayed in figure 5.14 dominates.

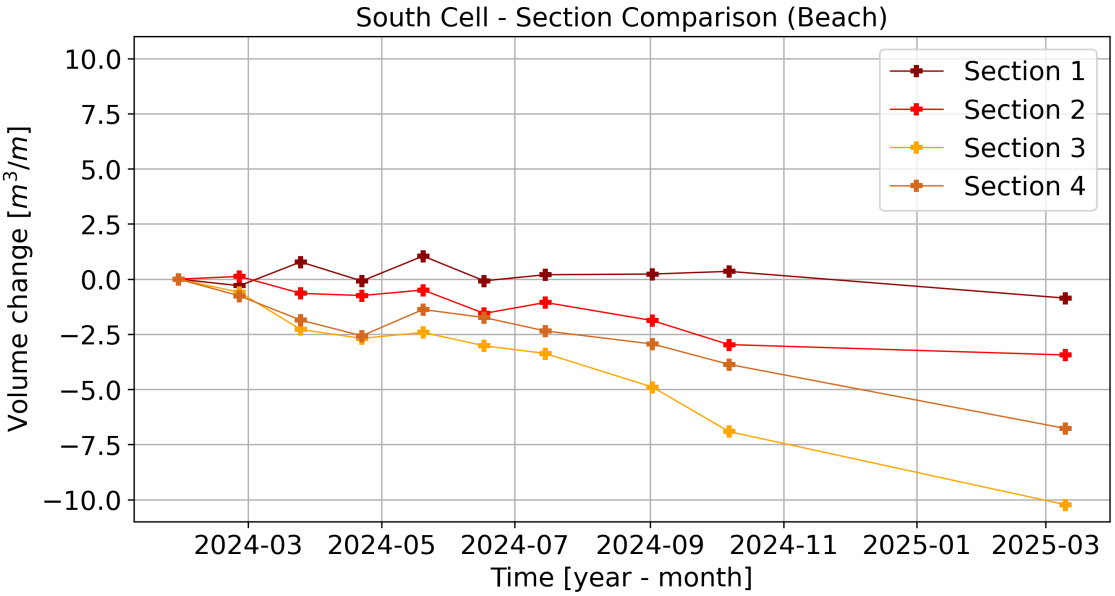

Figure 5.16: Cumulative volume change over longshore distance of the middle cell, split into the four longshore sections.

5.4. Morphology: Connection to site visit observations

The findings above can related to observations made during a site visit to the Oeverdijk (specifications of visit can be found under section 4.1). In cross-shore direction, site observations align with the results of data analysis that suggest offshore directed sediment transport, with waterline erosion and platform deposition. Ridges have formed in the sand, recahing 0.5 m high in some locations (see figure 5.17. From a side view, these ridges show to consist of both the additional 'top layer', and the original sand nourishment. The ridges are especially visible in the northern end of the middle cell, and the southern side of the southern cell, aligning with the results of the longshore erosion plots that those areas are a more dynamic stretch of coast as seen in figures 5.13 and 5.14. In both cells, the ridges flatten out beneath the breakwater, aligning with the data suggestion that the absolute volume change in the very corners of the cells is near zero. This ridge formation is a clear sign of cross-shore sediment transport, which is assumed to play a significant role in both the middle and southern cell.

Figure 5.17: Ridge observations (middle cell), with a hand for height indication

5.5. Morphology: Concluding remarks and next steps

To summarise, the morphological development of the Hoornse Oeverdijk over the course of the analysed year reveals distinct sediment transport patterns in both the cross-shore and long-shore directions. Cross-shore evolution is marked by consistent erosion near the waterline and deposition slightly offshore, indicative of the formation of a submerged platform (at about NAP -1 m), and an overall steepening of the nearshore profile (to roughly 1:10). These are features characteristic of low-energy beach systems. Long-shore analysis shows significant spatial variability in sediment volumes, with distinct erosion and (smaller) deposition zones. The southern cell morphology suggests a specifically uniform northward directed transport signal, the middle cell shows more longshore variability, likely related to cell curvature. These patterns confirm the dynamic nature of the nourishment, particularly in this early post-construction phase, and underscore the importance of considering both transport directions in (future) design assessments.

The observed patterns of erosion and sedimentation suggest transport signals that are, perhaps, in opposite direction between the analysed cells, in addition to a net sediment loss across both cells (roughly 12000 m^3 per cell). This cannot be understood or explained without understanding the hydrodynamic forcing that results in this sediment transport. Therefore, the following section will analyse the wind, and subsequent waves, currents and stresses that (can) form as a result, which is a requirement to build an explanation for the morphological development observed so far.

5.6. Hydrodynamics: General data analysis

Four main aspects of the hydrodynamic processes in the Markermeer are wind, water level (fluctuation), waves and current. These are discussed here, based on available or generated data. Essentially, the latter three are a (partial) result of the available wind (energy) that drives the dynamics of Markermeer.

Figure 5.18 displays the relative orientation of the middle and southern cells of the Oeverdijk, to allow for a clear comparison to the direction of forcing by waves and wind. The period that will be analysed here covers January 2024 to March 2025, covering all moments of morphological surveying.

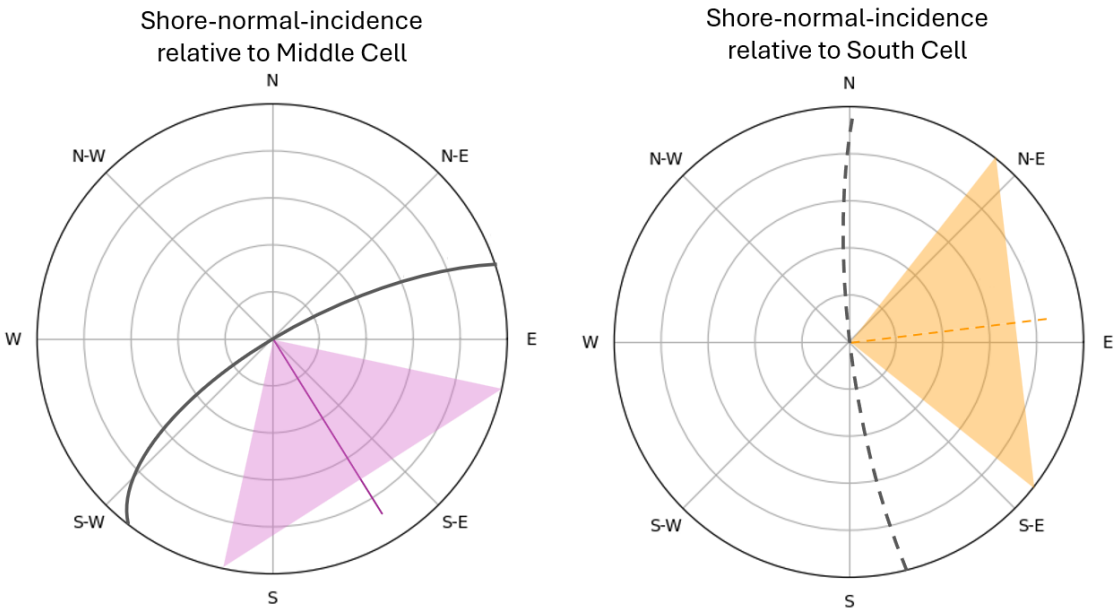

Figure 5.18: Orientation of the middle and southern cell in a compass (North = 0/360), with the direction of shore-normal-incidence range (for wind and waves coming from), marked for easy comparison to wind and wave data.

5.6.1. Wind

The full set of wind measurements over the considered period is analysed to create a wind rose (figure 5.19). The average hourly wind speed during the analysed period is 4.62 m/s, primarily coming from the south and southwest. The maximum wind speed that was measured is 19 m/s. During storms, strong winds come primarily from the south and southwest. Calmer periods see lighter winds from the east, west and sometimes even north. The most common southern winds align quite well with the longshore direction of the southern cell. The stronger winds, originating more from the southwest, generally come in to the southern cell at a much greater angle (see figure 5.20), introducing more longshore current potential.

Wave height shows a clear positive correlation to wind speed (see figure 5.20). When taking into account the direction of the wind (coming from), southwestern winds (250°) correlate to the highest wind speeds and subsequently the highest wave heights (orange and red dots). This is also the direction in which Markermeer facilitates its longest fetch distance, and the direction from which most storm winds blow. Figure 5.20 also shows that winds from 100° - 150° (south-east) generally yield higher waves for lower wind speeds, likely related to the opening of the Hoornse Hop bay in that direction.

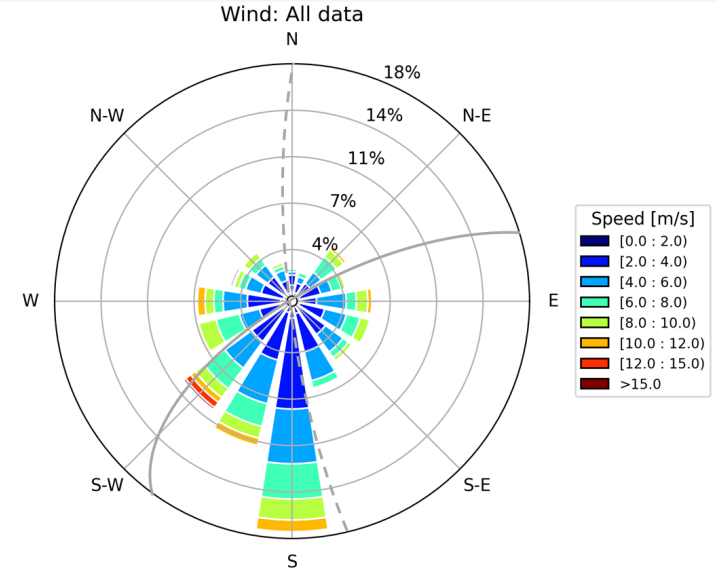

Figure 5.19: Wind rose of direction (coming from) and according wind speeds for the wind climate at the Berkhout KNMI station between January 2024 and March 2025. The dashed grey line represents the orientation of the southern cell, the full grey line that of the middle cell.

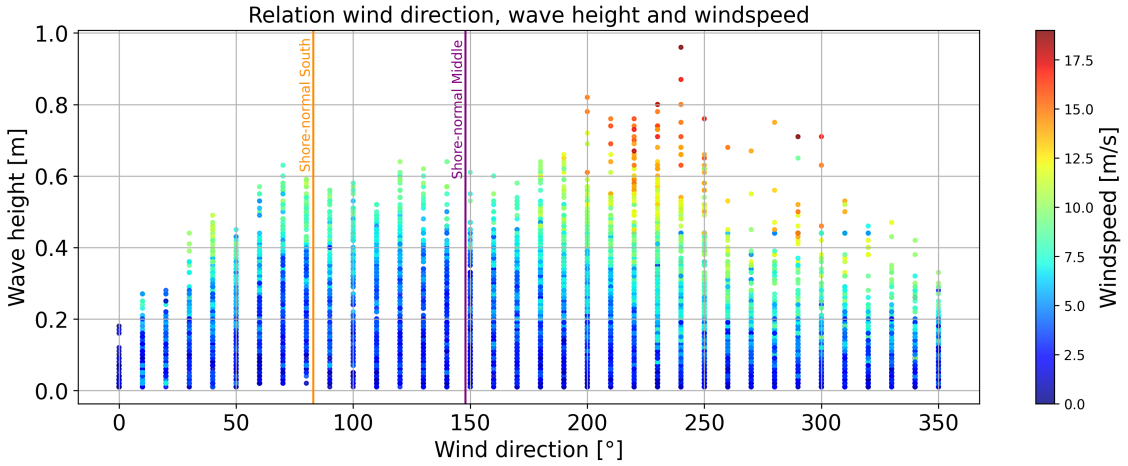

Figure 5.20: Significant wave height in m, plotted against the simultaneous wind direction (coming from), the colour of the points indicates wind speed in m/s.

5.6.2. Water level variation

The water level in Markermeer is regulated and set to a minimum of NAP -0.4 m during the winter, with allowed fluctuation between -0.1 and -0.3 during summer (Rijkswaterstaat, 2018). Generally, the water level is higher during summer months. On a smaller timescale, of hours to days, the deviation of water level measurements from a 10-day average water level can be interesting, as this may be a result of local wind climate instead of lake-scale regulation.

When the forcing winds are strong enough, water can be pushed to one end of Markermeer, creating higher water levels at that end of the lake, and lower at the opposite. Prior research and modelling has shown that, generally, the strongest winds coming from the southwest create maximum set-up at the Houtribdijk (northeast) side of the lake. The Oeverdijk is then located quite centrally, meaning it does not experience extreme levels of set-up or set-down. The water level at the Oeverdijk experiences more set-down than set-up. During lower wind speeds a fluctuation of set-up or set-down is found around 0, for higher wind speeds only increasing set-down is observed (figure 5.21).

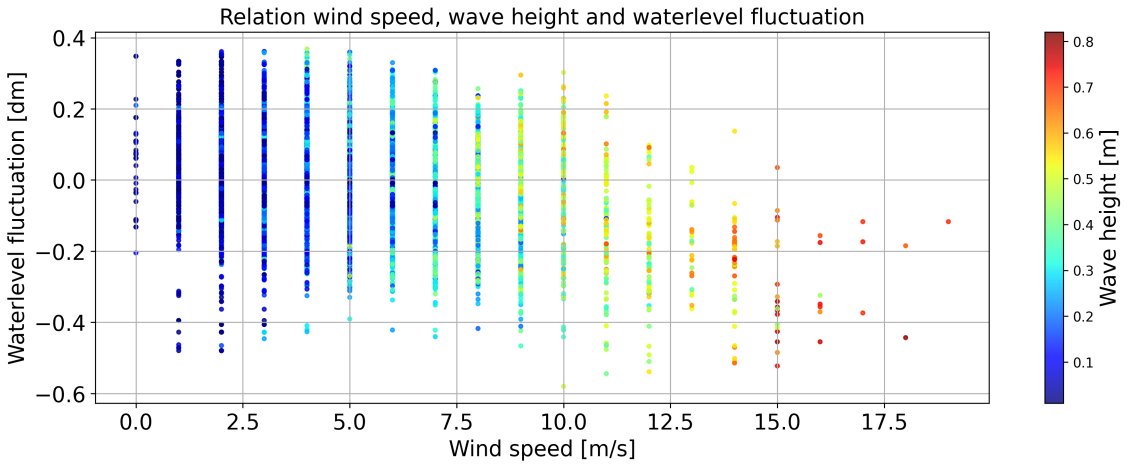

Figure 5.21: Hourly averaged wind speed in m/s plotted against the water level fluctuations (10-day average removed), the colour of the points indicates wave height in m.

5.6.3. Waves

Wave measurements were performed with an acoustic wave and current profiler (AWAC). The significant wave height (H_{m0}) will be used as indicator of wave height in the majority of this analysis, with an average of 0.19 m and a maximum recorded wave height of 0.96 m. The wave rose, figure 5.22, is constructed from the full period of measurements shows most waves come from the southeast, this does not directly align with the origin of dominant winds.

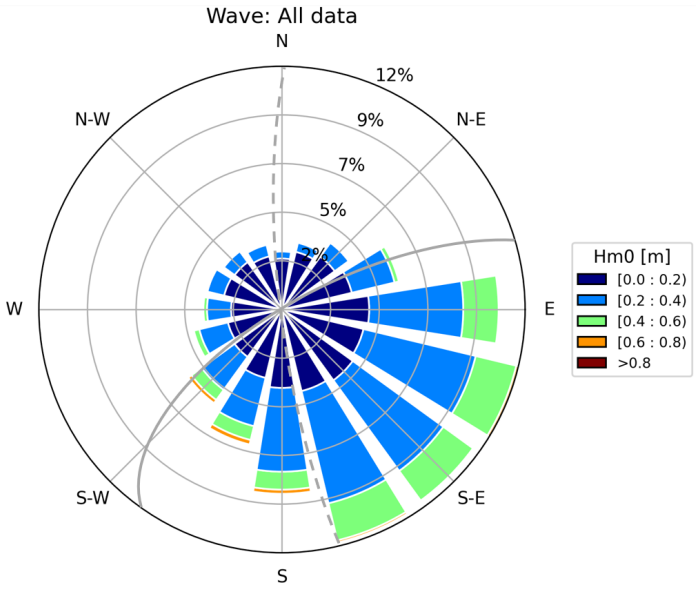

Figure 5.22: Wave rose of direction (coming from) and according significant wave heights for the wave climate at the buoy just offshore of the Oeverdijk. The dashed grey line represents the orientation of the southern cell, the full grey line that of the middle cell.

Waves as a result of wind at shore normal incidence, for both the middle and southern cell, are never extremes and barely reach wave heights above 0.6 m (see figure 5.23. When analysing wind speed, wind direction and water level fluctuation, higher wind speeds correlate to a wind direction between 200° and 300°, roughly from southwest to northwest, and higher wind speeds also correlate to increased set-down. Whether wind direction or wind speed are the determining factor for the occurrence of set-down can not be defined.

Where the wind direction corresponding to the highest wave heights was in the range of 200-300°, the resulting high waves show to be coming from a range in the order of 150-250°. This means the

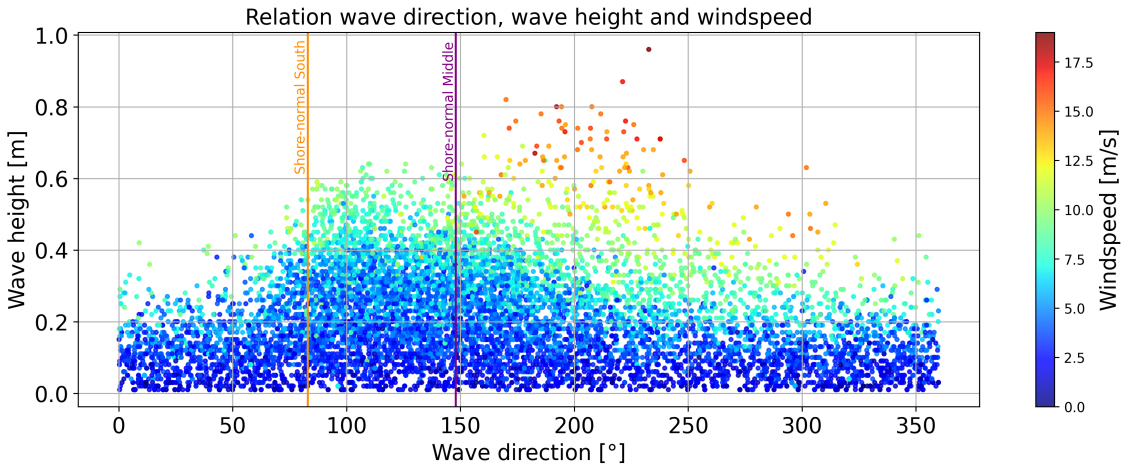

Figure 5.23: Significant wave height in m, plotted against the simultaneous wave direction (coming from), the colour of the points indicates wind speed in m/s.

incoming direction of the highest waves, in addition to the incoming direction of the majority of the waves (80-180°), is much closer to a shore-normal-incidence for the middle cell than for the southern cell.

5.7. Hydrodynamic variation in time

Forcing by wind, in terms of strength and direction, and the resulting waves, water level set-up and currents, vary over time. High energy events can have significant impact on rates of morphological change around the waterline. Through a peak-over-threshold analysis based on significant wave heights, 41 peak events (visualised in figure 5.24) are signalled in the analysed period. These peak events show a significant wave height of over 0.5 m, the peak prominence is at least 0.3m and the peak duration at 45% from the top is at least 5 hours. These demands are based on a combination of literature (Vila-Concejo et al. 2020, Ton et al. 2020, Wellen 2021) to select relevant peaks for the local climate whilst also facilitating comparisons to similar systems.

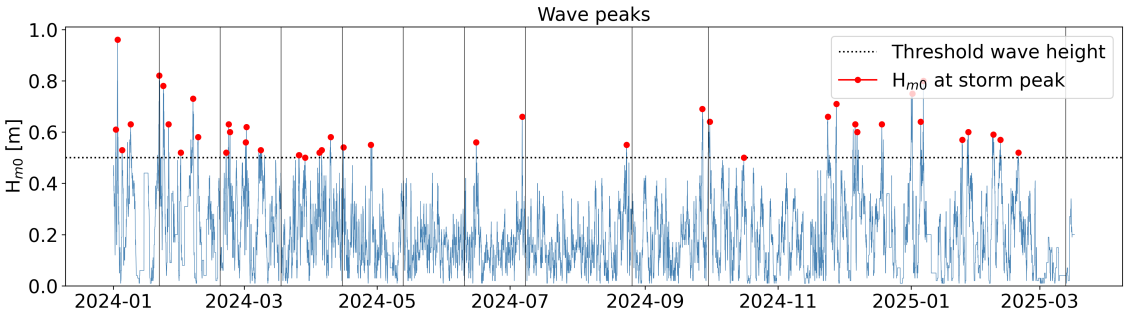

Figure 5.24: Significant wave height in time, where peaks that live up to the three storm demands are marked. Vertical black lines indicate the moments of surveying expeditions.

The time interval between surveying expeditions varies from roughly 4 weeks, to more than 20. This time scale differs significantly from the time scale of peak impact storm events, so aligning the impact of such peak events with morphological change that was observed, is very difficult. However, some characteristics that reflect the overall conditions of an interval between surveying expeditions can provide insights into what hydrodynamics shaped the coastline in that period. Table 3.1 shows, for example, that interval 9 shows a relatively low average wind speed at 4.60 m/s, yet saw a record number of 15 storms. Generally, intervals with more stormy periods show higher wind speeds (peaks above 15 m/s so a higher average), and those higher wind steeds come from a south to western angle. Calmer conditions show a broader range in wind directions. Overall, intervals 1, 2, and 9 have displayed the

most energetic conditions, where interval 5 is the most mild. This aligns with general summer-winter expectations.

Interval	Avg Wave Height (m)	Avg Wind Speed (m/s)	Avg Wind Dir (°)	Peak Count	Avg Peak Height (m)	Avg Peak Dir (°)
1	0.26	6.39	199	6	0.68	222
2	0.26	5.49	141	6	0.58	179
3	0.23	5.46	174	6	0.53	185
4	0.17	4.67	147	2	0.55	199
5	0.16	4.22	153	0	-	-
6	0.16	4.42	165	2	0.61	230
7	0.16	4.00	165	1	0.55	221
8	0.18	3.99	135	1	0.69	212
9	0.20	4.60	121	15	0.63	164

Table 5.3: Summary of environmental conditions and wave peaks over 9 time intervals

5.8. Hydrodynamics: Delft3D modelling output analysis

To focus on the development of waves, and the wind induced (nearshore) currents that form as a result, some idealised wind schematisations are put through a Delft3D run. The focus is on runs with a singular wind speed (15 m/s) and direction that were simulated over 24 hours. Hydrodynamic processes require a few hours to respond to forcing, so a full day is enough time for this response to form, without requiring too much computational time. The used wind speed, 15 m/s, is relatively strong, so that the effect of this wind direction can be clearly analysed. However, the uncommon strength and duration of the wind must be kept in mind when analysing results. Runs were executed with wind coming from 0°, 45°, 90°, 135°, 180°, 225°, 270° and 315° relative to north. This covers the (roughly) shore-normal-incidence onto the southern cell (90° to 83°) and middle cell (135° to 148°), as well as the main wind direction from the Berkhout KNMI station in data analysis (225°).

The coarse-grid, full lake runs primarily show that either a clockwise or anti-clockwise circulation can occur in the Hoornse Hop bay, at the Oeverdijk. The large grid size means very little precise local information is available, in addition to the effect of local bathymetry and breakwaters not being taken into account. The only assumption these runs do confirm is that flow velocities in the middle of the circulation cell at Hoornse Hop are very low, averaging at 0.1 m/s, aligning with the buoy observations and suggesting current measurements of the buoy are indeed not useful for analysing nearshore flow patterns. Therefore, only results of the fine-grid will be presented here.

Bed shear stress output, at the end of the simulated day, has been plotted spatially for all eight wind directions in figure 5.25. All grid points with a resulting bed shear stress of 0 have been made grey, to put focus on areas with sediment transport potential. Delft3D calculates bed shear stress including both current and wave induced shear stress, so these values incorporate the effect of flow speed and wave height in near shore locations, providing an all-round impression of sediment transport potential. Furthermore, bed shear stress is plotted in figure 5.25 as a magnitude instead of a vector for simplicity. Generally speaking, the longshore direction of the shear stress aligns with the dominant wind direction.

Based on figure 2.1, a rough indication of critical bed shear stress required for sediment transport can be calculated. Using ρ_s = 2650 kg/m^3, ρ = 1000 kg/m^3, D = 0.2 mm, ν = 1.25 x 10$^{-}6$, and g = 9.81, yields a critical bed shear stress of roughly 0.2 N/m^2. This means that certain wind directions most likely yield no transport for certain beach sections. For example, western and eastern winds (270° and 90°) create virtually no bed shear stress on the southern cell, suggesting little to no long-shore transport there under those circumstances. A similar effect is observed for shore-normal winds on the middle cell. However, the curved orientation of that cell means the effect is only observed for parts of the cell at a time, such as the northern edge of the middle cell for northern wind.

Winds from the north or the south (0° and 180°) are responsible for relatively high rates of bed shear stress along the southern cell, up to 0.6 N/m^2, indicating potential for sediment transport. This is to be expected, considering the roughly parallel shoreline orientation of the cell. Western and eastern winds

(270° and 90°) are responsible for strong bed shear stress in the middle cell, also reaching 0.6 N/m^2. However, winds from the north occur for less than 4% of the time, and fail to reach above 5 m/s (see figure 5.19). Eastern winds can reach speeds of 10 m/s, but still make up less than 7% of the time. Therefore, no significant impact of the flow patterns from those directions, is expected.

The strongest winds that realistically occur (see figure 5.19), come from a south to west range. The associated current patterns for those wind directions show a dominant long-shore direction of flow and bed shear stress: northward directed in both the southern and middle cell. Transport potential is highest in the southern cell for southern winds (bed shear stress above 0.4 N/m^2), and highest along the middle cell for south-western winds (bed shear stress above 0.5 N/m^2). Generally speaking, the southern half of the southern cell experiences stronger magnitudes of bed shear stress for all wind directions between 135° and 270°, with a slight exception for 225°. The middle cell experiences its peak bed shear stress magnitude at various longshore locations, depending on originating wind direction.

Significant bed shear stress at the outward-directed edge of the middle cell, along its northern breakwater, is also noticeable. For winds from 225° and 270°, the bed shear stress remains 0.2 N/m^2 or higher along the edge, peaking at 0.5 N/m^2 at the edge of the breakwater. Although it is not unlikely for significant flow speeds, and bed shear stresses, to occur for flows around a breakwater edge, it should be noted that this continued path of shear stress from the nearshore edge out to the breakwater tip is not observed along the southern cell breakwaters.

Finally, it is noticeable that the bed shear stress over the largest part of the lake bottom is not necessarily 0. However, the bed shear stress there does not show to reach above 0.1 N/m^2 for any wind direction, despite the relatively high wind speeds over an entire day. The areas of a bed shear stress of absolute 0 strengthen the suggestion that the lake bottom therefore has virtually no potential for significant sediment transport.

5.9. Hydrodynamics: Concluding remarks

To summarise, hydrodynamic forcing at the Oeverdijk is dominated by the local wind climate. Variations in direction and strength of these winds yields variations in wave height, wave direction, and local water level set-down, specifically during high-energy events. Seasonal variation in forcing is observed, both in average conditions (for example, average wave height per interval varies between 0.16 and 0.26m) and the number (0 to 15) of storm-events observed in those intervals. Delft3D modelling, although limited, confirms the presence of spatially variable alongshore currents and highlights the need to account for local bathymetry and shoreline orientation when interpreting hydrodynamic drivers. Southern winds are common, yielding significant bed shear stresses for the southern cell, whilst western (and eastern, although less common) winds yield most significant bed shear stresses in the middle cell. Wind from the south-western range right in the middle, of 200° to 250°, has the highest wind speeds (up to 17 m/s) and resulting highest waves (up to 1.0 m).

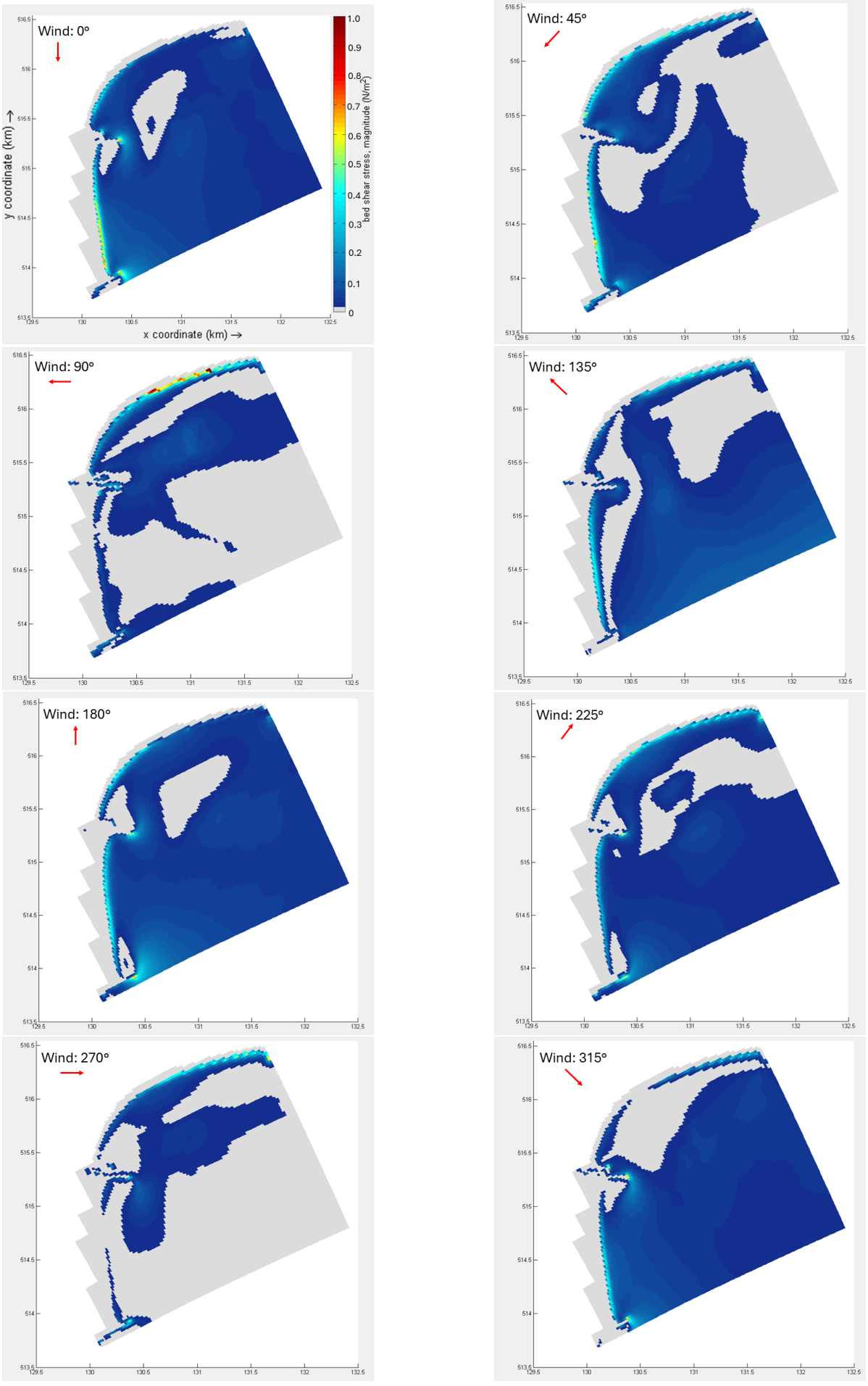

Figure 5.25: Magnitude of bed shear stress as a result of wind from a single indicated direction, for an entire day, at 15 m/s. Colour bar and axis label are uniform for all plots. Grey areas represent 0.

6

Link: Coupling morphology to hydrodynamics

In order to explain the observed local morphology using local hydrodynamics, a link between the two must be established. This chapter looks at potential for these explanatory links, both qualitative and quantitatively, by comparing the results of data analysis from different angles. First, an analysis is sought in cross-shore direction, analysing morphology and hydrodynamics on a time series, to detect patterns in time. Then, the statistical relationship between hydrodynamic characteristics and the different sections of the cross shore profile is analysed. In long shore direction, the CERC formula (see equation 2.5) is applied, to compare theory to observed transport signals and provide some insight into the likelihood of the observed long-shore transport quantities. Finally, measured local wind signals are used as driving force input for the nested Delft3D model, to analyse if and how modelled flow patterns match and explain the large-scale long-shore transport observations.

6.1. Combined data analysis: Cross-shore

6.1.1. Forcing and normalised volume changes on (interval) time series

The surveying expeditions mean morphological data is available at specific intervals. Hydrodynamic data is available in much smaller time increments (e.g. hourly), so the morphological data intervals are the limiting factor in windows of comparison. As wind is the main source of energy in this system, responsible for most wave and current action that leads to morphological change, the hypothesis is that a correlation exists between available hydrodynamic energy and morphology. Furthermore, the 95th percentile wave height was suggested to be a sediment transport indicatory by Ton (2023). Those two quantities are plotted on an interval time series against morphological change (indicated by normalised volume change, so m^3 / long-shore coastline meter / week) for both cells, in figure 6.1.

From a first look at total volume changes (grey planes in top panels), a very strong signal is not evident. This might be the result of some outlying offshore measurements. Therefore, the combined morphological change of beach and platform is also plotted, visualised by the black outlines. Those sections show somewhat of a pattern: a positive slope between intervals 1 and 3 (middle cell) or 4 (south cell). This positive slope indicates decreased rates of erosion. Following that, a period of steady or slightly increasing erosion is observed for periods 5 through 8. The strength of this signal varies per step, and is not strictly consistent. Finally, the middle cell still sees a high rate of erosion in interval 9, whilst the southern cell sees a drop to a much lower rate of erosion.

Hydrodynamically speaking, periods of higher and lower incoming wave energy can be clearly identified. Interval 1 to 5 shows a clear decrease in both 95th percentile wave height, and available wave energy. Intervals 5, 6 and 7 are specifically low-energy and look quite steady. When looking on a large scale however, intervals 5, 6 and 7 are part of a general trend of increasing wave height and energy from period 5 to 9. This expected pattern of decrease and increase aligns well with the expected seasonal variability: high energy in winter months such as February and December, against lower waves and calmer periods in June and July. It should be noted that interval 9 has a relatively low available wave energy compared to interval 1 for example, despite both intervals covering a stormy February and interval 9 experiencing the highest number of peaks of any interval (see Table 5.3). Likely, this is the result of interval 9 covering a much larger period, therefore reflecting more 'averaged' conditions.

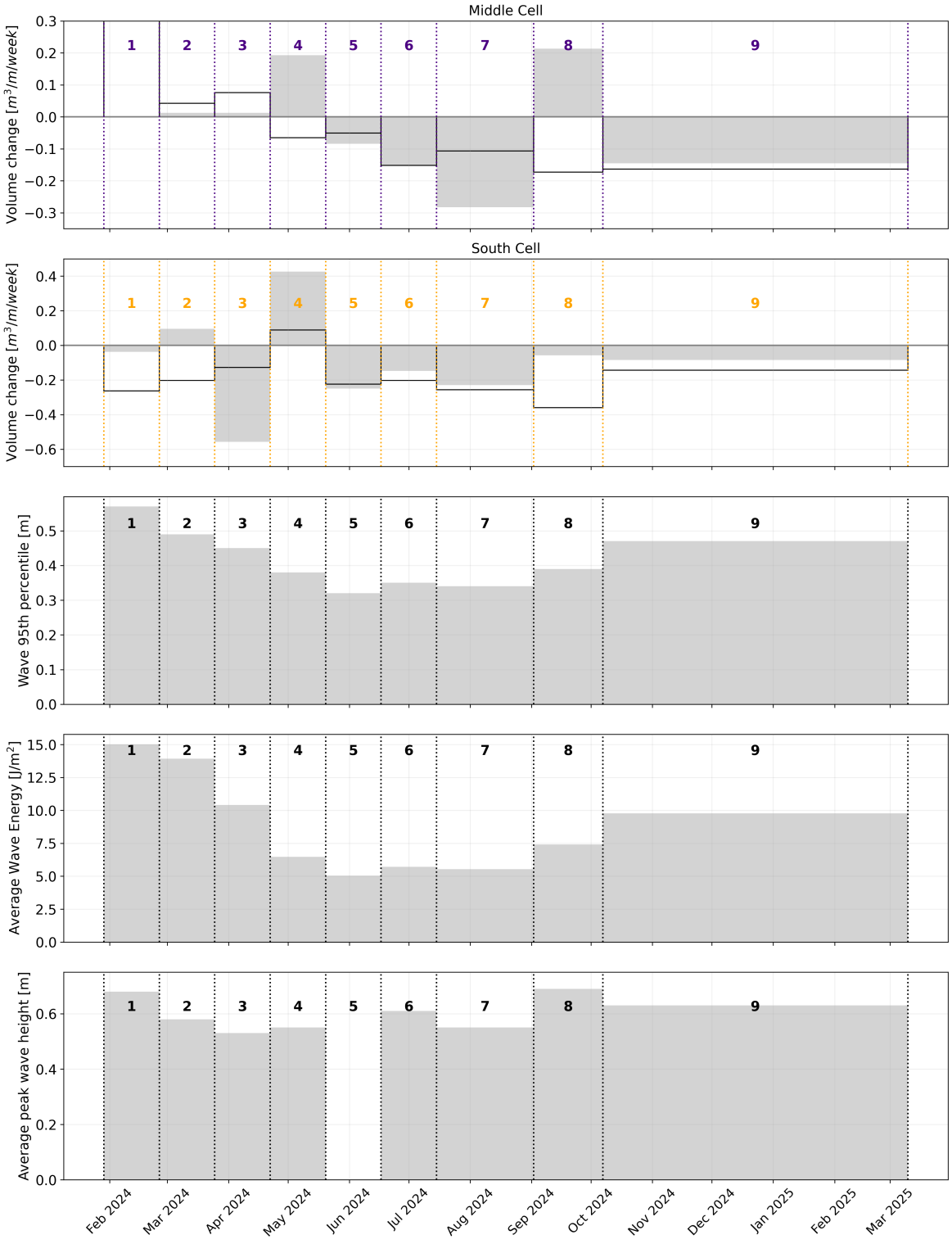

Figure 6.1: Time series over the surveying intervals plotting total normalised volume change [m^3/m/week] over time in the top panels for middle and south cell. The black outlines indicate the combined results of the beach and platform sections only, shaded grey is the entire cell (including offshore). The morphologic change of interval 1 of the middle cell is excluded. The three bottom panels plot 95th percentile wave height, average wave energy arriving, and the average wave height of storm peaks identified in Section 6.2.

When looking at the graphs in figure 6.1 (specifically the combined beach and platform morphology) in terms of a trend, the above suggests alignment with expectations: decreased rates of erosion over

the first half of the year, along with decreasing forcing. Then, a more slight increase in erosion, aligned with a more slight increase in forcing. Interval 4 appears to be a tipping point, yielding erosion in the middle cell and sedimentation in the southern cell. Interval 9 is also a slight outsider, especially for the southern cell. This is not completely unexpected considering the large period of time caught in that interval, averaging out a possible signal. However, when looking at the absolute values of erosion and sedimentation (for beach and platform), the results are less self-explanatory. For example, the southern cell shows very similar absolute rates of erosion for intervals 1 and 8, in addition to intervals 2 and 5, even though those duo intervals experience very different wave forcing. Intervals 1 and 8 show similar average peak wave heights that could indicate similar erosion rates during the intervals. This explanation does not hold up for the similarities in erosion between intervals 2 and 5. Additionally, the middle cell experiences no erosion over the first three (high energy) intervals, only sedimentation, despite the positive slope.

6.1.2. Correlation calculations between forcing and volume change

The graphic analysis of hydrodynamic drivers and morphological change shows general relationships between the two. To quantify these, values of hydrodynamic drivers are correlated against normalised volume changes over vertical sections. Pearson (PCC) and Spearman (SCC) coefficients, along with associated p-values, are calculated, as linear assumptions may offer initial insights into a relationship, but the expectation is that most drivers do not scale linearly with morphology. Correlations use 9 data points for the southern cell and 8 for the middle (first interval removed due to beach works). The interval without peaks is excluded from analyses correlating peak wave height and wind direction. Appendix E lists all correlations; only key findings are discussed in this section of the report. A PCC or SCC of 1 indicates perfect linear or rank correlation. A p-value below 0.05 is typically considered statistically significant.

Few strong relationships exist between drivers and total volume change. For both cells, the strongest correlations are observed between both average 95th percentile wave height (south: p = 0.24, 0.19; middle: p = 0.26, 0.32 respectively) and volume change, with all SCC values nearing 0.45. A relationship between wave height and morphologt is expected. However, this suggests higher waves result in more sedimentation, contrary to expected erosion under high energy. This may be the result of conflicting signals across the three vertical sections interacting, especially given the atypical offshore influence (see figure 6.1). Section-specific correlations follow in subsequent paragraphs.

In non-tidal, low-energy systems, storm events are expected to largely drive morphology. Therefore, a correlation is expected between average wave height across the peaks, where higher peaks lead to more significant sediment transport. For reference, a visualisation of this 'storm peak height', and how it is calculated, is presented in Appendix F. Accordingly, average wave height across peaks correlates with volume change: negatively for beach/platform (erosion), positively offshore (sedimentation). Trends persist in the middle cell despite less clear cumulative volume change (see figure 5.9). For the southern cell, SCC values for beach, platform and offshore morphology against peak average wave height are -0.21, -0.60, and 0.26 (p-values of 0.61, 0.12, 0.53); middle: -0.39, -0.32, 0.29 (p-values of 0.38, 0.48, 0.53). Despite not being statistically significant, these p-values are relatively low compared to other correlations. No clear relationship exists between volume change and number of peaks, suggesting that the intensity of peak events may more influential on local morphological change than the frequency of peaks.

A few statistically significant relationships appear. The strongest is average water level fluctuation vs. southern cell platform change (SCC = 0.80, p = 0.01), implying sedimentation with water level set-up, or more likely, erosion with set-down. As figure 5.21 shows, stronger winds yield increased set-down at the Oeverdijk, moving the waterline down towards the platform and likely increasing erosion there. In the middle cell, this correlation is weak (SCC = -0.19, p = 0.65). Another statistically significant correlation is the one between average peak wind direction and southern platform volume change (SCC = -0.88, p = 0.00). In this case, the average wind directions during a storm peak (see Table 5.3) range from 164° to 222°, so roughly south-south-eastern to south-western winds. The SCC value for the correlation is -0.88, suggesting more erosion for a higher wind angle in that range.

Other correlations are largely absent: p-values are mostly larger than 0.3, with many coefficients near 0. Both cells show similarly weak correlations overall, though the southern cell shows stronger links

to peak characteristics. This can indicate the southern cell being influenced by storm events more strongly. However, this also includes a correlation to the average wind direction during those storms, which varies more significantly compared to the orientation of the southern cell than that of the middle cell. From the storms whose wind directions that make up the averages in Table 5.3, only four storms had eastern winds (two in interval 9), possibly explaining the low erosion in that interval despite high wave energy (figure 6.1). However, data is insufficient to confirm this theory, but it does highlight the importance of considering wind as a vector in the wind-wave-sediment system. Therefore, next steps in this chapter will (amongst other things) look at the nearshore currents forming as a result of wind forcing, through modelling output.

6.2. Extended data analysis: Long-shore

6.2.1. Theoretical sediment transport: CERC formula

The cross-shore morphology follows expectations as a result of existing literature, with a steep waterline slope and underwater plateau developing as predicted. However, confirming longshore transport against theory is harder due to its high dependence on local orientation and clime. To estimate wave-driven transport in Hoornse Hop, the CERC formula is applied using the local wave climate (see full climate in Appendix B), resulting in figure 6.2). Waves are assumed to approach from the southeast (135°), based on analysed buoy data (figure 5.22). When using the incoming angle relative to shore-normal angles (figure 5.18), the middle cell is oriented at 58° and the southern cell at -7°, corresponding to transport rates of 9924 m³/year southward and 14548 m³/year northward, respectively. This aligns with morphological findings: stronger erosion in the southern cell, with transport patterns reversed between the two.

The southern cell's uniform orientation implies the theoretical rate (14548 m³/year) applies consistently along its length, and does not change greatly for a small orientation or shift on the graph. Observed erosion over the analysed period (1 year and 4 months) totals 12875 m³/year, but comparing this to the CERC value only holds if all sediment moves across a single cross-section. This would only be possible at the point 1200m alongshore, where erosion shifts to deposition (see figure 5.14). Since little material accumulates beyond that point, much of the difference in volume is likely lost offshore, indicating actual longshore transport is far lower than CERC suggests. The discrepancy likely stems from CERC's simplifications. It omits key influences like breakwaters, profile and sediment characteristics, and wind-driven system-scale currents. Therefore, comparing observed transport rates to calculations based on a single driving source does not make for a fair comparison here.

The middle cell's curvature makes its transport harder to capture with a single orientation. Its southern end aligns with the southern cell (-5°), while the northern end turns to 70°, implying a transport reversal across the cell. While the CERC formula estimate (9924 m³/year) roughly matches observed erosion (8826 m³/year), this observed eroded volume is distributed across the entire cell, enclosed by breakwaters on either end. Therefore, no single cross-section sees this entire volume pass, making it likely that the CERC overestimates transport here too. This long-shore direction reversal hints at opposing currents converging near the cell center, meaning more significant deposition is expected there. However, observed deposition in the middle of the middle cell is limited. Hence, it is likely that the CERC formula fails to capture exact longshore transport patterns quantitatively, but does provide a good indication of possible patterns qualitatively.

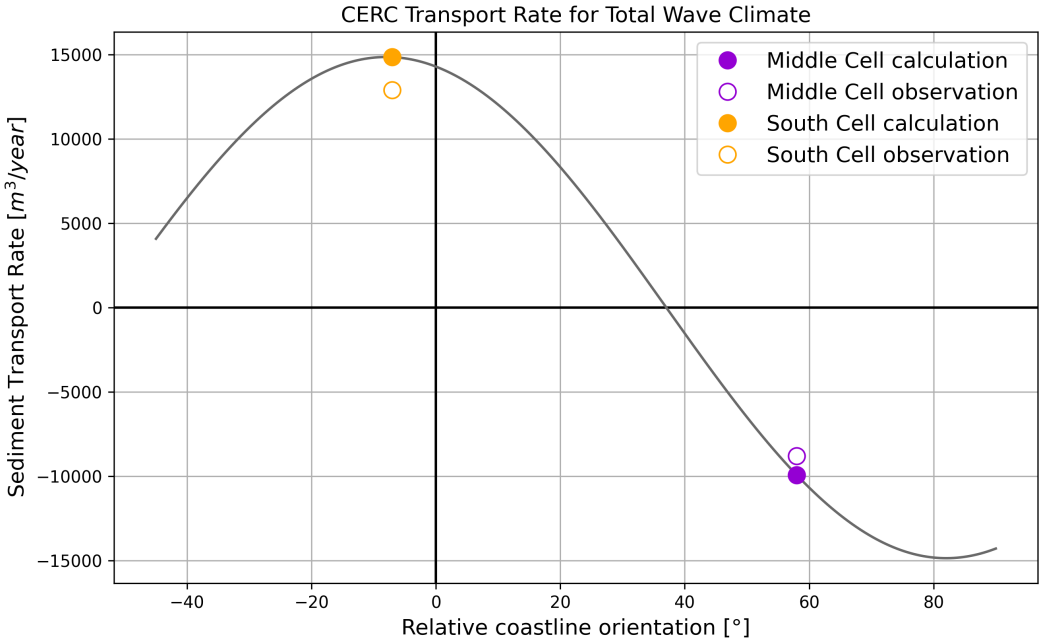

Figure 6.2: Sediment transport rates according to the CERC formula (calculation), against relative coastline orientation to North (0°). The observation data points are based on the integration of the the sediment budget plots in figures 5.13 and 5.14, to yield a total eroded volume over the year.

6.2.2. General long-shore signals: what do we (not) know

In long-shore direction the observations differ per cell, but in both cases data suggests longshore sediment transport, due to a long-shore gradient in the sediment gain / loss. This is also confirmed by the CERC formula calculations. The southern cell displays a clear trend of most erosion at the southern end, decreasing in magnitude towards a smaller section of deposition at the northern end. The dominant wind and wave conditions, with dominating southern winds and southeastern waves, mean waves coming in at an angle to the beach and generate a nearshore, northward directed longshore current that can yield this transport signal. These conditions occur for a large part of the time, considering the local wave roses in figure 5.22, making the observed northward directed longshore transport pattern at the southern cell very likely. The breakwater at the northern end of the cell can (partially) halt this longshore current, slowing down the flow to decrease sediment carrying capacity of the current and resulting in deposition there. However, this transport pattern has not been confirmed for low-energy calculations (only by the 15 m/s indicatory runs) and the net sediment loss over the entire cell is not explained by this pattern, under the assumption of no by pass around either breakwater.

The middle cell displays a more complex pattern of longshore erosion. The northern edge experiences the highest rate of erosion, and there are virtually no areas of significant deposition. This pattern initially suggests longshore sediment transport from north to south, reverse to the southern cell. However, most waves arrive at this beach section roughly shore-normal, with a few higher waves coming from a south-southwestern direction. This suggests northward directed currents instead. Furthermore, the middle of the middle cell experiences slight deposition, specifically during calmer summer months. This can be the result of a cross-shore process, as discussed in the literature of Chapter 2. In that case, shorter, calmer waves that arrive at shore-normal incidence can work to rebuild a coastline through onshore directed transport. Simultaneously, this sedimentation can be the result of reverse long-shore transport trajectories, where two sections of nearshore currents are directed towards the middle of the cell where they meet, (partially) cancelling eachother's flow velocity and resulting in a sediment drop. Essentially, wind and wave analyses only do not provide a clear explanation for this cell's erosion pattern and more information on nearshore hydrodynamic variation is required.

6.2.3. Modelling long-shore sediment transport (Delft3D)

In cross-shore direction, the available data allows for a more logical connection between forcing and morphology, than is possible in long-shore direction. Therefore the Delft3D model of the Markermeer, previously used to gain insight into flow patterns and sediment transport potential, is used here to simulate nearshore flows based on real-life wind patterns in an attempt to fill knowledge gaps. Output data collected at nearshore points along the coastline of the middle and southern cell is analysed to match observed long-shore transport signals to hydrodynamic driving forces.

Storm and calm weeks

First, one stormy week at the end of January 2024 (in which three storms with a south-western wind occur, wind speeds above 17 m/s) and one calm week in May 2025 (no storms, includes winds from the north and east, maximum wind speed of 7 m/s) were modelled to gain some insight into the possibilities of this modelling strategy. The aim of modelling these weeks is to reflect the impact of high-energy south-western storm events, and of low-energy wind scenarios from various other directions

Figure 6.3 shows a histogram of observed bed shear stresses during the week runs of both stormy and calm conditions. Assuming a critical bed shear stress of 0.2 N/m^2, as determined as minimum in Section 6.3.3, the model run of a stormy week shows this critical value is often exceeded, (significantly, sometimes reaching above 0.6 N/m^2), shown by the bars to the right of the dashed red line. This trend occurs along the majority of both coastlines (see Appendix G for histograms of all longshore output points). During a calm week, the critical bed shear stress is not exceeded at all, suggesting little to no transport potential during (such) calm conditions. Additionally, the direction of bed shear stress during a stormy week (with south western storms) is much more asymmetrical and predominantly northward directed. Shear stresses during a calm week show a more symmetrical distribution, as observed by the dark blue pyramid shape in figure 6.3.

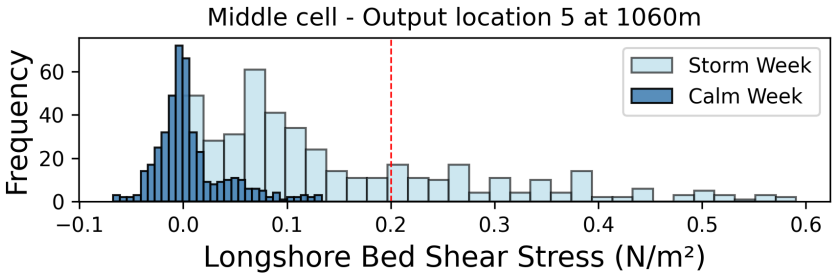

Figure 6.3: Histogram of longshore directed bed shear stress output during both high-energy (storm) and low-energy (calm) weeks, at an output point in the middle of the middle cell. Positive longshore direction is northward. Red dashed line indicates critical bed shear stress for sediment transport.

Bed shear stress gradient as transport indicator

The goal of this modelling is to see if modelled nearshore hydrodynamics can explain observed morphological development. For this, the gradient in time integrated bed shear stress can be used, in combination with the assumption that this bed shear stress is primarily northward directed for storm data output, to predict areas of potential sediment transport. Integrated bed shear stress is used instead of a peak value, as the integration over time provides a more cumulative insight into sediment transport potential. Erosional patterns are also a cumulative process. A positive gradient indicates increasing potential for sediment transport, suggesting more sediment may be picked up, leading to erosion. The opposite effect suggests deposition. Figures 6.4 and 6.7 plot the modelled gradients against observed cumulative volume change over the longshore of both cells. To make comparison easier, a positive upward gradient (indicating erosion) has been plotted against positive eroded volume, so that graphical alignment means expectations are confirmed.

For analysis of the middle cell, it must be kept in mind that it is possible that the third longshore output point, and therefore second gradient bar from the south, is the result of anomalous model output, possibly as a result of choosing an observation grid cell that is too close to dry land. The middle cell (see figure 6.4) shows some alignment between modelled and observed erosion at the southern edge, and around the 750m longshore marker. The southern edge of this cell (0 - 400m) should, based on

bed shear stress gradients, be eroding. That matches observations. However, significant deposition is modelled near 500m but not observed, potentially due to the anomalous model output. Significant contradiction between modelled and measured data occurs in the northern half of the middle cell, where model output suggests increased deposition from the middle towards the northern breakwater, yet observations show increased rates of erosion towards the northern breakwater. It is likely that either longshore currents are at play here that are not accurately modelled, or there is a significant impact of cross-shore sediment transport. Cross-shore processes are not accounted for in this modelling approach.

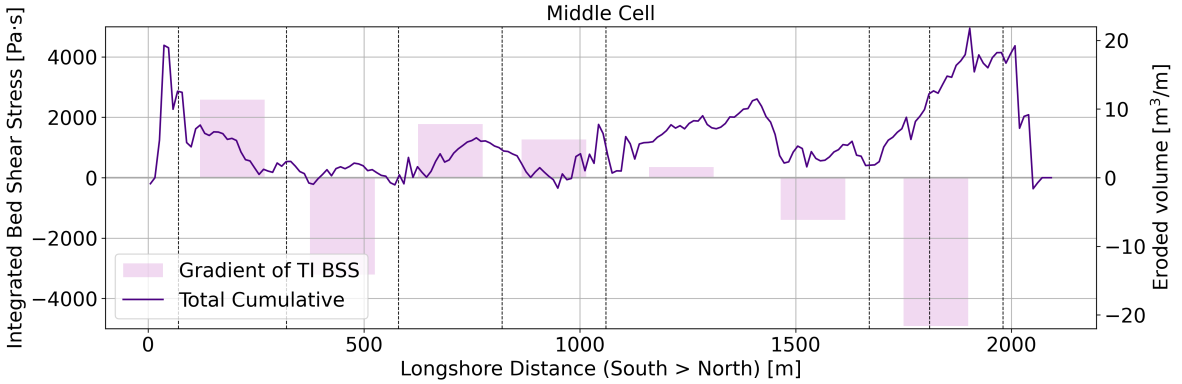

Figure 6.4: Gradient of time integrated bed shear stress over the longshore, against cumulative eroded sediment volume over the entire analysed period for the middle cell. Vertical dashed black lines indicate longshore positions of data output points.

The model output is also split and accumulated per interval, and plotted against observed morphological change over the interval (non-cumulatively) in figure 6.5, for the middle cell. This allows for an analysis at a smaller time scale. The running average volume change over 10m long-shore has been plotted here to smooth out the signal and enable a simpler comparison to the gradients bars. What is obvious here, too, is the clear mismatch between modelled sedimentation in the northern edge of the cell, against observed erosion during virtually all intervals. Overall, intervals 5, 7 and 8 show no clear longshore trend. Intervals 2 and 3 show a trend of decreasing erosion over the southern half of the cell, matching a similarly modelled trend when looking for very rough trend lines. This suggests erosion at the southern edge of the cell may be largely storm-driven. Contrastingly, intervals 4, 6, and 9 (of which 4 and 6 are clearly lower energy intervals) show an observed trend of increasing erosion from south to north, despite a clearly opposite modelled expectation. It is possible that this mismatch is a result of cross-shore processes that are not modelled.

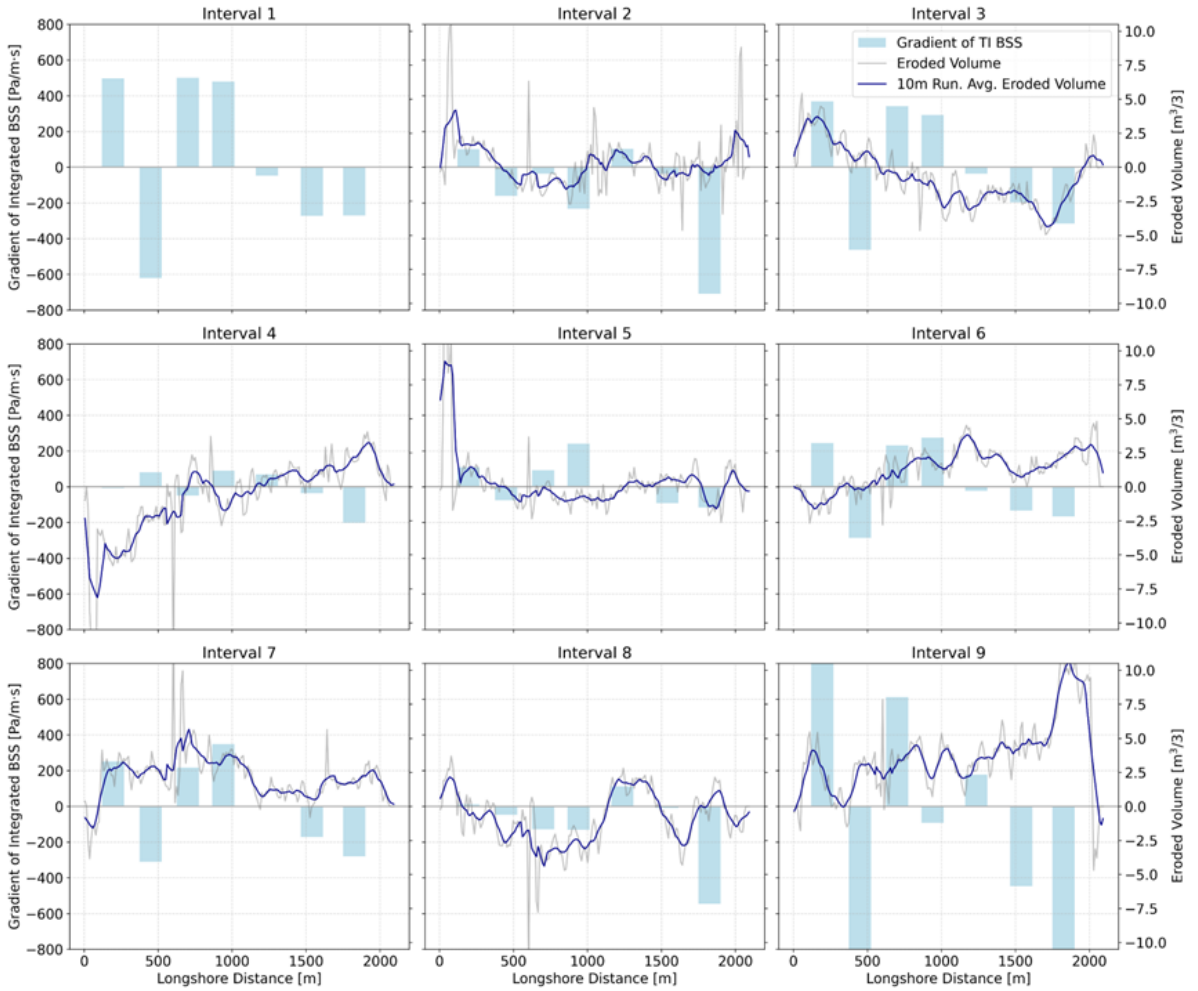

Figure 6.5: Plots of the gradient of time integrated bed shear stress between longshore model output points, against observed non-cumulative longshore volume change, per interval, for the middle cell. The grey line indicates direct bathymetry data output, the blue line plots a running average to simplify comparison of the graphs.

Taking into account earlier modelling output, the idea exists that the longshore current of the middle cell might bend around underneath the northern breakwater, jetting offshore, instead of coming to a halt. This could take (suspended) sediment with it. Therefore, an additional output point near the offshore edge of the northern breakwater bordering the middle cell, is modelled. This point is further offshore than the other modelled points, on the 'inside' edge of the breakwater. See figure 6.6 for a simple schematisation of where these observation points are. This offshore point shows longshore velocity and bed shear stress magnitudes in line with other longshore points, with the longshore direction being point offshore, parallel to the breakwater. This suggests the longshore current does not loose significant flow velocity or sediment carrying capacity as it turns the corner below the breakwater, potentially transporting eroded sediment offshore and contributing to the observed cumulative erosion over the northern half of this cell. However, that total eroded volume remains more than suggested by this modelling output.

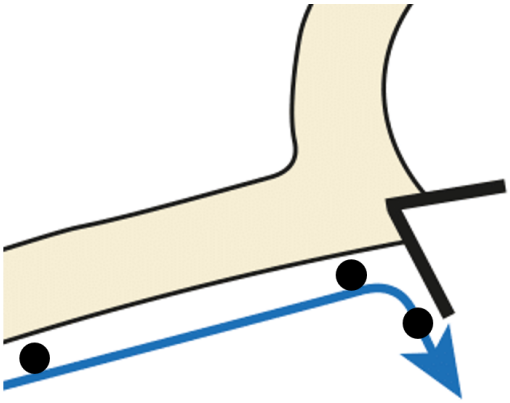

Figure 6.6: Schematisation of the three northernmost modelled longshore observation points in the middle cell; one along the shore, one along the shore in the corner of the cell and one at the inside offshore edge of the breakwater, indicated by black dots. This is not to scale. The blue arrow indicates the direction of the hypothesised nearshore current.

The southern cell (see figure 6.7) shows a more uniform modelled pattern of erosion and sedimentation, matching observations in terms of the two edges: significant sedimentation expected at the southern edge, significant deposition expected at the northern edge. The relative peak size (stronger modelled erosion than deposition in those edge zones) also aligns. However, the tilting point between erosion and sedimentation is modelled around 500m (erosion to the south of that, deposition to the north), whilst the observed tipping point lies closer to 1200m alongshore. Therefore, a large longshore section should experience deposition as suggested by modelling output, yet experiences erosion as a result of field data analysis. Additionally, the modelled erosion potential roughly balances the sedimentation potential, which does not align with the significant observed net sediment loss.

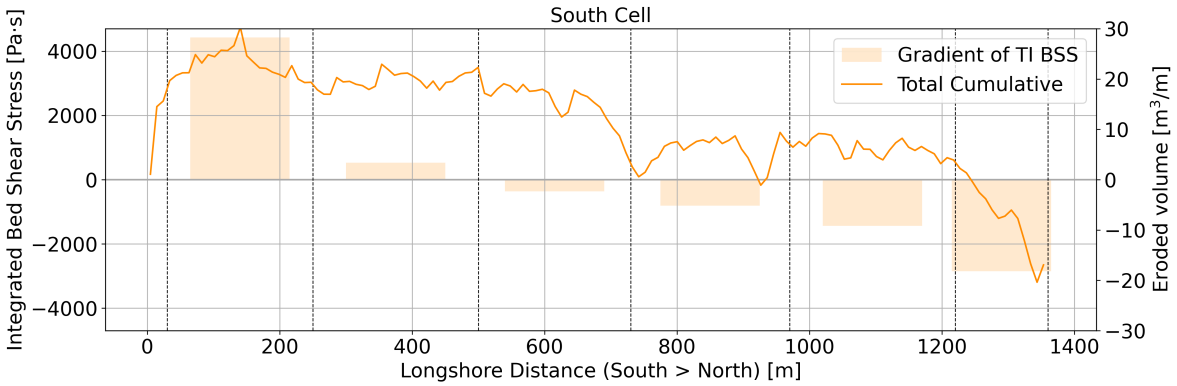

Figure 6.7: Gradient of time integrated bed shear stress over the longshore, against cumulative eroded sediment volume over the entire analysed period for the south cell. Vertical dashed black lines indicate longshore positions of data output points.

Although the observed trend in the southern cell appears uniform at first sight, this year-run signal can still be a cumulative result of contrasting processes. Therefore, integrated bed shear stress gradients are plotted against observed morphological change per interval for this cell in figure 6.8. In line with expectations, this reveals a primary signal of decreasing erosion from south to north (especially over the southern two-thirds of the cell) during intervals 1, 2, 3, 8 and 9. These also happen to be among the most energetic intervals. This matches the expected trend as a result of modelling output, although strength and erosion to sedimentation tipping points vary, with a long-shore sediment transport signal in northward direction. Intervals 4 and 5 show a different trend, with increasing erosion from south to north. This suggests a reverse long-shore transport direction, from north to south.

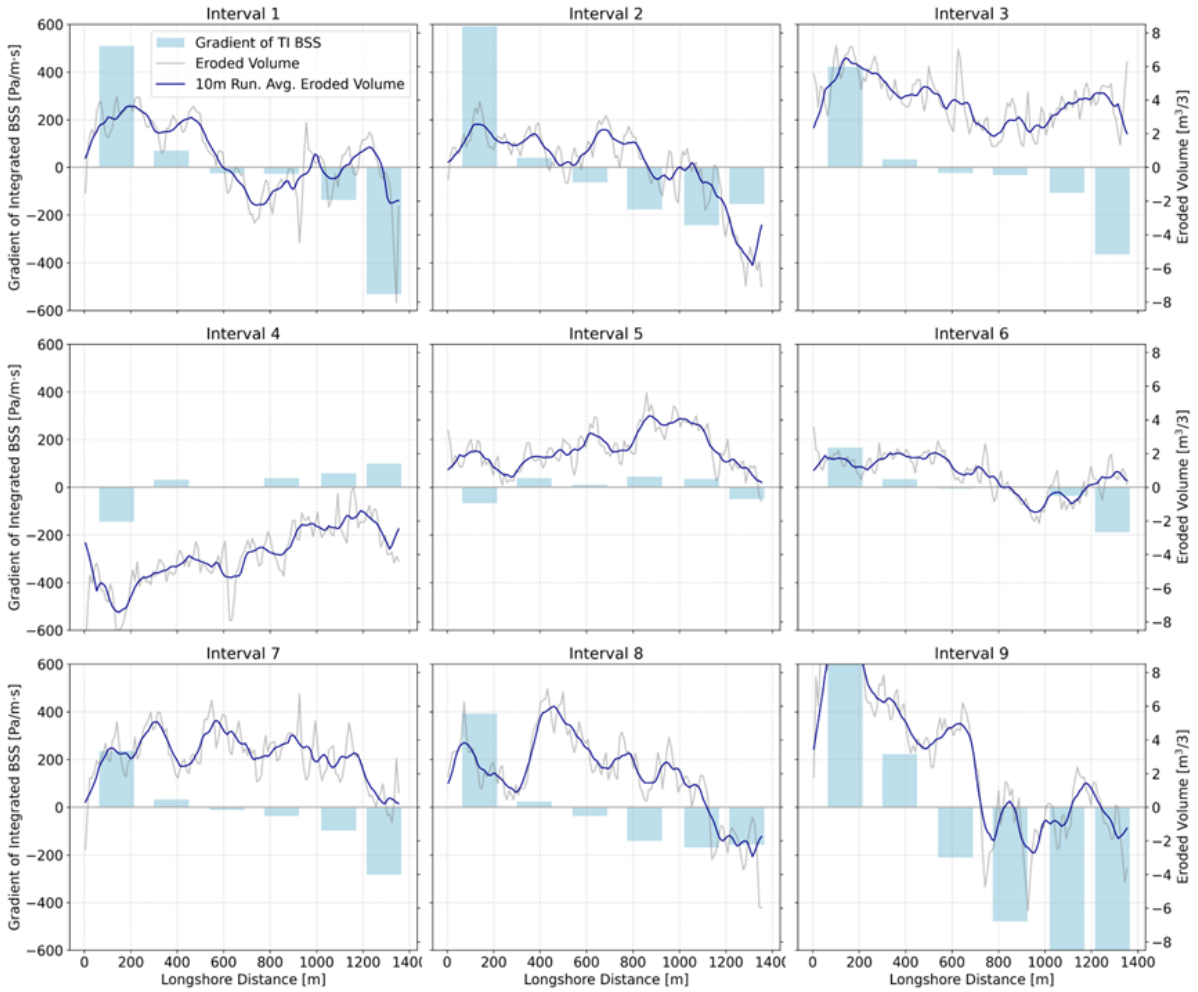

Figure 6.8: Plots of the gradient of time integrated bed shear stress between longshore model output points, against observed non-cumulative longshore volume change, per interval for the south cell. The grey line indicates direct bathymetry data output, the blue line plots a running average to simplify comparison of the graphs.

Transport in calm conditions

A final remark should be made regarding the observed transport signals, even over 'calm' intervals such as interval 5, which experienced no storm events. The originally modelled 'calm' week, based on figure 6.3, theoretically yielded no sediment transport. However, the results of, amongst others, the observed eroded volumes of interval 5, show that calm conditions can still result in (significant) sediment transport with a clear directional signal. Therefore, morphological development at this low-energy, non-tidal system is not necessarily dominated by high-energy events.

Observations made during the site visit to the Oeverdijk (specifications of the visit are in section 4.2), which took place on a specifically calm day with the water virtually flat, underline this idea that sediment transport also occurs during calm conditions. Results of very calm forcing could be observed during the visit, see figure 6.9. Sediment patterns such as this, slightly curved, small sandy hills, are likely to be flattened out by higher waves, and are therefore assumed to be a result of the calmer conditions during the visit. Mainly, the presence of this pattern suggests that even under calm conditions, some sediment transport does occur at the waterline in the middle cell.

Figure 6.9: Sedimentation patterns observed at the Oeverdijk, likely a result of very low-energy forcing, as this would be washed over and smoothed out by larger waves.

6.3. Concluding remarks

The integration of morphological and hydrodynamic datasets results in the strong indication that specific hydrodynamic drivers influence sediment transport at the Oeverdijk. Specifically, cross-shore volume changes show correlations with wave height and water level set-down, supporting the interpretation of wave energy as a primary driver of offshore directed cross-shore transport during high-energy events. In the long-shore direction, theoretical and model-based sediment transport estimates, particularly from the CERC formula and Delft3D simulations, align with observed patterns of erosion and accretion, specifically in the southern cell at the Oeverdijk. There, a clear northward directed long-shore sediment transport pattern is confirmed by both model and measurements. Morphological developments at the middle cell prove more difficult to explain, with complexities such as breakwater effects introducing uncertainty into transport predictions. This chapter reinforces that understanding morphological change in low-energy environments requires a nuanced, site-specific analysis of hydrodynamic variability and structural and bathymetric influences.

7

Interpretation: a concept system

This chapter brings all presented results (and links between them) together, to translate them into a generalised system description. This is done on two levels. The first is in cross-shore direction, presenting a way in which cross-shore results relate to expectations, and how they can perhaps be generalised for future reference and design. Following, the transport signals observed in long-shore direction are translated into scenarios as a result of their driving force: wind. These scenario's attempt to explain the basic situations that shape the current Oeverdijk coastline, in such a way that they can be applied for future morphological development predictions.

7.1. Cross-shore

7.1.1. Profile development

In the cross-shore direction, the Oeverdijk shows the literature based, expected, qualitative morphological change: a steep slope forming near the waterline and an extending underwater plateau. The waterline slope approaches 1:10, similar to Markerwadden findings and steeper than most profiles in Figure 2.2. This may be explained by those images often reflecting (small-range, but still) tidal environments that may smooth the profile. The Oeverdijk plateau depth still appears to be lowering, currently just above NAP -1 m, compared to an average waterline at NAP -0.3 m. Calculation methods for a depth of closure vary in use of H_s and T_p, but using Ton's (2021) 14-day method and buoy data, the calculated depth of closure is 0.8 m (±0.2 m). No exact waterlevel measurements for Markermeer are available, so the used water level of NAP -0.3m was based on an average of surveying expeditions. Therefore, it is possible the true average water level of the lake is closer to NAP -0.2 m. This aligns the plateau at NAP -1.0 m with Ton's (Ton et al., 2021) dynamic equilibrium theory and Hallermeier's (1980) depth of closure.

Hypsometric curves confirm the cross-shore sediment shift, with plateau growth visible through increased surface area at plateau height in both cells. Erosion is evident at the waterline and upper profile, but there is no compensating growth on the lake bottom (specificalle below NAP -2m). Though bordered by breakwaters and extending beyond the depth of closure, the sediment budget is not closed, raising questions about net sediment loss. Literature suggests possible post-nourishment sediment deposition beyond the depth of closure is possible (Jongh, 2017), yet the cross-shore volume data analysis doesn't fully support this. The middle cell shows no offshore growth, while the southern cell shows partial growth in deeper areas, suggesting some sediment crosses the DoC. Though low average flow speeds make lakebed transport seem unlikely, flows exceeding 0.15 m/s have been observed in indicatory Delft3D runs, likely due to lake-scale circulation. Dredging requirements in a southeastern shipping channel of the lake also supports the potential for deep sediment transport, implying cross-shore sediment loss into the lake may be possible (and permanent).

7.1.2. Equilibrium profile: generalisation potential

Although the Oeverdijk profiles are developing towards some clear characteristics as discussed in the previous section, an equilibrium profile has not been reached yet. Certain profiles, such as index 2 portrays in figure 5.5, have still shown large changes over the last surveyed interval. That does not indicate the profile development coming to a halt in equilibrium position. Instead, it invites the question of whether the profiles in this low-energy, non-tidal system have an equilibrium profile, and if so, at what time scale it will be reached. At the base of that question, lies the assumption that an equilibrium profile exists. Jackson et al. (2002) have reasoned low-energy beaches never reach an equilibrium. However, Ton et al. (2021) believe this should be possible for low-energy beaches under (semi-)constant hydrodynamic forcing.

The considered Oeverdijk is about 1, up to 1.5 years post-construction in the period analysed here. Markerwadden research (Ton, 2023) found profiles that still hadn't reached an equilibrium after 4 years in the same system. Extensive literature covers the general consensus that high-energy storm-events erode a coastline, and calmer periods allow the coast to undergo post-storm recovery. However, it may be the case that the very calm 'calm periods' of a low-energy, non-tidal lake environment are (sometimes) not enough to replenish a profile between storms. Following that thought, and the prior findings on profile development, it could be so that these low-energy profiles develop until the underwater plateau is large enough that virtually no wave energy (storm-event or not), reaches the waterline anymore. At that point no further erosion can take place, meaning no recovery is possible nor required anymore either. That may be the 'equilibrium' profile of such coasts.

In a broad search for an indication of the plateau width required to facilitate this equilibrium-profile idea, one could turn back to Dean's (1991) equilibrium profile. Although the shape of this profile (a smoothed curve due to the $x^{2/3}$ component), does not seem relevant for low-energy coasts, the cross-shore distance this profile takes to reach a depth of closure, might be. Using the range of A values determined at the Dutch coast, 0.055 - 0.093 (Bosboom et al., 2021), and a closure depth of 0.8 m, the offshore extent to the depth of closure varies from 55.5m to 25.2m. Considering the range and variability in possible input values for A, and d_s, and the profiles at the Oeverdijk already showing platform widths between 20-40m, compared to observations of widths in the order of 40-60m at the Markerwadden, this may not be an unreasonable estimation. Figure 7.1 provides a simple insight into the dimensions of this idea.

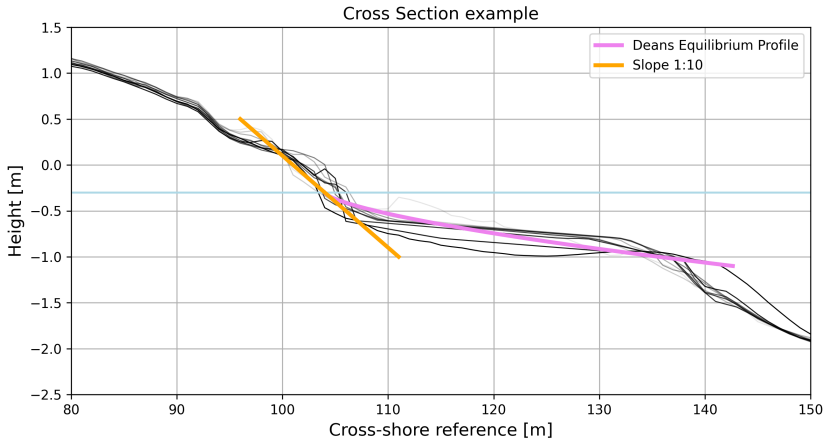

Figure 7.1: Development of an Oeverdijk profile over time, profiles becoming darker grey over time. The orange line shows a 1:10 waterline slope, the pink line reflects Dean's equilibrium profile using shape factor A = 0.07 to a depth of closure of 0.8 m below the waterline.

7.2. Long-shore

7.2.1. Scenario identification

It has become clear that the Oeverdijk, despite it's relatively sheltered location, is part of a very dynamic system, in which the strength and direction of its energy source is a relevant characteristic in explaining morphological trends. Morphological observations cannot be explained by a correlation with a single hydrodynamic factor, nor by the simplified modelling of a single time frame or direction of forcing, and require a complete system analysis. Therefore, explaining morphological development in a way that can be used to predict future developments, must be based on wind as the base of all local forcing. For this, combined insights of correlations between driving forces, morphology and system scale observations have resulted in the identification of two main scenarios that form the basis of the morphodynamics at the Oeverdijk. These scenarios are based on classified wind sections (the driving force), and their place in the range of occurring winds is visualised in figure 7.2

The identified scenarios are as follows:

- **Scenario 1:** occurs for winds from 135° - 270°. These wind directions regularly occur in combination with higher wind speeds, nearly all wind speeds above 10 m/s are recorded from within this range. This interval occurs often, representing 54% of the time.
- **Scenario 2:** occurs for winds originating from 315° - 90°. These winds generally have a lower wind speed, averaging 3.86 m/s, and only occur during 23% of the time.
- **Transitions:** The remaining two ranges (90° - 135° and 270° - 315°), are seen as transitional zones, during which the main trends in current direction and velocity from scenario 1 and 2 are switching.

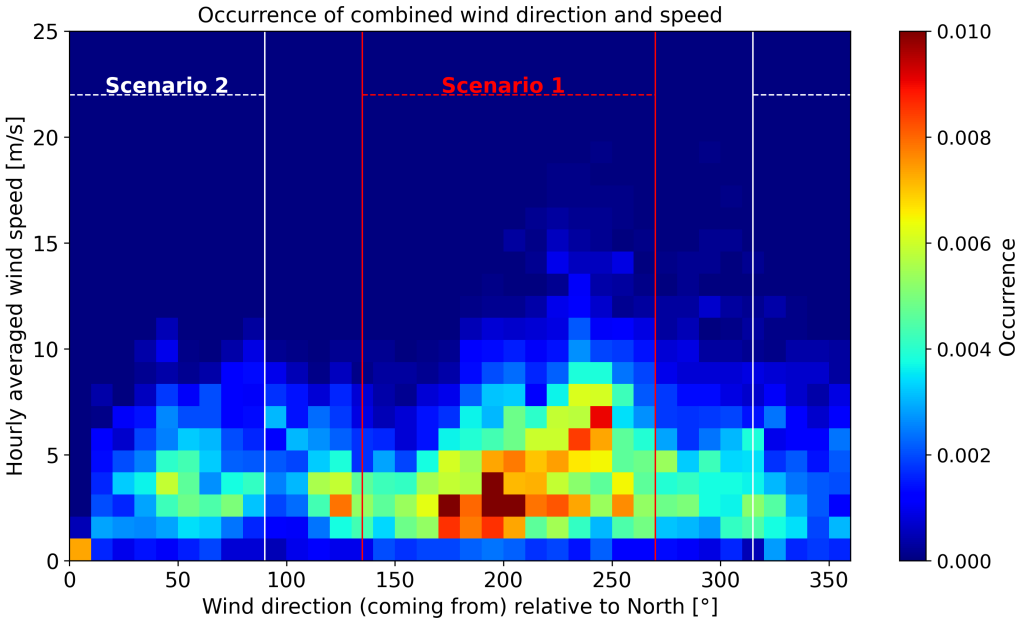

Figure 7.2: Double histogram to plot the direction from which the measured wind is coming, (in ° relative to north), against the hourly average wind speeds (in m/s) measured at the Berkhout KNMI station. The colourbar reflects the occurance of the different combinations of wind speeds and direction of origin. The scenarios, based on ranges of wind direction origin, discussed in this section are indicated by the red and white dashed lines.

7.2.2. Conceptualised system: Scenario 1

In this scenario, a lake-scale circulation occurs that circulates in clockwise direction throughout the Hoornse Hop at the Oeverdijk. This is a relatively strong current, roughly aligning with the wind fetch direction, resulting in a northward directed nearshore current in both cells.

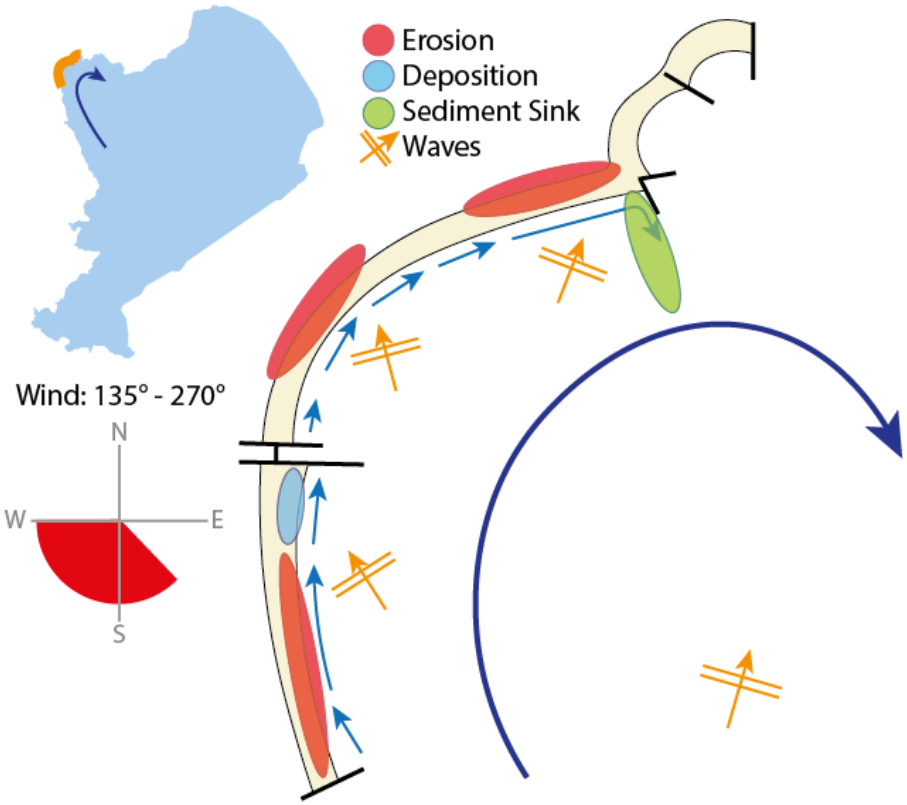

Figure 7.3: Scenario 1. The dark blue arrow represents the general lake-scale current, smaller blue arrows represent nearshore current. Black lines with arrow show wave direction.

In the southern cell, this current reaches its highest nearshore flow velocities for winds from 135°, and comes to a halt in the northern edge of the cell, at the meeting point with the breakwater. This means a positive gradient in flow velocity and bed shear stress occurs in the southern part of the cell, leading to erosion, and negative gradients occurs in the northern section, leading to deposition there. Relatively steady flow occur in the middle of the cell. When referring to the modelled and measured morphological signals per interval in figure 6.7, this scenario is specifically reflected in high-energy intervals 2, 8 and 9, showing southern erosion and a decreasing trend northward.

In the middle cell, a northward directed current also forms. This current picks up at the southern edge of the cell, just above the breakwater, leading to erosion there. The flow has its maximum flow velocity in the middle of the cell, but instead of the current coming to a halt when meeting the breakwater, it bends and connects into an offshore directed current along the northern breakwater (such as pictured in figure 6.6). This suggests that the negative gradient in flow velocity is not found in the corner of the breakwater, but beyond it, leading to sediment deposition there, offshore, instead of along the shoreline. This suggestion is supported by the lack of sedimentation near the breakwater, which was expected if the breakwater halted the longshore current.

7.2.3. Conceptualised system: Scenario 2

Here, the originating wind direction varies in such a way that both cells are under the influence of a southward directed current.

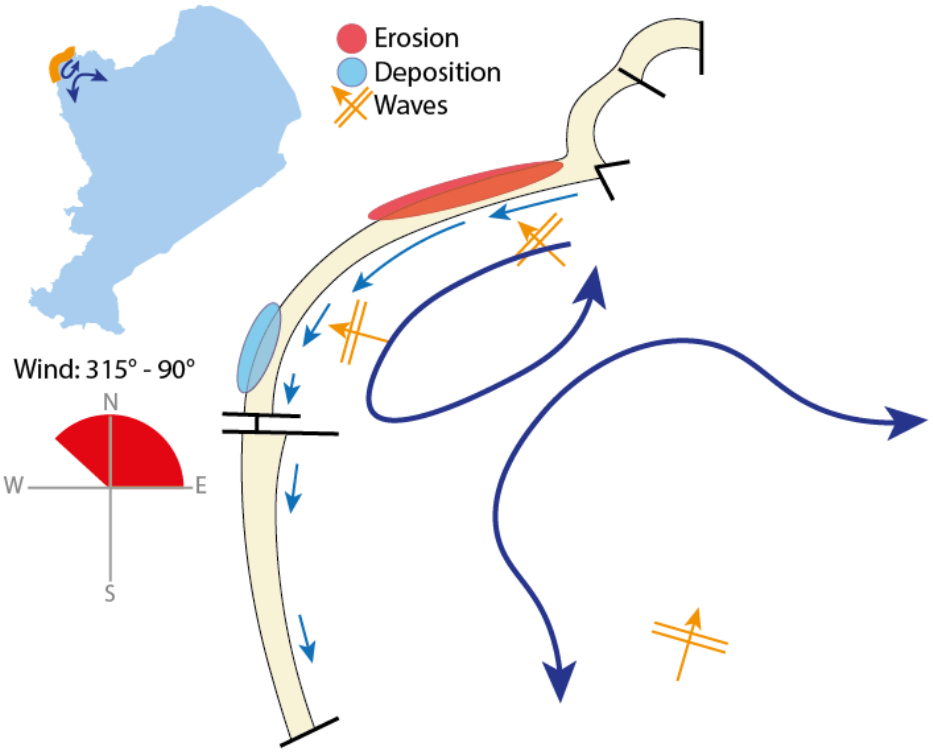

(a) Scenario 2 total

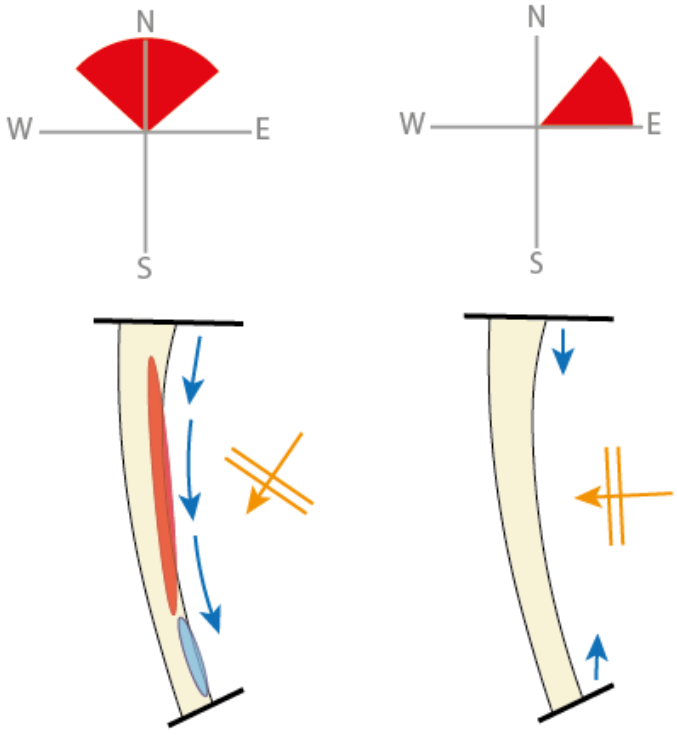

(b) Scenario 2 southern cell variation

Figure 7.4: Scenario 2

In this scenario, the middle cell is under the constant influence of a southward directed longshore current for all winds originating in this range, but strongest for winds coming from 90°. The rotation of this nearshore current is the same for all wind directions in this scenario. The southern cell experiences a southward current for a large part of this scenario (roughly for winds from 315° - 45°). The current reaches a maximum speed in the southern half of the cell for winds from 0°, but slows down for winds at an increasing angle to 0°. For a further increasing angle of incoming wind, the long-shore directed flow in the southern cell comes to a halt. Figure 7.4b displays these two options.

For this scenario as a whole, the main nearshore flow direction in both cells is southward directed. For the middle cell, this net effect is significantly stronger as it occurs for all wind directions in the scenario, and results in relatively higher flow speeds than the (less-common) southward directed currents in the southern cell do.

When referring to the modelled and measured signals per interval in figure 6.7, for the southern cell, this scenario is specifically reflected in low-energy intervals 4 and 6. The signal of southward directed transport in interval 4, and virtually a lack of signal during interval 6, reflect the two scenarios of figure 7.4b. In turn, modelled and measured signals during intervals 4 and 6 for the middle cell, shown in figure 6.4, show a southward directed signal of long-shore sediment transport with a positive gradient, also reflecting the impact of scenario 2 in figure 7.4.

7.2.4. Conceptualised system: Transition zones

The two main scenarios sketched above leave room for two transition zones for the remaining wind directions, specifically for wind coming from 270° - 315° and from 90° - 135°. In both of these cases, the wind comes from an angle that is roughly perpendicular to the middle cell's orientation. Therefore, waves arrive at nearly shore-normal somewhere in the middle of the cell, and create slight longshore currents at either end. The variability of these scenarios for the middle cell, with shifting of the neutral point relative to the incoming wind direction, further highlights the complex nature of the observed longshore erosion variability in this cell.

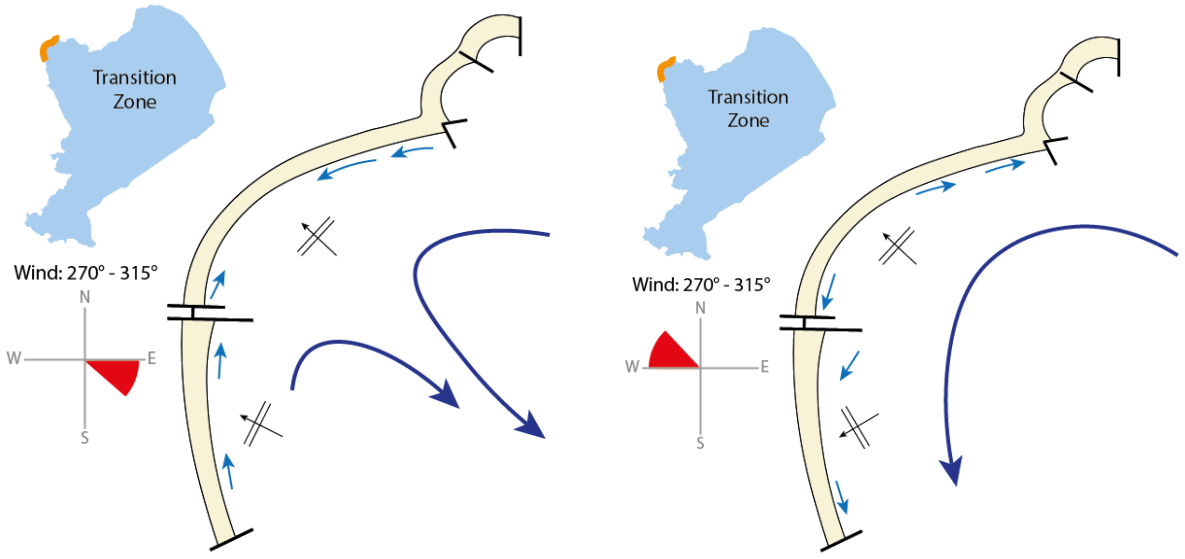

(a) Transition Scenario **(b)** Transition Scenario

Figure 7.5: Transitional scenario's between Scenario 1 and 2.

8

Design comparison

8.1. Similar system: Marker Wadden and Houtribdijk

As a way of validating the observed patterns and quantities of morphological change at the Oeverdijk, the results are compared to similar low-energy coasts. Specifically, the Marker Wadden and the Houtribdijk are two sandy nourishments in the same system (Markermeer), under slightly different hydrodynamic influence and orientation, that have also been heavily analysed. Their relative location and orientation is provided in figure 8.1. This comparison will specifically focus on doctoral thesis research by Anne Ton (2023) as much of the analysis here was done in a very similar way. This makes a comparison not only qualitatively, but also quantitatively, possible. Both analyses rely strongly on wind, specifically the consequent wave action, as indication of hydrodynamic conditions. For comparison purposes, significant wave height characteristics have been provided in Table 8.1. Evident is a milder wave climate at the Oeverdijk than at the Marker Wadden beaches. The Houtribdijk is comparable through mean significant wave height, but the 95th percentile height is significantly lower at the Oeverdijk.

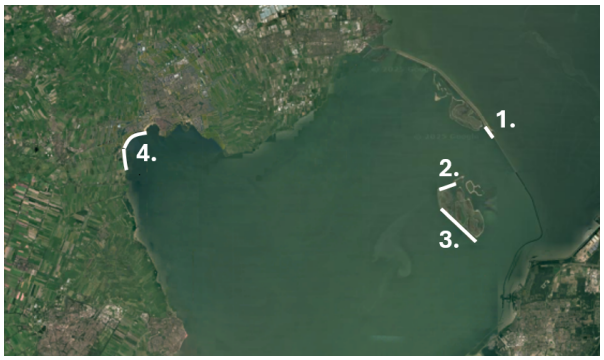

Figure 8.1: Relative locations of beaches at the Marker Wadden project: 1. Pilot Houtribdijk, 2. Noorderstrand, 3. Zuiderstrand & Recreatiestrand, 4. Oeverdijk (middle and south cells).

Location	Mean Hm_0 [m]	95% Hm_0 [m]	Period
1. Pilot Houtribdijk	0.20	0.54	Oct 2014 – Mar 2018
2. Noorderstrand	0.26	0.53	Apr 2019 – Sep 2019
3. Zuiderstrand & Recreatiestrand	0.27	0.63	Apr 2019 – Sep 2019
4. Oeverdijk Middle & South	0.22	0.47	Jan 2024 - March 2025

Table 8.1: Wave statistics at comparison locations: mean and 95th-percentile significant wave height (Hm_0). Houtribdijk and Marker Wadden information from Ton (2023).

In addition to local wave climate variations, it is important to note that the Houtribdijk, Zuiderstand and Recreatiestrand have an orientation that roughly aligns with south western wind and waves (225°) as shore-normal-incidence. Noorderstrand has a 335° shore-normal-incidence orientation. As shown in figure 8.1, the Marker Wadden, and Houtribdijk next to it, are located at the north-eastern edge of Markermeer, at the end of its longest (southwest to northeast) fetch length.

8.1.1. Morphology: cross-shore profile characteristics

In terms of cross-shore profile development, the Oeverdijk shows many similarities to the Marker Wadden and Houtribdijk coasts. For visual references, the four beaches analysed by Ton have been stacked on top of the analysed profiles of the Oeverdijk in profile 8.2. At first sight, the Houtribdijk profile, already

assumed to be an indicator of what the Oeverdijk would eventually look like, is a very good match. The platform width (smaller at the Oeverdijk) is the main visual difference, suggesting the Oeverdijk will likely develop towards a larger platform over time, thus experiencing more erosion, before reaching an equilibrium.

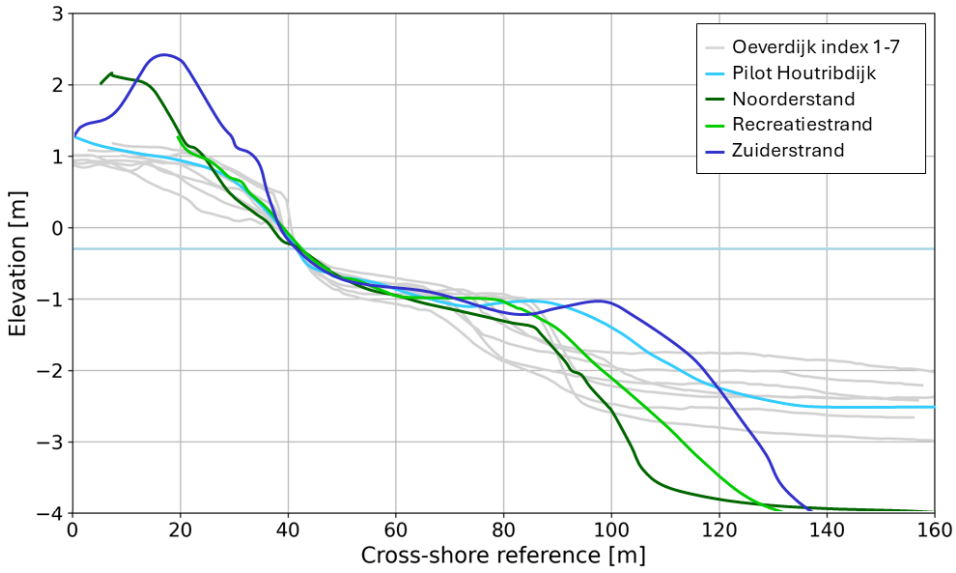

Figure 8.2: Average profiles of the beaches analysed by Ton et al. (2021), traced onto Oeverdijk profiles analysed in this research, and superimposed at the waterline for comparison.

With the exception of Noorderstrand (slope 1:20), the other coasts analysed by Ton have developed towards a waterline slope of around 1:10. This coincides with the average slope of the analysed profiles during the last Oeverdijk survey, despite the design slope of the Oeverdijk to be 1:40, whilst all Marker Wadden beaches had an initial slope of approximately 1:20. The alignment is visible in figure 8.2. This suggests the slope to which the waterline profile develops may be regardless of construction slope. However, Ton has already stated the Marker Wadden beaches have not reached an equilibrium state yet. Neither have the Oeverdijk beaches, considering the rate of change between latest measurements still far exceeding 0. Therefore, conclusions about an equilibrium profile cannot be drawn. Furthermore, Ton's work shows the development of a subaqueous plateau too, although the Marker Wadden and Houtribdijk coasts show platforms with widths varying between 30-60m, clearly extending further out than the Oeverdijk profiles. The Oeverdijk platforms do not exceed 40m yet, but are still growing and may reach similar size. Ton's explanation for the platform elevation assumes it to be in equilibrium around the Hallermeier depth of closure, which lies at a height of NAP -1 m at the Marker Wadden beaches. Although exact plateau heights at the Oeverdijk vary per section, the hypsometric curves also indicate the plateau development is moving towards NAP -1 m, or slightly shallower than that, clearly visible in figure 8.2. The hydrodynamic conditions at the Oeverdijk are also milder. Therefore, considering the depth of closure analysis is indeed closely related to incoming wave action, and the knowledge that that is noticeably lower at the Oeverdijk, the relation between plateau height and depth of closure would be feasible.

8.1.2. Morphology: volume changes

In addition to the previous cross-shore comparison, a quantitative comparison is interesting too. Figure 8.3 plots development of sections of the beach profile over time, for Oeverdijk and Marker Wadden beaches. Although not exactly similar, the vertical distribution of the sections 'beach', 'platform' and 'offshore' between the research methods bear close resemblance. Therefore, this volumetric comparison can be made. However, in these plots the reference (0 weeks) date is July 2018 for the Marker Wadden beaches, September 2014 for the Houtribdijk and January 2024 for the Oeverdijk. These projects were completed at different times, and at different rates. Therefore, the reference date is not at an equal distance to completion per project, and varying levels of morphological adjustments have

taken place between construction and the first (used) measurements. This must be taken into account when comparing the results.

An evident trend from this comparison is the relatively low rate of erosion and sedimentation at the Oeverdijk coasts. Specifically the middle cell nearly shows the absence of a trend, in the sense of cross-shore redistribution at this scale, in comparison to the Marker Wadden and Houtribdijk. All other beaches show an obvious offshore growth. Generally, the hydrodynamic conditions at the Oeverdijk are calmer than at the Marker Wadden. Therefore, it would not be unusual for the volume change rates to be lower there, whilst the spatial spread in erosion and deposition can still be confirmed as trend. Furthermore, due to the exclusion of results in the winter of 2023-2024 during and shortly after the completion of the Oeverdijk, it is possible that a phase of significant volume change during first adjustments is overlooked there.

At the Oeverdijk, the southern cell shows a pattern more distinctly. This trend of a growing offshore section against an eroding beach face and platform is reflected most clearly in the Zuiderstrand and Houtribdijk. This builds upon the assumption of cross-shore sediment transport where eroded waterline sediment is deposited offshore, acting at all low-energy beaches in this system. Additionally, despite the large net loss and relative total growth at the Recreatiestrand and Noorderstrand resepectively, those two beaches still also show a relative pattern of growth (or less erosion) of the offshore section, against more relative erosion of the beach and platform sections. It is unusual to note the large net loss of the Recreatiestrand against the Zuiderstand, despite their similar location and orientation, but this is likely related to the Zuiderstrand growing an offshore spit, compensating some (long-shore) loss.

Noorderstrand, in this time frame, does not show signficant beach face or platform erosion, like the middle cell. Instead, the entire profile at Noorderstrand is slightly growing, mostly due to the contribution of offshore growth. However, later research focused on Noorderstrand by Wellen (2021), analyses a period between 2019 Q3 and 2020 Q4, in which a trend of beach and platform erosion, against platform-edge and offshore deposition, does become visible. Furthermore, Ton's research shows the platforms of Marker Wadden beaches only start to lose volume after a period of 6 months (with steady or even increasing volumes). This adjustment period could last longer in a milder wave climate. Therefore, the middle cell could, although currently showing a relatively stable beach face and platform, still fall further into the expected cross-shore transport signal when given more time.

Ton's research also analyses morphological surveys over a period of 4 years, available for the Houtribdijk. This analysis shows beach face sedimentation for the first few months of measurements (visible in figure 8.3 too), after which an eroding trend sets in that becomes increasingly pronounced. This highlights that measurements of only a year after completion (such as in this comparison), may not yet show the expected trend clearly, (beach and platform erosion, offshore growth). This does not mean that will still develop over time. Therefore, it is likely that the qualitative suggestion of waterline erosion and offshore deposition, leading to profile steepening and platform growth, is enough of an indication that all these beaches are developing towards a similar shape, and that volume analyses will follow that trend when analysed over a large enough period.

Finally, the sum values presented in figure 8.3 show net loss across all beaches, except Noorderstrand (which is growing primarily due to offshore section growth). In all analyses, the offshore depth limit used for the volume calculations, lies on the lake bed, well beyond potential DoC limits. Additionally, the two beaches with the largest sediment loss (Recreatiestrand and Oeverdijk southern cell) are bordered by a breakwater on either end. Hence, the Oeverdijk-based suggestion of (significant) cross-shore sediment transport, (primarily lakeward directed) at full lake depth is supported, even when no sediment transport is originally expected there.

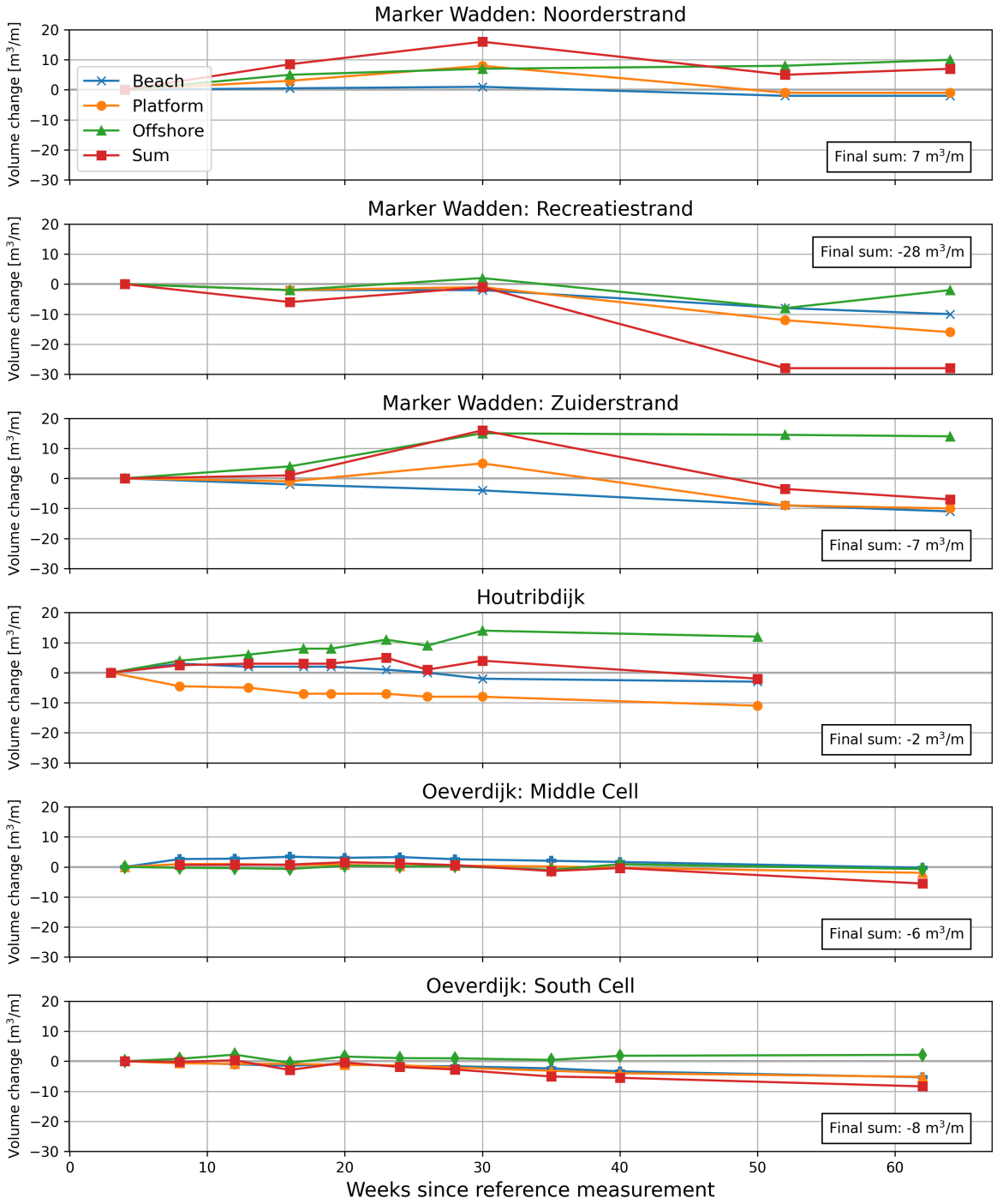

Figure 8.3: Volume changes over various beaches, compared over time. Data for the Marker Wadden and Houtribdijk beaches is extracted from graphs in Ton,(2023), and may not be exact. Layout is also adapted from Ton, for easy comparison. Note that the reference measurement varies in time and time relative to completion per project.

8.1.3. Hydrodynamics: water level set-up and set-down

The research by Ton (2023) and, in its extension by Wellen (2021), both point to a significant influential factor for nearshore hydrodynamics: water level set-up. This set-up leads to large-scale, horizontal circulations, which have been known to exist for longer. Those circulations contribute to current direction at the Oeverdijk. However, local water level set-up is also relevant in determining the height on the profile at which waves reach the coastline. Steezel et al. (2017) showed a strong positive corre-

lation between wave height and wind set-up. The strongest winds over Markermeer generally come from the south-west, with resulting set-up at the Marker Wadden end of the lake. This yields higher water levels there, up to 0.4m higher than average, with higher local wave heights, coming in at roughly shore-normal for the Houtribdijk, Recreatiestrand and Zuiderstrand; a logical superposition of impact. The Oeverdijk is located in a very different part of the Markermeer, much more at a 'tipping point' in the set-up gradient over the lake, for winds from the southwest. During strong south-western winds, the Oeverdijk beaches even experience a slight set-down of local water levels (up to 0.1m). As the highest waves at the Oeverdijk still coincide with south-western winds (see figure 5.20), the scenario of the highest waves reaching sediment unusually high up on the profile, is not as relevant at the Oeverdijk as it is at the Markerwadden. This may be another contributor to lower total rates of erosion at the Oeverdijk compared to most Marker Wadden beaches, in addition to the overall milder wave climate for example.

8.2. Original design

8.2.1. Cross-shore development

The difference between the design profile the Oeverdijk and the actual profile into which it has developed can provide useful insights about design choices. Four profiles were designed per cell, one per section. For comparison, the cross section in the middle of each section has been plotted against the design profile there. Figures 8.4 and 8.5 show the development of two profiles against their design profile. For the other profiles, refer to Appendix C. In all profiles, the wear layer volume in higher parts of the profile, specifically above NAP +0.5 m, remains almost untouched. Some profiles, such as in the middle cell, section 4 (figure 8.4), have barely eroded the wear layer at all, and platform deposition visually compensates for a large part of the 'losses'. Others, such as in the south cell, section 3 (figure 8.5), show much higher rates of erosion across the entire profile, losing up to a third of wear layer volume within this first year of measurements and showing very little plateau deposition to compensate.

In all cases it is evident that the profile has already started adjusting between completion and the first survey considered, as some waterline erosion is already visible in the light green profiles of 2024 wk04 (first used survey) in figure 8.4 and 8.5, compared to the design profile (orange outline). This means that in some cases the eroded volume compared to the wear layer is larger than calculated in the graphs. However, the largest part of further erosion around the waterline occurs in the plotted time frame, which is expected as that covers a much longer time frame, in addition to an entire seasonal cycle. In most cases, the erosion does not reach the design safety profile yet but is getting close, as was already suggest by the numbers on waterline retreat in Table 5.2. In cases where the erosion has reached the safety profile, a significant part of the wear layer volume is still left higher up in the profile. The height at which the breach of the design profile occurs, or likely will occur, is always between the waterline and NAP -1 m.

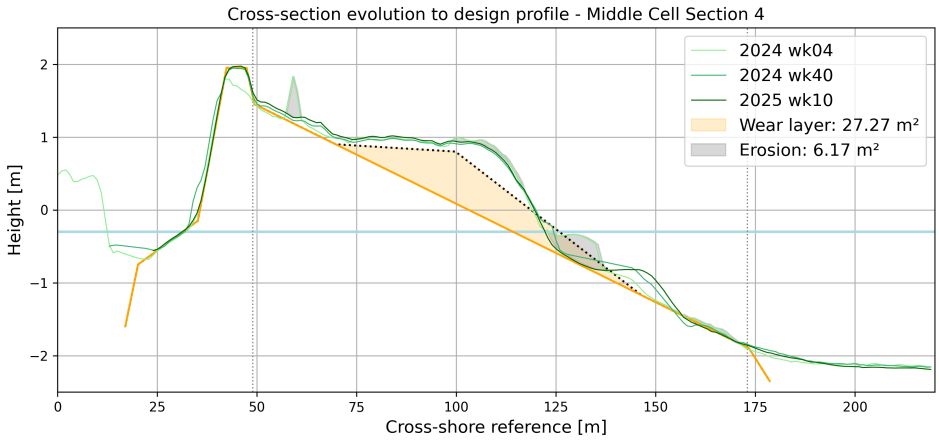

Figure 8.4: Development of the cross section in the middle of section 4, Middle cell, against the design profile of that cell. Eroded volume [m^3/m] between week 04 of 2024 and week 10 of 2025 is calculated, next to the volume [m^3/m] of the wear layer in that design profile.

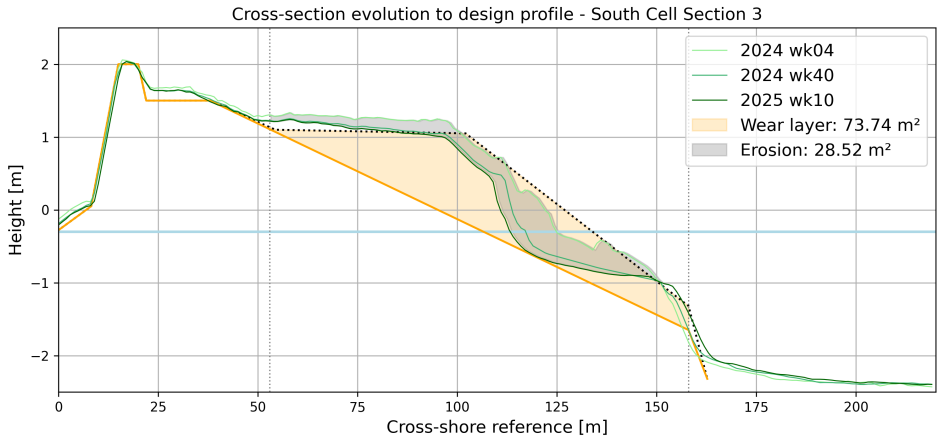

Figure 8.5: Development of the cross section in the middle of section 3, South cell, against the design profile of that cell. Eroded volume [m^3/m] between week 04 of 2024 and week 10 of 2025 is calculated, next to the volume [m^3/m] of the wear layer in that design profile.

When spatially comparing the original design profiles to the morphological development per long-shore section, some points of interest stand out. The wear layer increases in volume from north to south along the south cell, with a slight decrease from section 3 to 4. At first glance, this correlates with the expected, and observed, pattern of erosion along the southern cell, showing increasing rates of erosion from north to south. However, the two southernmost sections (3 and 4) show roughly equal amounts of erosion (refer to Appendix A for the volume changes per section), whilst the wear layer of section 3 is significantly larger than that of section 4 (74 m^3 against 36 m^3). This has resulted in the erosion of section 3 only touching upon the safety profile after a year of erosion, whilst this safety profile has already started to erode in section 4. This indicates that the expected or predicted erosion pattern in the southern cell is not fully reflected by what is observed. Specifically, the erosion in section 4 is larger than expected. This could be due to the influence of wind (and waves) from a south-eastern and eastern angle. These winds are not very common (winds from 80° - 135° account for 10% of the time), and are rarely observed at speeds above 8 m/s. However, they still yield a northward directed current and resulting waves are not too impacted by the sheltering effect of the southern breakwater, meaning section 4 is also under the influence of an accelerating nearshore current. Additionally, eastern waves are assumed to have greater impact on cross-shore sediment transport, and loss. Therefore, if erosion predictions are based on high-energy events (from south-western winds) only, this additional impact of northward directed nearshore current at the southern edge of the cell, may have been underestimated.

Contrastingly, the wear layer volumes in the middle cell decrease from northern to southern sections, and although the observed erosional pattern over the longshore shows a less distinct pattern here, it roughly matches a decreasing pattern from north to south. Therefore, the safety profile is virtually untouched along the entire middle cell. However, the significant erosion in the northern edge of the middle cell, does mean the wear layer of section 1 has already lost over a third of its volume.

Erosion causing the active outline of the profile to touch the safety profile underneath the wear layer does not mean the safety standard of the Oeverdijk is immediately in danger, as enough dynamic sediment is still left in the profile. This sediment is just higher up in the profile, and will likely slide into the lower parts when enough erosion occurs around the waterline. This development does indicate that the Oeverdijk is not always changing (at a rate that is) as expected, partially because too little is known about the cross-shore development of low-energy, non-tidal profiles.

8.2.2. Long-shore erosion patterns

The design team for the Oeverdijk project carried out morphological research prior to finalising the design, in an attempt to gain insight into potential longshore sediment transport, and losses. That way, design profiles with varying volumes could be suggested over the long shore. Two calculation methods were used for this, the first (a condition approach), uses Delft3D to simulate morphological changes for each hydrodynamic condition separately, then computes an annual average based on a weighted mean.

Results of this method are shown in figure 8.6. The second method (morphological summation approach), uses XBeach to simulate morphological evolution over a time series of hydrodynamic forcing, constructed from locally relevant conditions (Alliantie Markermeerdijken, 2016). The second method predicted lower losses for both cells. Noticeably, the negative black values are predicted cross-shore losses out of the active zone, suggesting this modelling process also already assumes a (significant) volume will be 'lost' from the Oeverdijk, as was the case.

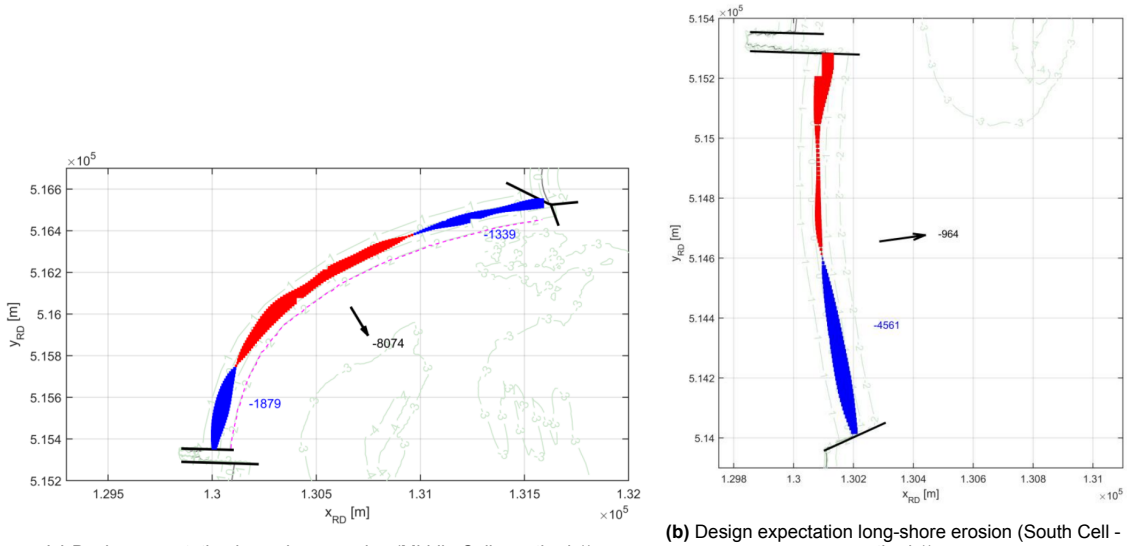

(a) Design expectation long-shore erosion (Middle Cell - method 1)

(b) Design expectation long-shore erosion (South Cell - method 1)

Figure 8.6: Erosion zone plots taken from the research report of Alliantie Markermeerdijken (2016), as part of the morphological consideration design research.

The middle cell design predictions show some similarity to observations, plotted in figure 5.13. Mainly, a shorter erosive zone indeed forms in the south, along with a larger erosive zone in the north. However, the middle part of the middle cell is observed to stay relatively stable, whilst this modelling method predicted deposition here. The total cross-shore loss (modelled at 8074 m^3, observed around 12500 m^3) is still a significant underestimation, but of the same order of magnitude, indicating that perhaps the relative rates of modelled against observed erosion and deposition are not too different.

The southern cell design predictions show the simple distribution this research has also found: erosion in the south, deposition in the north. However, this model outcome shows an erosive zone that covers roughly half the longshore distance of the southern cell, whilst observations indicate the erosion covers more than three quarters of the cell. In terms of cross-shore losses, the model shows significant underestimation. Only 964 m^3 per year is modelled, against observations showing a rough 11500 m^3 per year. Spread out over the cell, this has resulted in a stronger shoreline retreat than expected, hence the current profile is touching on the safety profile, virtually along the entire cell.

8.2.3. Possibility for unforeseen erosion

Across the Oeverdijk, more erosion is observed than was expected. However, the expected losses were based on erosion as a result of waves and currents in the lake (via Delft3D and XBeach modelling). Field observations revealed another observed pattern of erosion that may contribute, visible in figure 8.7. Although these gully's were mostly observed in the southern cell during the site visit, it is not ruled out they cannot occur elsewhere. The gullys are likely a result of water eroding sediment along a path of least resistance back to the lake. This could be from water reaching higher up in the profile, but is more likely to be related to rainwater run-off. If these gully's are indeed a result of rainwater seeping out, this is an indication that rainfall can play a role in beach face erosion, by loosening sediment around the waterline. Periods of more rainfall usually also coincide with stormy periods and higher wave heights. Young et al. (2021), in following of earlier research by Young et al. (2009), found maximum cliff coast line erosion occurred during the wettest period, specifically correlating rainfall to upper cliff erosion, and lower cliff erosion to wave impacts. This research looked at sedimentary coastal cliffs on the southern

coast of California, a very different situation to the Oeverdijk. However, this research does suggest it is possible that rainfall can have an influence on (top-down) erosion rates of a steep waterline profile, an effect that is likely to be more uniform over the Oeverdijk than that of hydrodynamic forcing. This effect (not) being accounted for in design calculations may relate to deviations from predicted sediment loss, increasing erosion across both entire beach sections, as this process can make more cross-shore sediment transport, and loss, possible under similar hydrodynamic conditions.

Figure 8.7: Gully (southern cell

9 Discussion

This chapter discusses the findings of this thesis and puts them into perspective. First, a statistical data analysis is done to assess uncertainty margins in the data, followed by a discussion on the observed significant net sediment loss. Following, model limitations of the Delft3D Markermeer model that was used, are discussed. Finally, a reflection upon the likelihood of the presented conceptual system description is provided.

9.1. Data quality and statistical likelihood of results

The reliability of results and conclusions drawn in this research largely comes down to the quality of the morphological surveying data that was used. As described in Chapter 3, the data was collected through three different methods, each with stochastic variability around the GPS output.

A +/- 3 cm stochastic error margin around the surveying data is of relatively small effect in this analysis. The qualitative development of the cross-shore profile is of a much larger order, as is seen in figure 9.1, and the error margin does not influence general observations such as steepening of the profile at the waterline. It may be of very slight influence on the calculated gradients on these slope, but as they are of indicative nature, there is no significant impact. This stochastic error is also of a very small relative impact on the analysis of observed volume changes. The error, using $\sigma = 0.03$, acts on the surface of a volume column only, scaling to total volume in such a way that it has no significant impact on volume change trends. Therefore, qualitative profile development can be assumed trustworthy.

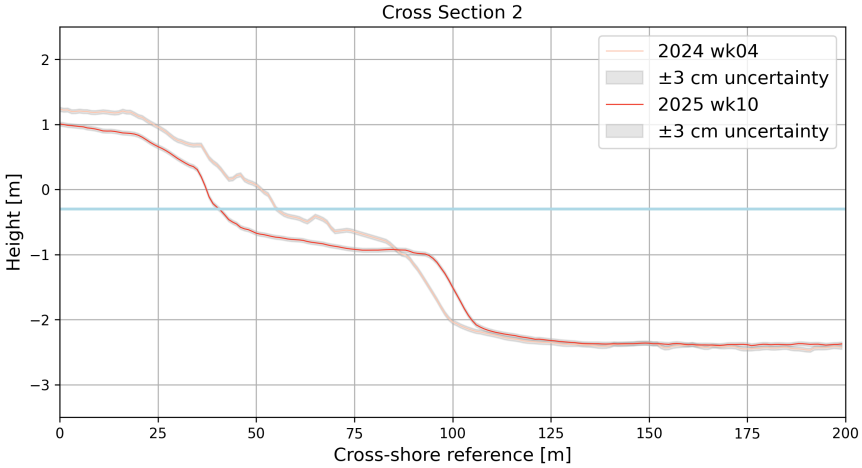

Figure 9.1: Stochastic 3 cm error margin around cross-shore profile at index 2.

Contrary to stochastic, the type of error that could be very influential on the results presented in this report, is a systematic error. As is evident from the hypsometric curves and cross shore evolutions (figures 5.7 and 5.5), vertical shifts in larger surface areas can be in the order of 0 to over 10 centimeters per surveying interval. A systematic error can come about during a surveying interval via a range of ways. Examples of this include that LiDAR drone technology can experience latency or synchronisation issues between timing of different components, where a systematic timing offset can lead to spatial error. Bathymetry data is collected using a multibeam echosounder, which is susceptible to input values of water temperature and salinity for example. If not aligned correctly, this can systematically offset output

data. A handheld GPS can experience human errors such as the user putting it together at the wrong offset, or a component being held at an angle throughout the survey. The main takeaway here is that there are a large number of reasons that may lead to systematically incorrect datasets. The result of this is that entire sections of bathymetry or topography in the analysed datasets may be off by a few centimeters.

Although the size of this error can vary depending on the source, an assumed offset of 0.03 m is used to provide an indication of the possible effect on the data analysis results. Figure 9.2 and 9.3 plot the total volumes in each cell (within the limits as indicated in figure 5.8). The error range (black bars) indicate the consequence of a 0.03 m offset, for all total volumes in both cells over time. On the entire volume, this section is relatively small. However, the focus of the results in this report is on the change in these volumes over time. The local morphological changes are also the results of surface shifts in the order of centimeters, putting into perspective the impact of measurement error on the volumes we are trying to analyse. Although it would be unlikely for the individual measurements to show a decreasing trend this explicitly, in a pattern that follows expectations, it may still be possible no sediment was lost from either cell at all. A systematic error like this could be reflected in the hypsometric curves, with a clear shift, but that does not look apparent.

To gain insight into the likelihood of a trend existing within these data points, despite uncertainty margins, a fitted trend line is plotted, using the Pearson correlation coefficient assuming a linear trend for simplicity, where the negative slope indicates the likelihood of a trend of erosion over time. For both Oeverdijk cells, the linear slope roughly indicates a loss of 30 m^3 / day, which is spread over a smaller surface area for the smaller southern cell. The trends yield a p-value of 0.002 for the middle cell and 0.00003 for the southern cell. In both cases this p-value suggests a statistically significant relationship, indicating that both cells are truly eroding. As it is possible that the true trend in this data is non-linear, and more seasonal, a linear fit wouldn't be the best option. Therefore a Spearman Correlation Coefficient (SCC) has also been calculated, yielding SCC = -0.7 and -0.9, with p-value = 0.002 and 0.0005 for the middle and southern cell respectively, confirming the declining trend.

A confidence interval of ±1σ is plotted around the lines (red zone in figures 9.2 and 9.3). As a result of the spread of collected datapoints, the uncertainty interval becomes largest around the final collected data in 2025. This is logical, as there is a big time step between the second to last and last measurement, in addition to that period experiencing relatively high rates of erosion (in theory). If the final data point of 2025 were to be removed, to test the influence of this seemingly significant data point, both cells would still show a negative fitted slope. However, the middle cell would then only have a fitted slope of -16 m^3 /day, an R^2 of 0.4 and a p-value of 0.09, the southern cell of -32 m^3 / day, 0.8 and 0.001. For the southern cell the last measurement is not of great impact, but for the middle cell that survey doubles the fitted slope gradient, and determines whether or not the p-value is classified as statistically significant. This reflects the influence of single data points on the reflected trend here, especially for the middle cell. Having more data points that cover significant impact periods, mostly winter months, is therefore relevant in determining observed trends with (more) confidence.

In addition to trends over time, an analysis of the residuals was carried out, plotted in figures 9.4 and 9.5. In theory, no trend of residuals over time, or residuals against total volume, should exist if these errors are random around a significant trend. This is not the case, further suggesting the negative trend observed over the total surveying time frame can be deemed reliable. The maximum difference of the plots on the right can be used as an indication for a 'simple' error margin in the observations of volume plots presented earlier. When normalising the maximum residual volume per cell over the length of the cell, a range of 1.4 and 1.5 m^3/m for the middle and southern cell are found, respectively. Using those numbers to take a second look at the volume changes per vertical section presented in figures 5.9 and 5.10, the beach erosion in both cells can still be seen as 'true' erosion. The same holds for platform erosion and offshore growth in the southern cell, signalling the clear cross-shore transport signal there. The platform and offshore section of the middle cell still lie within the error margin.

Although no residual specifically stands out, this could be explained by the fact that these residuals are calculated based off of the 'complete' data sets, eventhough they were collected in three sections, by three seperate measurement techniques. Therefore, the systematic error (even if the overall consequence is not significant, as seen in this section), can effect one vertical profile section specifically. Looking at figures 5.9 and 5.10, it could be stated that the 8th offshore datapoint for the middle cell (week

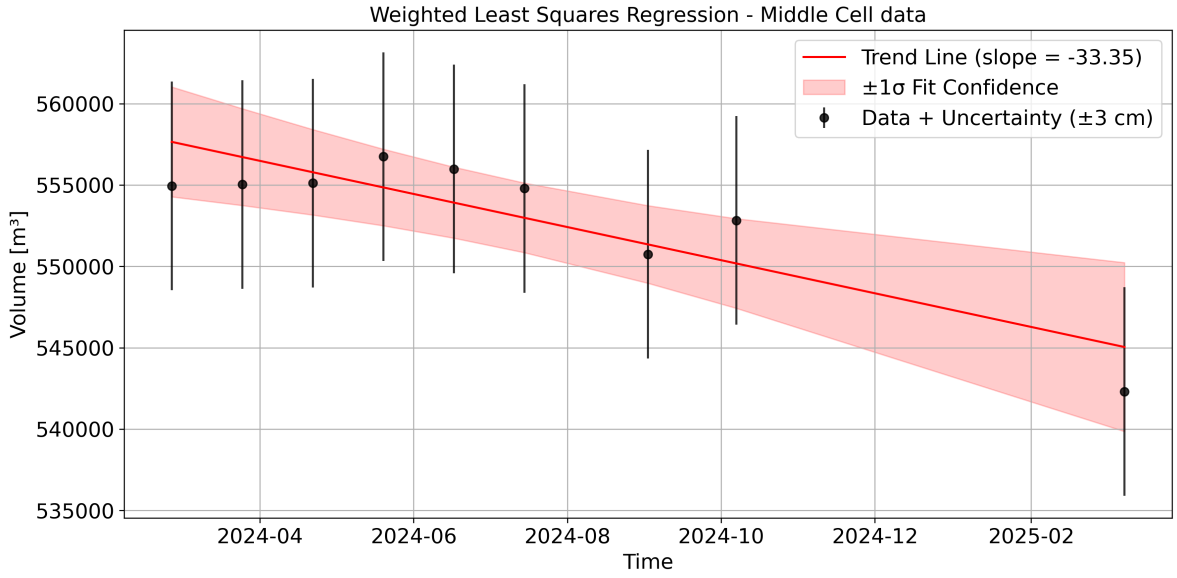

Figure 9.2: Trend and uncertainty of middle cell volume calculations. Black lines represent the error margin around total volumes of the middle cell as a result of a 3 cm systematic offset over the entire surveying datasets. The red line is the fitted relationship (using Pearson's correlation coefficient: R^2 = 0.76, p-value = 0.002), with a red confidence interval of ±1σ (68%) around the fitted relationship.

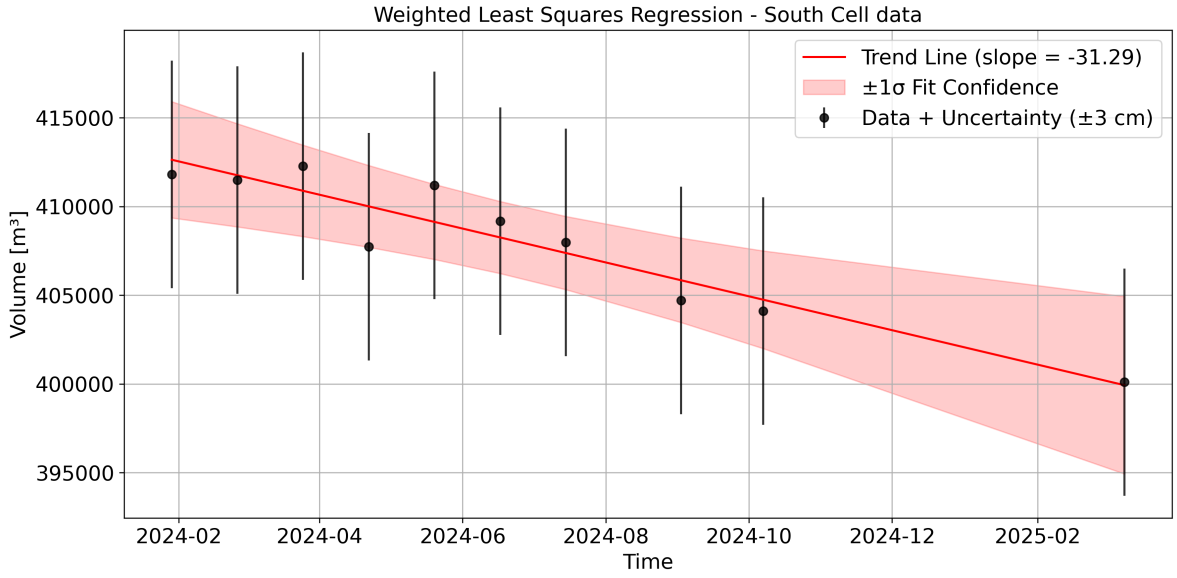

Figure 9.3: Trend and uncertainty of middle cell volume calculations. Black lines represent the error margin around total volumes of the middle cell as a result of a 3 cm systematic offset over the entire surveying datasets. The red line is the fitted relationship (using Pearson's correlation coefficient: R^2 = 0.89, p-value = 0.00003), with a red confidence interval of ±1σ (68%) around the fitted relationship.

40, September), and the 4th offshore datapoint in the southern cell (week 16, april), are anomalous. However, the offshore datasets are collected for both cells in a single surveying expedition, meaning an anomalous measurement in one cell should be visible in both cells. As that is not the case, the likelihood of significant offset for those surveys becomes more unlikely again.

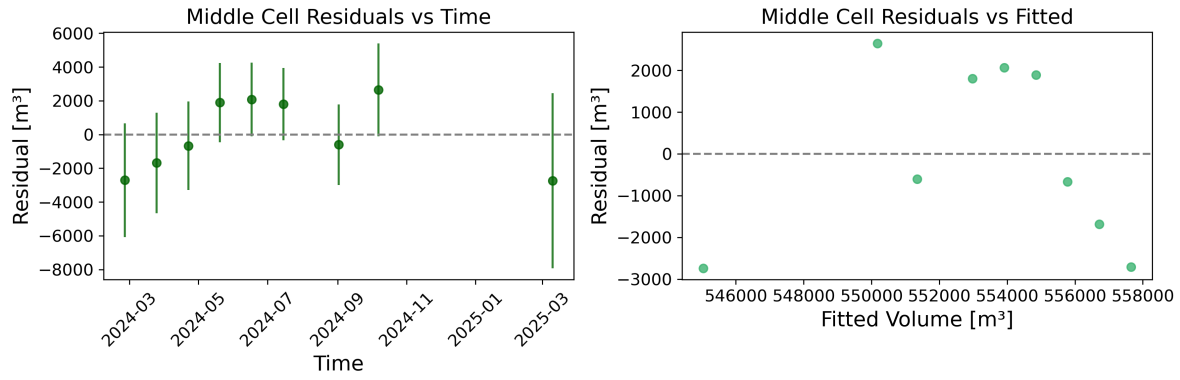

Figure 9.4: The left graph plots the residual (measured - fitted) volumes of the middle cell over time. The error bars indicate the confidence interval range around the data points. The right graph shows the same residuals, but against the total fitted volume.

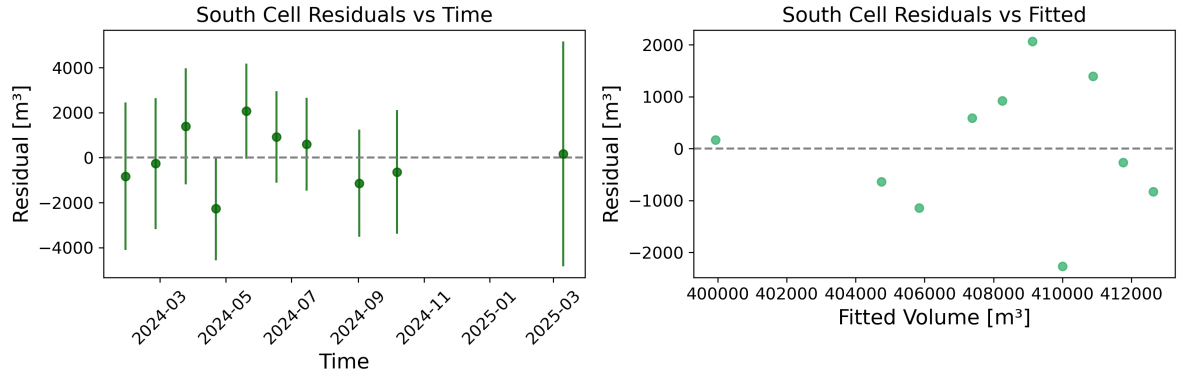

Figure 9.5: The left graph plots the residual (measured - fitted) volumes of the southern cell over time. The error bars indicate the confidence interval range around the data points. The right graph shows the same residuals, but against the total fitted volume.

9.2. Hydrodynamic drivers

On a smaller scale, most hydrodynamic analysis results are in line with expectations such as highest waves coinciding with strongest winds. However, two significant large lake-scale phenomena are observed. The first is lake-scale wind set-up and consequent circulation patterns, relevant for Oeverdijk dynamics. Prior research (such as Vijverberg et al., 2011, Ton et al., 2022 and Wellen, 2021) already discussed these circulations. The hydrodynamic analysis in this thesis confirms the large-scale circulations in lake Markermeer can result in current directions at an angle, or even reverse, to the wind direction as a result of wind-set-up. This is primarily based on modelling results and confirmed by field-data confirming local water-level set-down during high south-western wind speeds. Two important points emerge when considering the Oeverdijk as part of a lake-scale system. First is that the combination of orientation and Oeverdijk location here, mean that nearshore current directions can differ significantly to wind directions, relevant for assumed dominant longshore transport directions. Second, storm events can yield a water-level set-down here, contrary to expectations for storm conditions and different to Marker Wadden observations. Therefore, the designed 'dynamic zone' in the profile might have the tendency to reach further down instead of higher up onto the profile, influencing optimal placement of the wear layer. The impact of the resulting lake-scale current cannot be easily quantified.

Furthermore, an unusual finding is that the wind and wave rose at the Oeverdijk do not align in dominant strength and direction, indicating another large scale process influences local wave direction. Local wave direction is an important parameter for determining the direction of nearshore, longshore current, and thus sediment transport. The Berkhout wind rose (figure 5.19) and the Hoornse Hop wave rose (figure 5.22) differ by 45° - 90°, with wind coming from the south and south-west, against waves from the

south-east. One explanation for this is that the direction of longest fetch over lake Markermeer reaches from Amsterdam to the Houtribdijk; roughly in line with the strongest and most common southwestern winds. Possibly, waves formed over the first section near Amsterdam diffract around Volendam, curving into the Hoorsne Hop at an angle relative to the wind.

Finally, an interesting observation, in wind and wave plots (see figures 5.20 and 5.23), is that for wind speeds of 5.0 m/s and below, higher waves form for winds from roughly 70° - 150°. Although the highest waves occur for wind directions of about 60° higher, those require much higher wind speeds to generate higher wave heights. For example, wind around 0.75 m/s from 140° generates waves of 0.5 m, whereas the same speed from 210° only yields waves of 0.3 m. However, the highest wind speeds do not occur in the 70° - 150° range, meaning the highest waves are formed at higher wind angles. This suggests wind from 70° - 150° (roughly south-east), transfers energy to waves more efficiently. That incoming direction aligns well with the longest fetch distance of lake Markermeer, relative to the Hoornse Hop bay, in which the Oeverdijk lies. Wind from all other angles either forms waves over a smaller fetch length, or forms waves that must diffract in order to reach the Oeverdijk. The fact that this direction of longest fetch (south-east) does not align with the direction of strongest winds (south-west), may provide natural storm protection for the Oeverdijk, and partly explain why observed morphologic change is less extreme than at the more exposed Marker Wadden.

9.3. Model limitations

When using a (nested) Delft3D model to fill knowledge gaps, as done here due to lack of field measurements, the results and interpretation thereof can come with some critical remarks. The development of the original Markermeer Delft3D model, as a 3D suspended matter model, included validation using various measurement campaigns (Deltares, 2012). However, it is difficult to draw conclusions about the accuracy of the model at a small scale (such as the order of nearshore current velocities), in a specific location (such as the Overdijk), when validation and calibration efforts have been made with the focus on other output functions of the model in various other locations. Essentially, model output cannot be confidently trusted without validation with local, relevant data. However, the only available (hydrodynamic) data is that of the measuring buoy. This has already been compared to the model output in figure 4.6, resulting in the main observations that modelled waves have lower peaks than measured waves, and that modelled waves follow the direction of wind (input) more closely. Timing of peaks and direction changes matches well, and during periods of lower wind speeds more close overlap is observed.

This observation concerning lower modelled peak heights is a relatively small issue for the goal of the modelling analysis in this report, as the quantitative output of the model is only used as indication of relative magnitude and location, not for computational purposes. The lag in wave direction is considered more relevant, as wave direction is a driving factor in nearshore current as a result of wave incidence. However, the difference between observed and measured wave direction doesn't reach an average above 20°, which is much smaller than the direction intervals in which the explanatory conceptual scenario's are divided. Therefore, the deviation in wave direction is likely to be small enough for the effect of both the measured and modelled waves to contribute to the same scenario.

One of the main simplifications made in the Delft3D model of this research is the use of 2D instead of 3D velocity calculations (so only 1 vertical layer). The effect of 3D calculations, which generates a vertical velocity profile to indicate undertow for example, would allow us to analyse cross-shore processes. However, the purpose of modelling in this report is an indication of long-shore currents. That does not require 3D velocity profiles. Earlier research using this Delft3D model to model Markermeer currents (Wellen, 2021) compared 2D depth-averaged modelling, to 3D modelling and nearshore ADCP measurements. Their measurements showed no significant change in current direction over depth, matching the 3D modelling output. As a result, they deemed 2D, depth-averaged velocity calculations an acceptable indication for current direction and strength.

As a result of the chosen grid size in the nested model, roughly 15 x 15 m cells, the inclusion of certain aspects of the bathymetry on and around the Oeverdijk in the model, is limited. For example, the underwater plateau is less than 15m wide in some parts of the analysed cells and the steep waterline slopes only span a few horizontal meters, thus disappearing in this model. Therefore, the impact of this

(changing) local bathymetry on nearshore hydrodynamic processes is not necessarily included in the model output. For example, the drying and flooding process at the waterline, which is already difficult to model, is made increasingly hard to represent realistically, even though the hydrodynamics at the waterline are likely the determining factor for rates of erosion there. Other relevant aspects, such as the breakwaters on either end of all cells, are included in the model in the form of thin dams, but they only span over a few underwater grid cell lengths. On the one hand, these settings yield model output with variations in nearshore current velocities that indicate a response to the bathymetry and thin dams. For example, higher, angled velocities occur around the edge of the breakwaters. However, research by Wellen (2021) revealed a reversed nearshore current as a result of a thin dam, on a nested grid with similar grid cell size but a much longer breakwater and a wider under water plateau. This raises the question of whether the nest grid cells at the Oeverdijk are definitively small enough in relation to local features to reveal all resulting local flow patterns.

Finally, the long-shore bed shear stress analysis presented in Chapter 6 knows some limitations that should be mentioned. In the shown results, only a few long-shore output points have been used, roughly every 250m longshore. This means many intermediate signals can be lost. Additionally, the third longshore point in the middle cell is likely anomalous as a result of the minimum depth of one of the corners of the cell (see Appendix G) at the waterline. This means interpretation of gradients as a result of that point should be analysed with that possibility kept in mind. We have attempted to generate output with denser output points (every 50m longshore), from the same grid. However, this proved difficult as the order of magnitude of bathymetry changes often matches the grid cell size, whilst we want to specifically analyse bed shear stresses on the forming underwater nearshore platform. That, in addition to the difficulty of modelling flooding and drying processes, and the use of a 1D model here, meant many longshore locations are unsuitable for output points. Although detailed modelling is beyond the scope of this research, it would be useful to have a more detailed longshore data ta analyse sediment transport potential (perhaps even both in cross-shore and long-shore direction) when looking to explain morphological change. Therefore, it is important to note this was not possible within the time frame and scope of this research, but would be a suitable direction for further research.

9.4. Likelihood of conceptualised system description

In essence, this research expresses the developed understanding of the Oeverdijk system in the form of a concept system, presented in Chapter 7. How realistic this concept system is, is important in determining the reliability of the conclusions drawn. This can be split into separate aspects of the conceptualisation.

9.4.1. Over-simplification

Combining and linking morphological and hydrodynamic data was a requirement to generate a concept system description of how the Oeverdijk develops. This lead to the formulation of two 'main' scenario's, which might be an over-simplification on its own. After all, wind coming from such a broad variety of directions will never yield a single flow pattern in all cases. However, wind also never naturally occurs from a single direction for long enough to establish the unique flow pattern related to that wind direction. Therefore, it is more likely to assume that wind comes from a 'cluster' of directions at a time, establishing a general flow pattern as a result, from which deviation can occur. The aim of this thesis is to establish an explanation for general trends, hence requiring an analysis of general flow patterns. Nevertheless, this 'clustered' representation of scenario's is not a 'true' reflection of natural occurrences and must not be thought of in that way. Instead, it is a simplified reality used to describe general trends at the Oeverdijk. How well this simplified reality can explain observations, determines the likelihood of it being a useful representative of reality.

9.4.2. Generalised cross-shore profile

As discussed in the section on statistical data analysis, the uncertainty around the surveying data is small enough to deem the qualitative results on cross-shore profile development reliable. Therefore, the generalised profile development at the Oeverdijk is assumed very likely, supported by the fact that various existing literature already predicted this development (of waterline steepening and plateau formation). However, the suggestion to quantify and generalise this development using a 1:10 slope, and a Dean's profile (1991) to Hallermeier's (1980) depth of closure, as is done in figure 7.1, has not

been thoroughly analysed or proven. No general Dean's profile has been determined for the Oeverdijk profiles (or really any low-energy coastal environment in literature), and discussion remains about the 'correct' way to calculate a depth of closure. Therefore, although it is a suggestion that may prove useful or likely related, based on existing literature confirmed by findings in this thesis, it is not a proven concept.

9.4.3. Long-shore erosion pattern explanation in perspective

In terms of long-shore, it is difficult to determine whether the conceptualised system scenarios in Chapter 7 realistically form the base of the morphological development of the Oeverdijk. The Delft3D runs, indicating sediment transport potential in figure 5.25, show alignment between areas of increasing bed shear stress, observed erosion, and erosion areas in scenario diagrams for corresponding wind directions. A slight misalignment in modelled and measured wave directions means the longshore positioning of modelled erosion-prone areas may differ slightly in reality. On the other hand, the conceptualised scenario's combine a large enough section of wind origin directions, that these small modelled shifts may not be relevant over large periods of time. The southern cell specifically has an erosive pattern that can be well explained by the short but strong influence of high-energy events, combined with longer periods of low-energy impact.

For the middle cell, explaining its total erosive pattern through the concept scenarios relies on the formation of an offshore jet into a sediment sink during south-western winds of Scenario 1. Although this offshore flow is supported by model output, no nearshore current measurements exist to confirm it. Additionally, the modelling suggests an offshore current in the same order of magnitude as the nearshore current is sometimes observed, it does not indicate a significant increase in flow velocity or bed shear stress to explain the exceptionally high rates of erosion there. In fact, this northern edge erosion of the middle cell is larger than the erosion anywhere along the cell, suggesting both high and low-energy periods contribute. As the offshore jet is not associated with low-energy conditions, this suggests a large part of the net middle cell sediment loss may instead result from cross-shore loss, perhaps driven by shore-normal wave arrival and the low but non-zero flow velocities and bed shear stresses at and beyond the plateau edge. Additionally, the neutral zone (roughly 1500-1600m longshore) in the erosive northern zone of the middle cell does not see a clear explanation in the scenario's, although analysis of that stretch is already made more difficult by last-minute land works there.

One unresolved aspect that remains after the long-shore transport analysis is the net sediment loss across both cells, roughly 11500 m^3 in the middle cell, 12500 m^3 in the southern. Although long-shore patterns explain the redistribution of settlement, modelling does not suggest overall sediment loss. When looking for a long-shore explanation, a possibility is that the assumption of no long-shore bypassing of the breakwater is incorrect. This suggests that sediment from the southern cell bypasses the breakwaters and reaches the middle cell, which is the most likely option considering the dominant northward directed transport in the southern cell, and the smaller net loss in the middle cell despite longer length. However, modelled flow velocities do not suggest such currents around the breakwater, and the fact that the breakwaters reach to well beyond the DoC makes this scenario unlikely to explain such significant volume loss through a single location (around the breakwater head). Therefore, it is assumed that, along with the concept system scenarios, significant cross-shore sediment transport occurs to explain sediment loss. This leads to the cross-shore profile development as discussed, but also to sediment being lost from the system, across the DoC. For the southern cell this effect is assumed to occur evenly across the cell, whereas in the middle cell it is focused at the northern sediment sink (see figure 7.3). The general elevation difference plots (figures 5.2 and 5.1), appear to confirm this. In the middle cell (figure 5.2), the northern edge shows the strongest waterline erosion and the strongest rates of deposition at the offshore platform edge, with a height difference exceeding 30cm on either side, indicating cross-shore transport. This effect is much less pronounced along the southern half of the cell. Along the southern cell, the strong waterline erosion and offshore deposition occur more uniformly over the entire cell, supporting the assumption that the southern cell experiences a steady cross-shore sediment loss more uniformly, while the middle cell shows northern-edge-focused losses.This is further supported by the northern edge's orientation, which is most perpendicular to the primary direction of incoming waves compared to the rest of the cell, unlike the more uniform orientation of the southern cell. Modelled longshore transport rates from bed shear stress gradients compared to observations

(figures 6.4 and 6.7) further support the suggestion of localised versus widespread cross-shore losses. Those figures show the southern cell eroding more than expected across nearly the entire cell, while the middle cell's discrepancy is concentrated at the northern edge, matching the strongest cross-shore transport signals.

9.4.4. Upper losses: aeolian transport and settlement

Another point of discussion regarding the morphological development of the Oeverdijk, is the higher part of the profile, above NAP + 0.9m, showing clear sediment loss. This loss is not included in the volume calculations, due to the NAP +0.9m cutoff to limit the research to marine processes, but is still signficant and remains unexplained. This loss is a very visual 'sinking' of the surface on the left edges of profile development figures such as figure 5.5. It primarily concerns the top of the wear layer, visualised in design plots such as figure 8.4. The actual 'top' of the dike profiles remains relatively stable. The strength of this effect differs over the cross sections. The southern cell shows a much more uniform decline along the entire cell, with the top of the wear layer dropping between 0.1 and 0.2 m. The middle cell shows more variation, with the top of the wear layer staying virtually stable at the southern edge, but also dropping up to 0.15m nearer to the northern edge. The settlement predictions for the safety profile of the dike, as discussed in Chapter 3, predict no more than (a conservative) 0.05m of settlement across the profile in this year. These predictions have been a good match with measurements over the course of construction, making it unlikely that this significantly larger loss is now settlement. Two other options may, instead, explain the profile 'sink' and subsequent sediment loss. This first is some form of dynamic shifting of the wear layer, where sand from the upper wear layer slides down the profile into areas experiencing more erosion. In some ways this is the goal function of the wear layer, for the entire layer to be dynamic enough to balance out areas of significant erosion. However, it is difficult to predict exactly how this process would work. Additionally, if this upper sand really did 'fall' into the gaps or erosion lower in the profile, this would form a sediment source for the analysed section, and mean that in theory the sediment loss over the cells is even larger than is now the assumption. The other explanation relates to aeolian transport. The wear layer has a significant, relatively flat surface area, higher up in the profile around NAP +1.0 m. This could make it more susceptible to aeolian transport, although that possibility still depends on many factors beyond surface elevation, including moisture, local vegetation etc. (Hoonhout et al., 2016).

10

Conclusions and recommendations

This chapter brings all presented results and discussion together to provide a conclusion, as answers to the posed research questions. Additionally, recommendations are made for suggested follow-up research in various directions.

10.1. Conclusions

The aim of this thesis was understanding how hydrodynamic processes drive the morphological development of the Oeverdijk, in Hoorn. The research to achieve that has been structured by asking specific research (sub)questions. Here, those questions are answered.

RQ1: What patterns and quantities of erosion and deposition can be observed at the Hoornse Oeverdijk beach?
Over the monitoring period (January 2024 - March 2025), cross-shore profiles consistently evolved from a 1:40 design slope towards a steeper 1:10 profile at the water line, with a 20–40 m underwater plateau forming at NAP -1 m, roughly matching Hallermeier's depth of closure as expected. Volume analysis showed cross-shore sections to experience erosion of up to 30 m^3/m, and deposition zones with gains up to 20 m^3/m. However, losses are primarily from the beach and platform section, and are not fully compensated by (primarily offshore) gains. Alongshore, the middle cell is stable in the southern half but erodes in the north, ending in a sediment sink beneath the northern breakwater. The southern cell shows erosion in the south and slight sedimentation northward, with a tipping point at 1200 m alongshore. Both cells show net sediment loss (11500 m^3 in the middle cell and 12500 m^3 in the southern). This is likely cross-shore sediment loss, under the assumption of no breakwater bypass.

RQ2: What local hydrodynamic forcing yields sediment transport at the Hoornse Oeverdijk?
The Oeverdijk is exposed to locally generated wind waves, with winds coming primarily from the south, and stronger winds (>10 m/s) from a south-western direction. Winds from the north are barely observed. Peak storm events yield wave heights up to 0.8m, and the highest waves coincide with strongest winds, in addition to noticeable water level set-down. These high-energy characteristics correlate noticeably with (lakeward-directed) cross-shore transport patterns, where both higher waves and stronger set-down yield increased beach and platform erosion, and offshore growth.

The nearshore currents that form as a result of local wave and wind action are responsible for long-shore sediment transport, through bed shear stresses that surpass the critical bed shear stress for sediment transport (roughly 0.2 N/m^2). Southern winds result in the highest long-shore bed shear stresses in the southern cell, south-western winds achieve this effect for the middle cell. Although this effect is especially strong during storm periods, calmer (no-storm) intervals also experience bed shear stresses high enough to yield sediment transport, with clear longshore transport signals being observed (see figures 6.4 and 6.7). The direction of bed shear stress, and consequent transport, is strongly related to wind-direction. Modelling output confirms a primarily northward directed bed shear stress in both cells as a result of longshore currents, generated by a primarily south-originating wind climate. However, modelled and measured transport signals do not always match, suggesting a significant role for cross-shore transport too.

RQ3: How do the morphological developments of the Oeverdijk compare to other sandy coasts in the Markermeer, and to the original design profile and expectations?
The Oeverdijk profile develops in a very similar matter to other Marker Wadden beaches, both displaying steep foreshores (both roughly 1:10) and low-gradient submerged platforms at similar height. This supports the generalisability of observed morphotypes (Ton et al., 2021). Plateau width is smaller at the Oeverdijk (20 - 40m against 40 - 60m), but still growing. Absolute volumes of transport at the Oeverdijk also appear smaller (losses of 3 and 8 , likely related to the milder hydrodynamic climate at

the Oeverdijk. Long-shore sediment transport patterns vary per beach, as this is highly influenced by (relative) orientation. A common occurrence between virtually all analysed Marker Wadden beaches is a total sediment loss, suggesting significant cross-shore sediment transport beyond the depth of closure, even in this low-energy environment.

The design process for the Oeverdijk already considered the potential of a 'Houtribdijk Profile' developing, which is thus indeed what happened. Observed profile evolution diverged from the initial 1:40 design, trending instead toward the common double-slope structure with a steep nearshore face and a gradual underwater plateau. This development confirms design assumptions of a dynamic layer between NAP +0.5m and -1.0m. However, the cross-shore extent and volume redistribution exceeded original wear layer estimations in some locations, suggesting that current models may under-represent real transport volumes. The vertical distribution of the wear layer over the design profile might mean less sediment is available near the water line than perhaps required, longer monitoring will provide more insight here. In long-shore direction, the expected erosive patterns generally aligned. However, the longshore extent over which erosion would occur, in addition to volumes of net (cross-shore) sediment loss, were underestimated in the southern cell especially. In future design processes, a closer analysis of the system interaction between hydrodynamic drives, geomtery, structures and morphological change might be able to lower this gap.

Main RQ: How do local hydrodynamics shape the morphological evolution of the Hoornse Oeverdijk beach?

The morphological evolution of the Hoornse Oeverdijk is primarily wind-driven, through associated wave and currents. The redistribution of sediment, both in the cross-shore and long-shore directions, reflects a response to (seasonal) variations in wave energy and directionality. In cross-shore direction, wave action results in the development of a low-energy coastal profile that aligns with literary research, as discussed, with a steep waterline profile (1:10) and underwater plateau (stretching up to 40m already, around NAP -1 m). Waterline retreat (up to 15 m/year) is observed more significantly than locations of lakeward growth (up to 4m / year), suggesting erosive cross-shore processes dominate. In long-shore direction, the basis for a total system explanation lies in defining the effect of the driving force of morphological change: wind. Figures 7.3 and 7.4a show the development that occurs as a result of two main incoming wind sectors, where scenario 1 represents the most common, and most energetic wind sector. Depending on the strength of the wind from those directions over time, a weighted effect of the long-shore patterns that develop as a result of those winds can provide insight into expected long-term morphological development at the Oeverdijk. Net sediment losses of around 12000 m³ per cell remain, that are not simply explained by cross-shore redistribution within the DoC, or settlement, instead pointing to significant cross-shore losses via a breakwater-induced sediment sink and strong offshore directed transport across the expected transport boundary.

10.2. Recommendations

Recommendations are split into three topics. The first relates to further research in the direction of deepening our understanding of the developments at the Oeverdijk as part of the Markermeer system. The second is focused on improving and validating output of the Delft3D model of the Markemeer, however, multiple rounds of validation and calibration have already bean applied to various locations within this model and fine-tuning the Hoornse Hop area is not assumed to yield significant improvement of results in the scope of this analysis. Finally, a direction of research is proposed from a more zooomed-out perspective of application, working towards using the things learnt about low-energy coastal systems for future design approaches in similar settings.

Measurements & interpretation

- In order to validate and verify the suggested long-shore transport scenario's at the Oeverdijk in this research, nearshore current and wave measurements need to be collected and analysed. Specifically, hydrodynamic data should be collected near cell edges to trace potential sediment loss and validate and verify the long-shore conceptual system description. A step gauge (STB) can be used to measure water level fluctuations and wave height, whilst an ADCP can be used to measure current magnitudes and directions.
- Currently, the outline of the coastal cells (middle and south) was done under the assumption that

the offshore border of the cell, in combination with breakwaters on either side of the cells, meant no significant sediment transport out of the cell would occur. However, data analysis reveals a net sediment loss over the cells, possibly explained by sediment bypassing the breakwaters, being deposited inside the rocky structure of the breakwater, or crossing the DoC further into the lake. Data analysis (if all required data is available, otherwise collection is required first) of a larger area in the Hoornse Hop can be carried out, specifically a sediment balance analysis, in an attempt to trace (cross-shore or bypass) sediment loss.

- Research into additional settlement of the dike (for example due to original lake bed composition), and an analysis on potential for aeolian transport in the area, can be done to validate the hypothesis of those causes (not) leading to significant wear layer volume loss.
- Continued monitoring is suggested to discover trends over elongated time frames. Monitoring least twice a year (e.g. September and May) is required to capture seasonal variation, and confirm the rate of the suggested sediment loss as discovered here. However, short-interval monitoring throughout winter is also suggested (for example bi-weekly or post-storms), to be able to distinguish the effect of storm characteristics on morphological development.
- Similar research to this thesis, consisting of bathymetry data analysis on profile development of other low-energy coasts can confirm expectations on profile characteristics outside of Markermeer. That knowledge can help confirm generalisation potential of low-energy equilibrium profiles for future design references, to lower design sediment requirements.

Delft3D Markermeer Model

- Currently, the observed long-shore transport signals at the Oeverdijk are based on model output of longshore variation in bed shear stress and depth averaged flow velocity. Calibrating and validating (the trend in) these nearshore hydrodynamics with collected field-data, using an ADCP, on local flow velocity profiles can strengthen the reliability of conclusions drawn as a result of this model output.
- Further use of this model can allow for the studying of various phenomena around the Oeverdijk, or a sensitivity study of design decisions. For example, the impact of an extended breakwater at the northern edge of the middle cell can be studied, or changing the angle of the breakwater. This can lead to more insights on the conditions under which the conceptual sediment sink there, is formed, and perhaps how to adapt it to mitigate sediment loss.
- In this research, a depth-averaged version of the D3D model was used, with a (still relatively coarse) grid cell size of 15 x 15m. However, using a layered model (for example, 7 layers over the vertical depth profile), on a finer grid, allows for the inclusion of cross-shore processes such as undertow, to help gain insight into the potential for cross-shore sediment transport. Additionally, it allows for close analysis of nearshore dynamics on and near the underwater platform. This is an important step in explaining the (assumed) cross-shore losses and long-shore erosional patterns.
- Experimentation with the inclusion of morphological change in runs of this Delft3D Marker Wadden model can work towards a better modelled understanding of the morphological development of low-energy coastal systems. However, Delft3D uses empirical sediment transport formulas, which means the output of these runs could be very far off real-life and require significant model alterations before becoming a reliable source for morphological development analysis.

Application

- Even if a generalised low-energy coastal profile can be determined on the basis of this, and other comparable research, a long road likely follows towards implementation. Changing design profiles, when they form the basis of coastal protection projects, can require adjustments to safety regulations or policy requirements. Contractors will need a way to validate the efficiency of a design to clients. Research that combines available (empirical) evidence for the existence and efficiency of a generalised low-energy coastal profile, in addition to ensuring it meets any regulation requirements, can go a long way to minimising time to implementation.

References

Alliantie Markermeerdijken (2016): Morfologische beschouwing Oeverdijkvarianten. Tech. rep. AMMD-01299.

Alliantie Markermeerdijken (Sept. 2017): Ontwerpbasis Oeverdijk DO. Dutch. Tech. rep. Alliantie Markermeerdijken.

Alliantie Markermeerdijken (July 2018a): Ontwerp buitenprofiel Oeverdijk DO. Tech. rep. AMMD-004710. Alliantie Markermeerdijken.

Alliantie Markermeerdijken (Nov. 2018b): Ontwerpnota DO Oeverdijk M2 en M3. Tech. rep. Alliantie Markermeerdijken.

Alliantie Markermeerdijken (2022): Vrijgave Formulier Ophoogslagen. Tech. rep. AMMD-009476.

Aragonés, L., J.I. Pagán, M.P. López, J.C. Serra (Sept. 2019): "Cross-shore sediment transport quantification on depth of closure calculation from profile surveys". en. In: Coastal Engineering 151, pp. 64–77. ISSN: 03783839. DOI: https://doi.org/10.1016/j.coastaleng.2019.04.002.

Bosboom, J, M. J. F. Stive (Jan. 2021): Coastal Dynamics. ISBN: 978-94-6366-371-7. URL: https://doi.org/10.5074/T.2021.001.

Bruun, Per (1954): Coast Erosion and the Development of Beach Profiles. en. U.S. Beach Erosion Board.

Cooper, J.A.G., F. Navas (June 2004): "Natural bathymetric change as a control on century-scale shoreline behavior". In: Geology 32.6, pp. 513–516. ISSN: 0091-7613. DOI: https://doi.org/10.1130/G20377.1.

Davidson-Arnott, Robin G.D., Robert A. McDonald (Apr. 1989): "Nearshore water motion and mean flows in a multiple parallel bar system". en. In: Marine Geology 86.4, pp. 321–338. ISSN: 00253227. DOI: https://doi.org/10.1016/0025-3227(89)90091-1.

De Vriend, Huib J., Mark Van Koningsveld, Stefan G.J. Aarninkhof, Mindert B. De Vries, Martin J. Baptist (June 2015): "Sustainable hydraulic engineering through building with nature". en. In: Journal of Hydro-environment Research 9.2, pp. 159–171. ISSN: 15706443. DOI: https://doi.org/10.1016/j.jher.2014.06.004.

Dean, Robert G (1991): "Equilibrium Beach Profiles: Characteristics and Applications". en. In: Journal of Coastal Research 7.1.

Deltares (2012): Validation suspended sediment model Markermeer – version II & Application to silt screen. Tech. rep.

Freire, Paula, Óscar Ferreira, Rui Taborda, Filipa Oliveira, A. Rita Carrasco, Ana Silva, Catarina Vargas, Rui Capitão, Conceição Fortes, Alexandre Braga Coli, João Santos (Jan. 2009): "Morphodynamics of Fetch-Limited Beaches in Contrasting Environments". In: Journal of Coastal Research SI 56, pp. 183–187.

Guillén, Jorge, Gonzalo Simarro, Daniel Calvete, Francesca Ribas, Angels Fernández-Mora, Alejandro Orfila, Albert Falqués, Rinse De Swart, Amanda Sancho-García, Ruth Durán (Feb. 2024): "Sediment leakage on the beach and upper shoreface due to extreme storms". en. In: Marine Geology 468, p. 107207. ISSN: 00253227. DOI: https://doi.org/10.1016/j.margeo.2023.107207.

Hallermeier, Robert (Jan. 1978): "Uses for a calculated limit depth to beach erosion". In: Coastal Engineering Proceedings 1, p. 88. DOI: https://doi.org/10.9753/icce.v16.88.

Hallermeier, Robert J. (Jan. 1980): "A profile zonation for seasonal sand beaches from wave climate". en. In: Coastal Engineering 4, pp. 253–277. ISSN: 03783839. DOI: https://doi.org/10.1016/0378-3839(80)90022-8.

Harley, Mitchell D., Gerd Masselink, Amaia Ruiz De Alegría-Arzaburu, Nieves G. Valiente, Tim Scott (May 2022): "Single extreme storm sequence can offset decades of shoreline retreat projected to result from sea-level rise". en. In: Communications Earth & Environment 3.1, p. 112. ISSN: 2662-4435. DOI: https://doi.org/10.1038/s43247-022-00437-2.

Hegge, Bruce, Ian Eliot, John Hsu (July 1996): "Sheltered Sandy Beaches of Southwestern Australia". en. In: Journal of Coastal Research 12.3. Number: 3. ISSN: 0749-0208.

Hoonhout, Bas M., Sierd De Vries (Aug. 2016): "A process□based model for aeolian sediment transport and spatiotemporal varying sediment availability". en. In: Journal of Geophysical Research: Earth

Surface 121.8, pp. 1555–1575. ISSN: 2169-9003, 2169-9011. DOI: https://doi.org/10.1002/2015JF003692.

Jackson, Nancy L, Karl F Nordstrom, Ian Eliot, Gerdhard Masselink (Nov. 2002): "'Low energy' sandy beaches in marine and estuarine environments: a review". en. In: Geomorphology 48.1-3, pp. 147–162. ISSN: 0169555X. DOI: https://doi.org/10.1016/S0169-555X(02)00179-4.

Jongh, L. de (2017): "Initial morphological evolution of a mega nourishment". en. In.

Kamphuis, J. William (Nov. 1991): "Alongshore Sediment Transport Rate". en. In: Journal of Waterway, Port, Coastal, and Ocean Engineering 117.6, pp. 624–640. ISSN: 0733-950X, 1943-5460. DOI: https://doi.org/10.1061/(ASCE)0733-950X(1991)117:6(624).

Kirk, R. M., P. D. Komar, J. C. Allan, W. J. Stephenson (Apr. 2000): "Shoreline Erosion on Lake Hawea, New Zealand, Caused by High Lake Levels and Storm-Wave Runup". en. In: Journal of Coastal Research 16.2. Number: 2. ISSN: 0749-0208.

Makaske, Bart (1998): "Morphologic Changes of a Micro-Tidal, Low Wave Energy Beach Face During a Spring-Neap Tide Cycle, Rhone-Delta, France". en. In: Journal of Coastal Research 14.

Masselink, Gerhard, Andrew Short (Jan. 1993): "The effect of tide range on beach morphodynamics and morphology: a conceptual beach model". In: Journal of Coastal Research 9, pp. 785–800.

Mil-Homens, João, Roshanka Ranasinghe, J. S. M. van Thiel de Vries, M. J. F. Stive (May 2013): "Re-evaluation and improvement of three commonly used bulk longshore sediment transport formulas". In: Coastal Engineering 75, pp. 29–39. ISSN: 0378-3839. DOI: https://doi.org/10.1016/j.coastaleng.2013.01.004.

Nordstrom, Karl F., Nancy L. Jackson (Feb. 2012): "Physical processes and landforms on beaches in short fetch environments in estuaries, small lakes and reservoirs: A review". In: Earth-Science Reviews 111.1, pp. 232–247. ISSN: 0012-8252. DOI: https://doi.org/10.1016/j.earscirev.2011.12.004.

Nutz, A., M. Schuster, J.-F. Ghienne, C. Roquin, F. Bouchette (Feb. 2018): "Wind-driven waterbodies: a new category of lake within an alternative sedimentologically-based lake classification". en. In: Journal of Paleolimnology 59.2, pp. 189–199. ISSN: 0921-2728, 1573-0417. DOI: https://doi.org/10.1007/s10933-016-9894-2.

Penning, W E, H J Steetzel, R Van Santen, J Fiselier, H J De Lange, V Vuik, S Ouw Erkerk, J S M Van (2015): "Natural foreshores as an alternative to tradiitonal dike re-enforcements: a field pilot in the large shallow lake Markermeer, the Netherlands". en. In.

Raad van State (2021): Versterking Markermeerdijken kan doorgaan.

Ranasinghe, Roshanka, Rob Holman, Matthieu De Schipper, Tom Lippmann, Jennifer Wehof, Trang Minh Duong, Dano Roelvink, Marcel Stive (Oct. 2012): "Quantifying nearshore morphological recovery time scales using argus video imaging: Palm Beach, Sydney and Duck, North Carolina." en. In: Coastal Engineering Proceedings 33, p. 24. ISSN: 2156-1028, 0589-087X. DOI: https://doi.org/10.9753/icce.v33.sediment.24.

Robert G. Dean (1977): "Equilibrium beach profles: US Atlantic and Gulf coasts". In.

Seymour, Richard J. (2005): "Cross-Shore Sediment Transport". en. In: *Encyclopedia of Coastal Science*. Ed. by Maurice L. Schwartz. Dordrecht: Springer Netherlands, pp. 352–353. ISBN: 978-1-4020-3880-8. DOI: https://doi.org/10.1007/1-4020-3880-1_104.

Shields, A. (1936): "Anwendung der Ähnlichkeitsmechanik und der Turbulenzforschung auf die Geschiebebewegung". German. PhD thesis.

Shipman, Hugh (2010): The Geomorphic Setting of Puget Sound: Implications for Shoreline Erosion and the Impacts of Erosion Control Structures. en. Scientific Investigations Report. Series: Scientific Investigations Report.

Steezel, C. (July 2017): The behaviour of sandy shores of the Markerwadden. Tech. rep.

Stive, Marcel J.F., Huib J. De Vriend (Aug. 1995): "Modelling shoreface profile evolution". en. In: Marine Geology 126.1-4, pp. 235–248. ISSN: 00253227. DOI: https://doi.org/10.1016/0025-3227(95)00080-I.

Ton, A. M. (2023): "Sandy beaches in low-energy, non-tidal environments". en. In: DOI: https://doi.org/10.4233/5978034d-f9e5-4094-99dc-dd8591828125.

Ton, Anne, Vincent Vuik, Stefan Aarninkhof (Dec. 2022): "Longshore sediment transport by large-scale lake circulations at low-energy, non-tidal beaches: A field and model study". In: Coastal Engineering 180, p. 104268. DOI: https://doi.org/10.1016/j.coastaleng.2022.104268.

Ton, Anne M., Vincent Vuik, Stefan G. J. Aarninkhof (Feb. 2021): “Sandy beaches in low-energy, non-tidal environments: Linking morphological development to hydrodynamic forcing”. In: Geomorphology 374, p. 107522. ISSN: 0169-555X. DOI: https://doi.org/10.1016/j.geomorph.2020.107522.

Ton, Anne, Vincent Vuik, Rinse Wilmink, Stefan Aarninkhof (Dec. 2020): “Morphodynamics of sandy beaches in low energy, non-tidal environments”. en. In: Coastal Engineering Proceedings 36v. Number: 36v, pp. 47–47. ISSN: 2156-1028. DOI: https://doi.org/10.9753/icce.v36v.sediment.47.

Travers, Ailbhe (Mar. 2007): “Low-Energy Beach Morphology with Respect to Physical Setting: A Case Study from Cockburn Sound, Southwestern Australia”. en. In: Journal of Coastal Research 232, pp. 429–444. ISSN: 0749-0208, 1551-5036. DOI: https://doi.org/10.2112/04-0275.1.

Vijverberg, Thomas, Johan Christian Winterwerp, Stefan Gert Jan Aarninkhof, Hans Drost (Mar. 2011): “Fine sediment dynamics in a shallow lake and implication for design of hydraulic works”. en. In: Ocean Dynamics 61.2-3, pp. 187–202. ISSN: 1616-7341, 1616-7228. DOI: https://doi.org/10.1007/s10236-010-0322-2.

Vila-Concejo, Ana (Jan. 2024): “Morphodynamics and management challenges for beaches in modified estuaries and bays”. en. In: Cambridge Prisms: Coastal Futures 2, e11. ISSN: 2754-7205. DOI: https://doi.org/10.1017/cft.2024.7.

Vila-Concejo, Ana, Shari L Gallop, John L Largier (2020): “Sandy beaches in estuaries and bays”. en. In.

Wellen, Fleur Willemijn (July 2021): “Development of a nonequilibrium beach in a lowenergy lake environment”. In.

Yin, J.-H., J. Graham (May 1989): “Viscous–elastic–plastic modelling of one-dimensional time-dependent behaviour of clays”. en. In: Canadian Geotechnical Journal 26.2, pp. 199–209. ISSN: 0008-3674, 1208-6010. DOI: https://doi.org/10.1139/t89-029.

Young, A.P., R.T. Guza, H. Matsumoto, M.A. Merrifield, W.C. O’Reilly, Z.M. Swirad (Feb. 2021): “Three years of weekly observations of coastal cliff erosion by waves and rainfall”. en. In: Geomorphology 375, p. 107545. ISSN: 0169555X. DOI: https://doi.org/10.1016/j.geomorph.2020.107545.

Young, Adam P., R.T. Guza, R.E. Flick, W.C. O’Reilly, R. Gutierrez (Nov. 2009): “Rain, waves, and short-term evolution of composite seacliffs in southern California”. en. In: Marine Geology 267.1-2, pp. 1–7. ISSN: 00253227. DOI: https://doi.org/10.1016/j.margeo.2009.08.008.

A

Longshore sections volume splits

Here, the remaining graphs that complete the long-shore split of cross-shore profile development for both beach cells are presented.

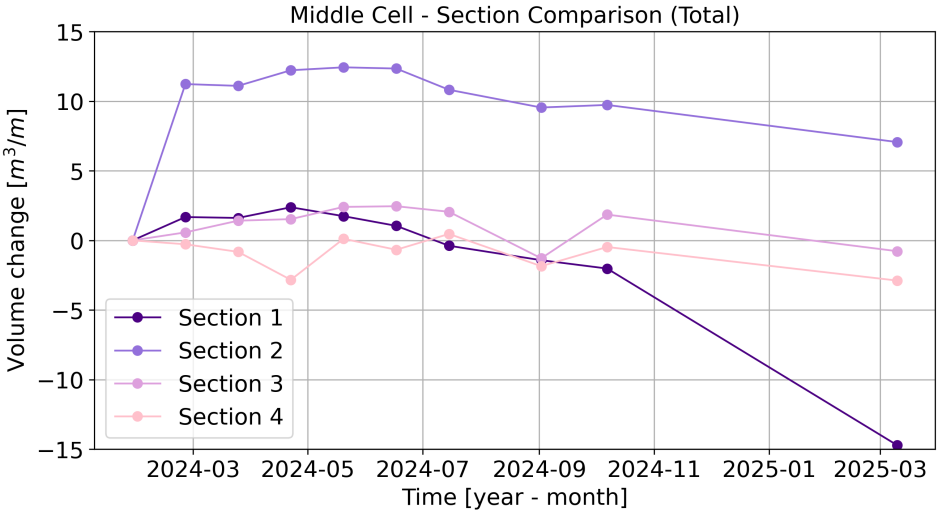

Figure A.1: Volume change over longshore distance of the middle cell, split into the four longshore sections, for the vertical total section.

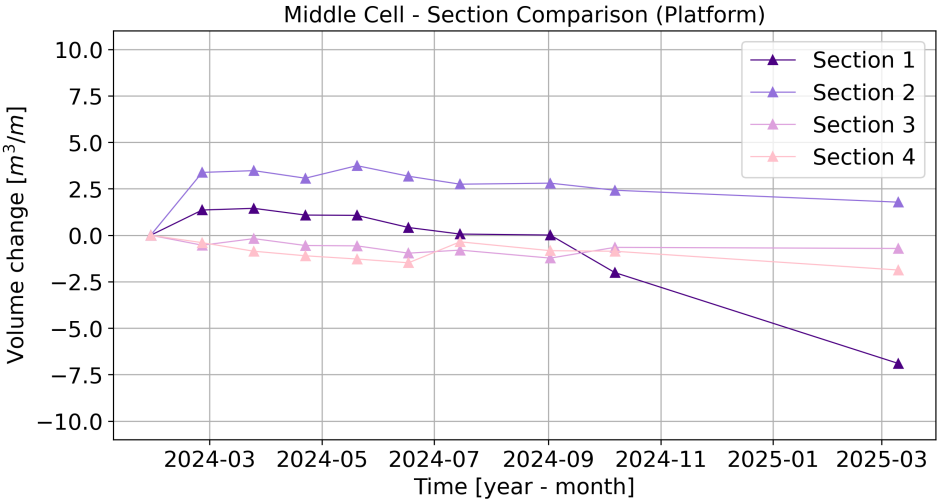

Figure A.2: Volume change over longshore distance of the middle cell, split into the four longshore sections, for the vertical platform section.

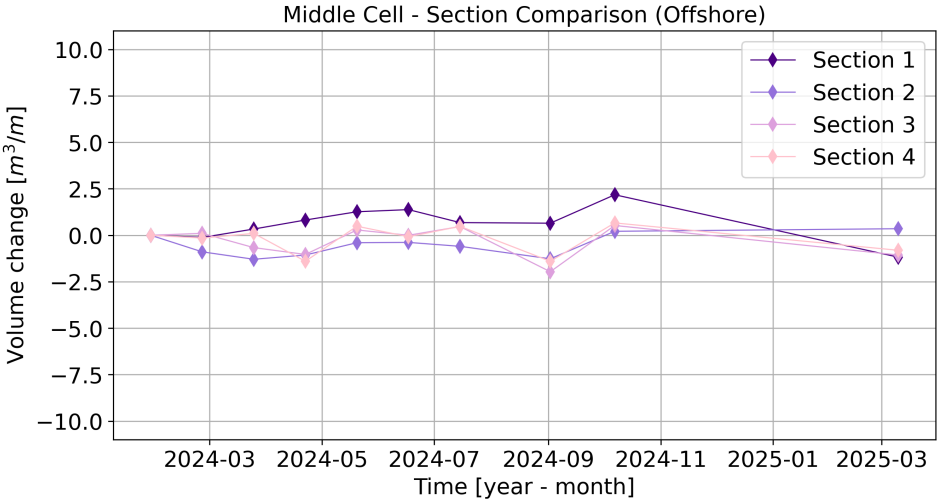

Figure A.3: Volume change over longshore distance of the middle cell, split into the four longshore sections, for the vertical offshore section.

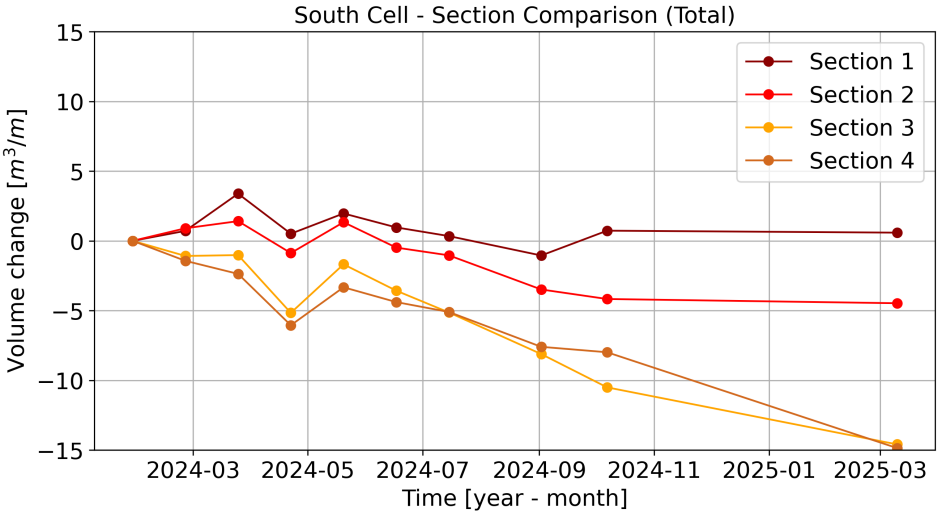

Figure A.4: Volume change over longshore distance of the south cell, split into the four longshore sections, for the vertical total section.

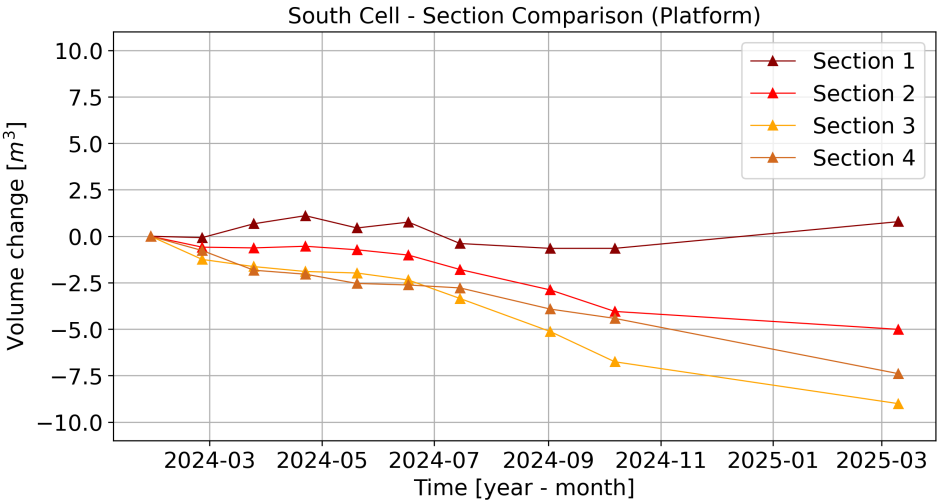

Figure A.5: Volume change over longshore distance of the south cell, split into the four longshore sections, for the vertical platform section.

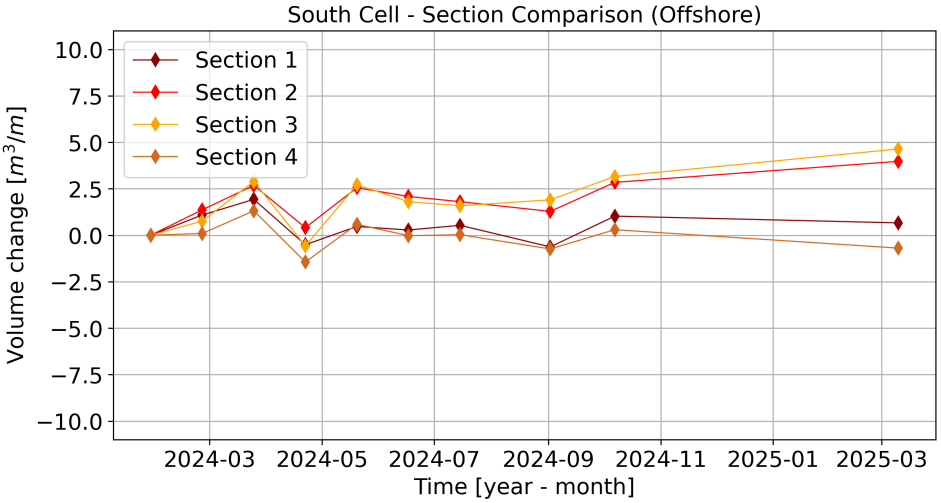

Figure A.6: Volume change over longshore distance of the south cell, split into the four longshore sections, for the vertical offshore section.

B

CERC wave climate

The wave climate used for the CERC sediment transport formulation, was determined from the available buoy data (using wave height, period and direction), and split into climates with according categorisation:

H_3 ; T_p	-45°	-30°	-15°	0°	15°	30°	45°	60°	75°
0.1 m ; 1.25 s	1309	168	151	169	168	169	191	152	1227
0.2 m ; 1.75 s	474	75	115	170	193	203	169	212	1030
0.3 m ; 2.0 s	37	15	61	86	102	114	165	130	321
0.4 m ; 2.5 s	12	12	62	135	219	130	131	129	201
0.5 m ; 2.75 s	0	0	1	11	23	11	3	6	28
0.6 m ; 2.75 s	0	0	0	0	0	0	0	0	5
0.7 m ; 3.0 s	0	0	0	0	0	0	0	0	1

Table B.1: Wave climate by occurance for various wave heights and peak periods across incident angles.

C

Design profiles

The morphological development of all 8 design sections (4 for both beach cells) relative to their design profile are presented here.

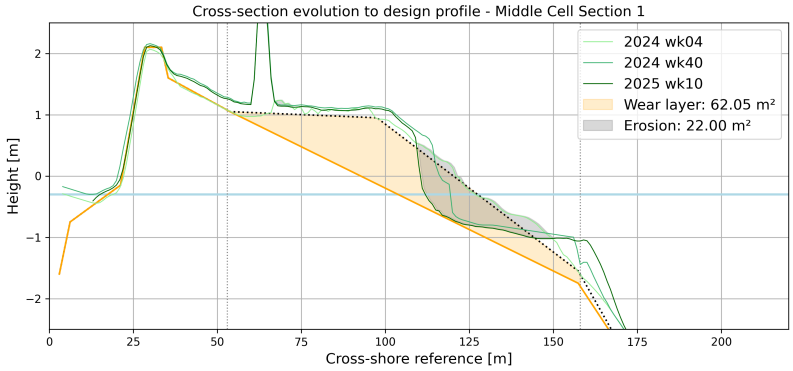

Figure C.1: Development of the cross section in the middle of section 1, Middle cell, against the design profile of that cell. Eroded volume [m^3/m] between week 04 of 2024 and week 10 of 2025 is calculated, next to the volume [m^3/m] of the wear layer in that design profile.

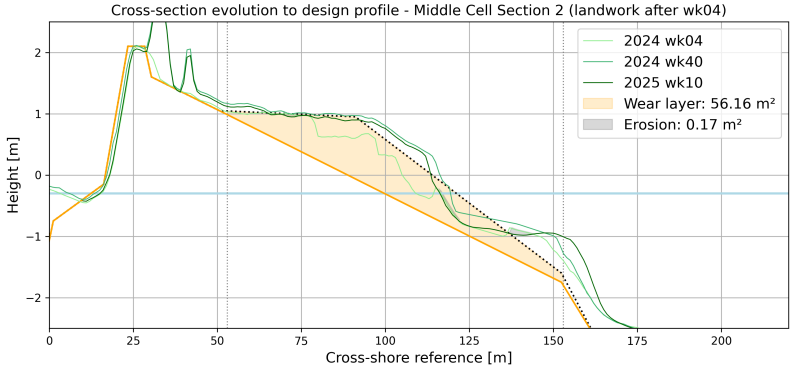

Figure C.2: Development of the cross section in the middle of section 2, Middle cell, against the design profile of that cell. Eroded volume [m^3/m] between week 04 of 2024 and week 10 of 2025 is calculated, next to the volume [m^3/m] of the wear layer in that design profile.

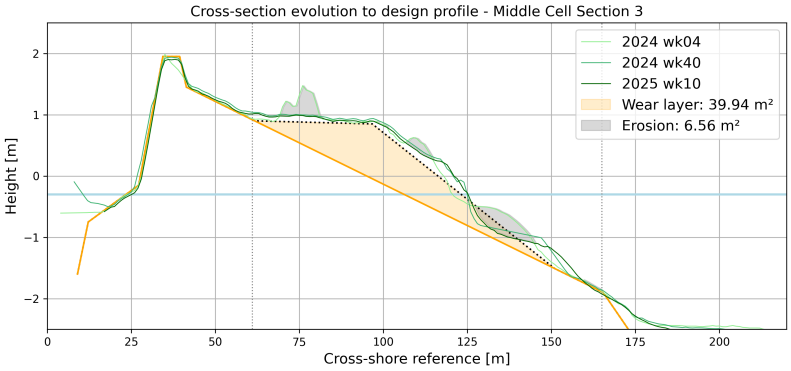

Figure C.3: Development of the cross section in the middle of section 3, Middle cell, against the design profile of that cell. Eroded volume [m^3/m] between week 04 of 2024 and week 10 of 2025 is calculated, next to the volume [m^3/m] of the wear layer in that design profile.

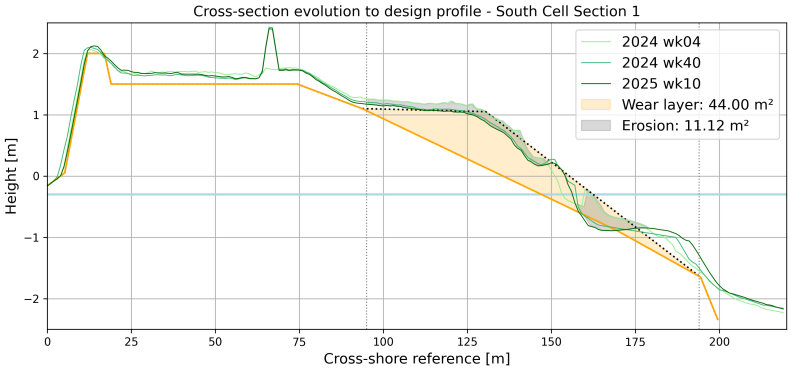

Figure C.4: Development of the cross section in the middle of section 1, South cell, against the design profile of that cell. Eroded volume [m^3/m] between week 04 of 2024 and week 10 of 2025 is calculated, next to the volume [m^3/m] of the wear layer in that design profile.

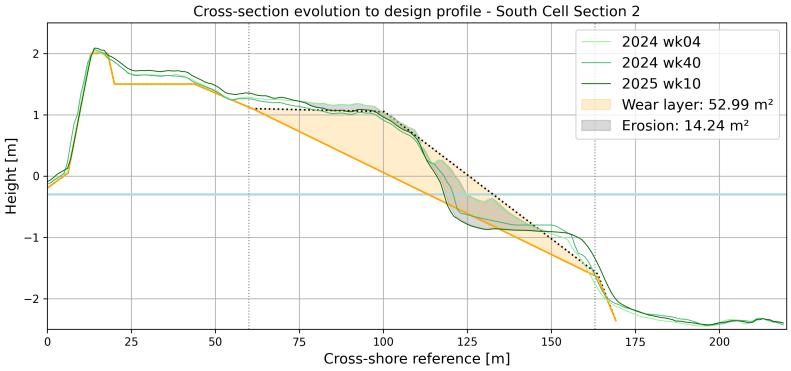

Figure C.5: Development of the cross section in the middle of section 2, South cell, against the design profile of that cell. Eroded volume [m^3/m] between week 04 of 2024 and week 10 of 2025 is calculated, next to the volume [m^3/m] of the wear layer in that design profile.

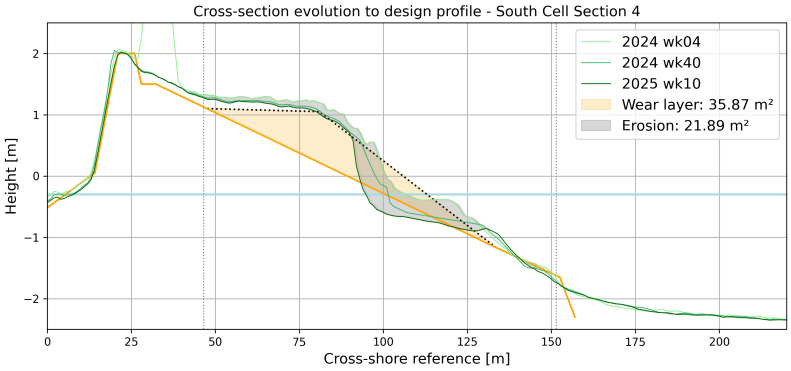

Figure C.6: Development of the cross section in the middle of section 4, South cell, against the design profile of that cell. Eroded volume [m^3/m] between week 04 of 2024 and week 10 of 2025 is calculated, next to the volume [m^3/m] of the wear layer in that design profile.

D

Model validation

The graphs displaying the model validation tests for a calm week are presented here.

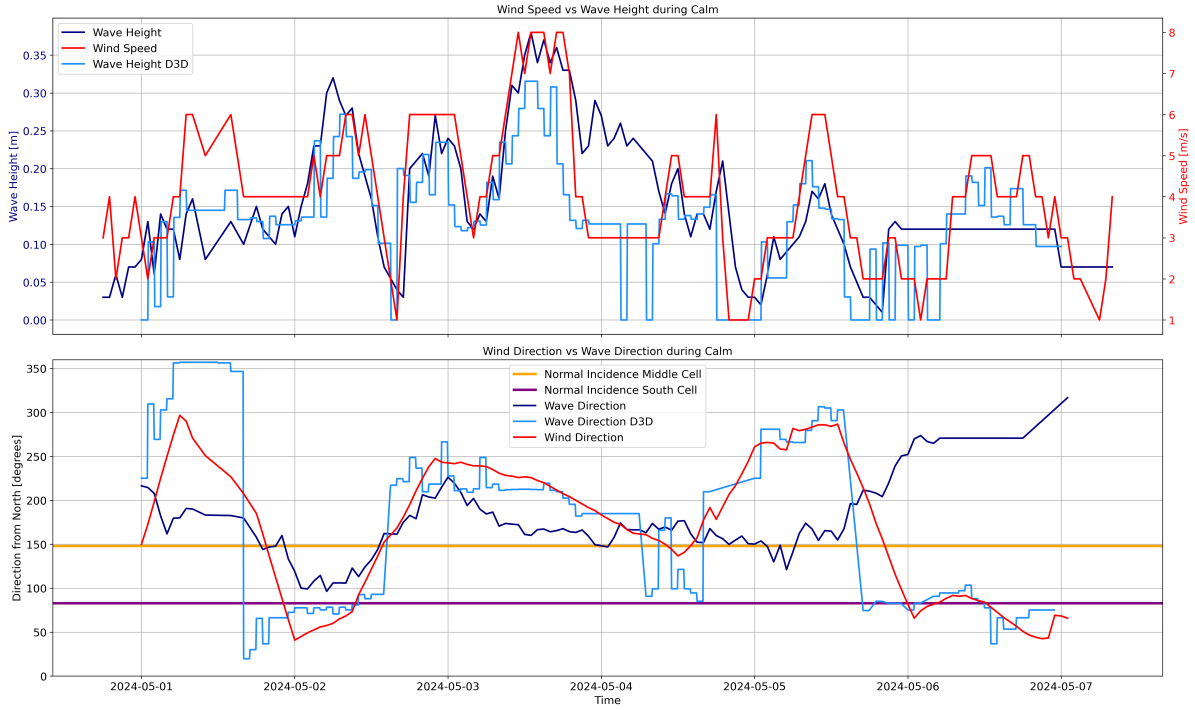

Figure D.1: Graph to show measured wind data (KNMI station), measured wave data (buoy) and wave data (Delft3D) as a result of measured wind input. The Delft3D output is based on numerical output at an observation point in the location of the buoy, in the Hoornse Hop bay.

E

Correlations

All correlation coefficients and corresponding p-values for the correlations between the volume change of all cross-shore sections against selected hydrodynamic drivers are provided here.

Correlation coefficients and p-values between hydrodynamic variables (Table 5.3) and normalised volume changes (Figures 5.11 and 5.12) in total, and per section, for each cell. Both Pearson (PCC) and Spearman (SCC) correlation coefficients and associated p-values are provided. A PCC of 1 indicates a completely linear relationship, an SCC of 1 indicates a perfect association of ranks. A low p-value, in statistics often below 0.05, means a statistically significant correlation is likely.

Hydrodynamic Variable	**South Cell total**				**Middle Cell total**			
	PCC	**p-val**	**SCC**	**p-val**	**PCC**	**p-val**	**SCC**	**p-val**
Ave. wind speed	0.02	0.96	0.37	0.33	0.19	0.65	0.19	0.65
Ave. wind direc.	-0.31	0.42	-0.37	0.33	-0.29	0.49	-0.42	0.29
Ave. wave height	0.01	0.97	0.43	0.24	0.21	0.61	0.45	0.26
95th pth wave height	0.09	0.81	0.48	0.19	0.22	0.61	0.40	0.32
Ave. waterlevel fluc.	-0.23	0.55	-0.35	0.36	-0.03	0.94	0.02	0.96
Wave energy	0.07	0.85	0.48	0.19	0.15	0.72	0.40	0.32
Peak counts	-0.04	0.93	0.26	0.51	-0.18	0.67	0.01	0.98
Ave. peak wave height	0.13	0.76	0.24	0.57	0.23	0.62	0.14	0.76
Ave. peak wind direc.	-0.02	0.96	-0.14	0.74	-0.13	0.78	-0.29	0.53

Table E.1: All correlations for total volume changes

Hydrodynamic Variable	**South Cell beach**				**Middle Cell beach**			
	PCC	**p-val**	**SCC**	**p-val**	**PCC**	**p-val**	**SCC**	**p-val**
Ave. wind speed	0.02	0.96	0.28	0.46	0.59	0.12	0.19	0.65
Ave. wind direc.	0.04	0.91	0.08	0.83	0.28	0.50	0.36	0.39
Ave. wave height	-0.24	0.54	0.02	0.97	0.52	0.19	0.19	0.65
95th pth wave height	-0.10	0.79	0.12	0.77	0.32	0.44	0.07	0.87
Ave. waterlevel fluc.	0.21	0.58	0.02	0.97	0.50	0.21	0.40	0.32
Wave energy	-0.22	0.58	0.12	0.77	0.39	0.33	0.07	0.87
Peak counts	-0.03	0.94	0.41	0.27	0.06	0.89	-0.10	0.82
Ave. peak wave height	-0.38	0.36	-0.21	0.61	-0.49	0.26	-0.39	0.38
Ave. peak wind direc.	0.11	0.79	0.21	0.61	-0.51	0.23	-0.39	0.38

Table E.2: All correlations for beach section volume changes

The correlation coefficients are calculated using normalised volume changes, provided in Table E.5.

Scatter plots for correlations between morphology changes and average peak wave heights:

Hydrodynamic Variable	South Cell platform				Middle Cell platform			
	PCC	p-val	SCC	p-val	PCC	p-val	SCC	p-val
Ave. wind speed	0.16	0.69	0.18	0.64	0.22	0.61	0.43	0.29
Ave. wind direc.	-0.29	0.45	-0.13	0.73	0.15	0.72	0.05	0.91
Ave. wave height	0.22	0.56	0.12	0.77	0.05	0.90	0.12	0.78
95th pth wave height	0.08	0.84	-0.02	0.97	0.03	0.94	0.14	0.74
Ave. waterlevel fluc.	0.74	0.02	0.80	0.01	-0.28	0.50	-0.19	0.65
Wave energy	0.13	0.73	-0.02	0.97	0.05	0.91	0.14	0.74
Peak counts	0.34	0.38	0.13	0.74	-0.11	0.79	0.35	0.39
Ave. peak wave height	-0.58	0.13	-0.60	0.12	-0.34	0.45	-0.32	0.48
Ave. peak wind direc.	-0.89	0.004	-0.88	0.003	0.32	0.48	0.21	0.64

Table E.3: All correlations for platform section volume changes

Hydrodynamic Variable	South Cell offshore				Middle Cell offshore			
	PCC	p-val	SCC	p-val	PCC	p-val	SCC	p-val
Ave. wind speed	-0.02	0.96	0.23	0.55	-0.23	0.59	-0.07	0.87
Ave. wind direc.	-0.30	0.44	-0.48	0.19	-0.36	0.38	-0.33	0.42
Ave. wave height	0.05	0.90	0.38	0.31	-0.15	0.73	0.07	0.87
95th pth wave height	0.12	0.76	0.42	0.26	-0.07	0.87	0.04	0.91
Ave. waterlevel fluc.	-0.48	0.19	-0.32	0.41	-0.28	0.50	-0.5	0.21
Wave energy	0.12	0.75	0.42	0.26	-0.16	0.71	0.04	0.91
Peak counts	-0.10	0.79	0.18	0.64	-0.30	0.46	-0.22	0.60
Ave. peak wave height	0.37	0.36	0.26	0.53	0.51	0.24	0.29	0.53
Ave. peak wind direc.	0.11	0.79	-0.19	0.65	0.19	0.69	0.25	0.59

Table E.4: All correlations for offshore section volume changes

Interval	Middle Total	South Total	Middle Beach	South Beach	Middle Platform	South Platform	Middle Offshore	South Offshore
1	-0.05	-	0.66	-0.10	0.24	-0.16	-0.07	0.21
2	0.14	0.01	0.03	-0.16	0.01	-0.05	-0.03	0.34
3	-0.81	0.01	0.16	-0.13	-0.09	0.00	-0.07	-0.68
4	0.62	0.19	-0.09	0.18	0.03	-0.09	0.26	0.53
5	-0.36	0.08	0.06	-0.20	-0.12	-0.03	-0.04	-0.14
6	-0.22	-0.15	-0.18	-0.01	0.03	-0.19	0.00	-0.01
7	-0.33	-0.28	-0.08	-0.10	-0.03	-0.15	-0.18	-0.08
8	-0.08	0.21	-0.08	-0.20	-0.09	-0.16	0.38	0.28
9	-0.12	-0.15	-0.09	-0.09	-0.08	-0.05	-0.07	0.01

Table E.5: Summary of morphology volume changes, values that form figure 5.11 and 5.12. These form the base for correlation coefficients. All volume changes are in [m^3/m/week].

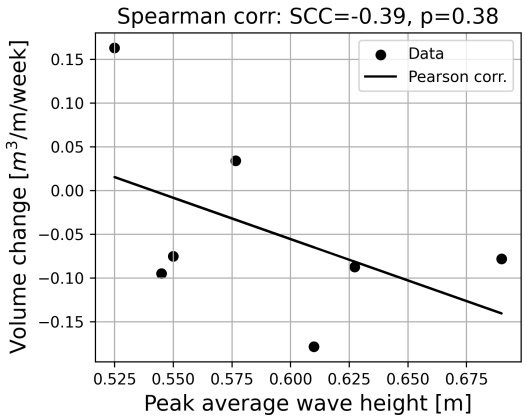

(a) Middle Cell - Beach

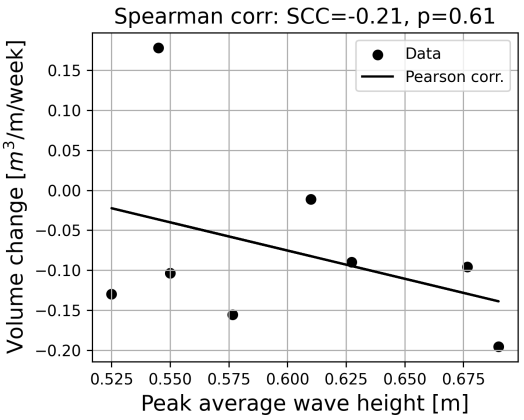

(b) South Cell - Beach

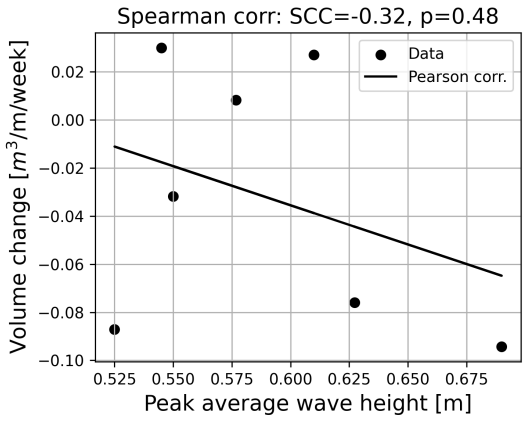

(c) Middle Cell - Platform

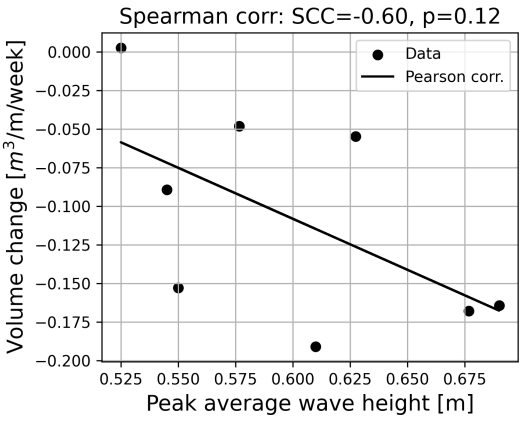

(d) South Cell - Platform

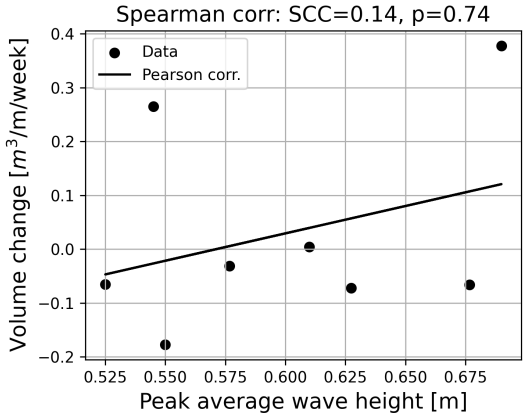

(e) Middle Cell - Offshore

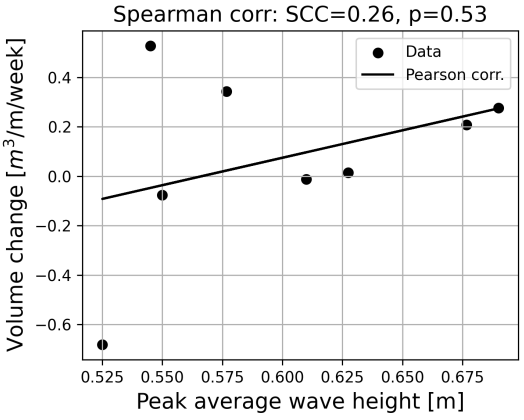

(f) South Cell - Offshore

Figure E.1: Normalised measured volume change per beach section against average wave heights of classified peaks per interval.

F

Storm peak wave height calculation

Visualisation of graph to show the calculation of average peak storm height is provided here.

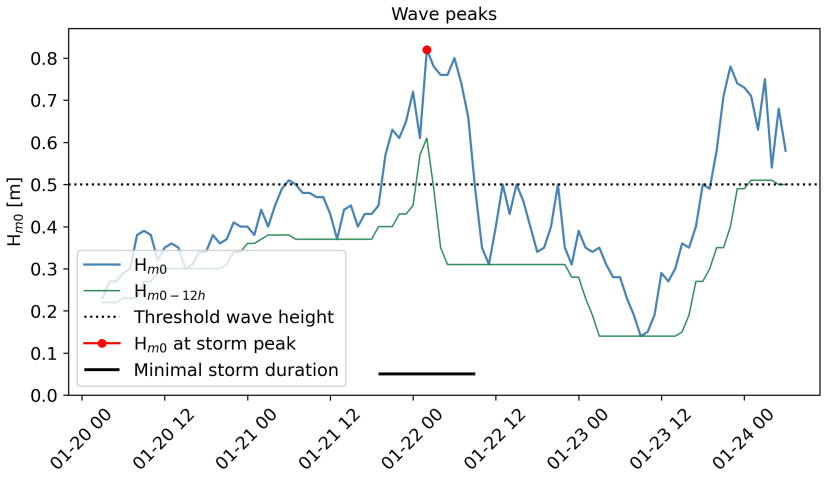

Figure F.1: Visualisation of 'Average Peak Wave Height' calculation. Storms are selected based on criteria (minimum peak height, prominence, duration), and average wave height is computed over the storm duration indicated by the black bar.

G

Bed shear stress modelling

Here, the minimum depth of the corners of each output grid cell for the bed shear stress calculations are used, where positive values are downward relative to NAP. So, the average waterline is at 'depth = 0.3'. Evidently, the third output point of the middle cell has an anomalously low depth.

South Cell loc	Min. depth [m]	Middle Cell loc	Min. depth [m]
1	0.7	1	0.7
2	0.8	2	0.8
3	0.9	3	0.2
4	0.9	4	0.8
5	0.9	5	0.8
6	0.9	6	0.9
7	0.7	7	0.8
-	-	8	0.8

Table G.1: Summary of the minimum depth at the four corners of the grid cell used for bed shear stress output.

Here, bed shear stress histograms are plotted for all output locations along the shores of both the middle and southern cell.

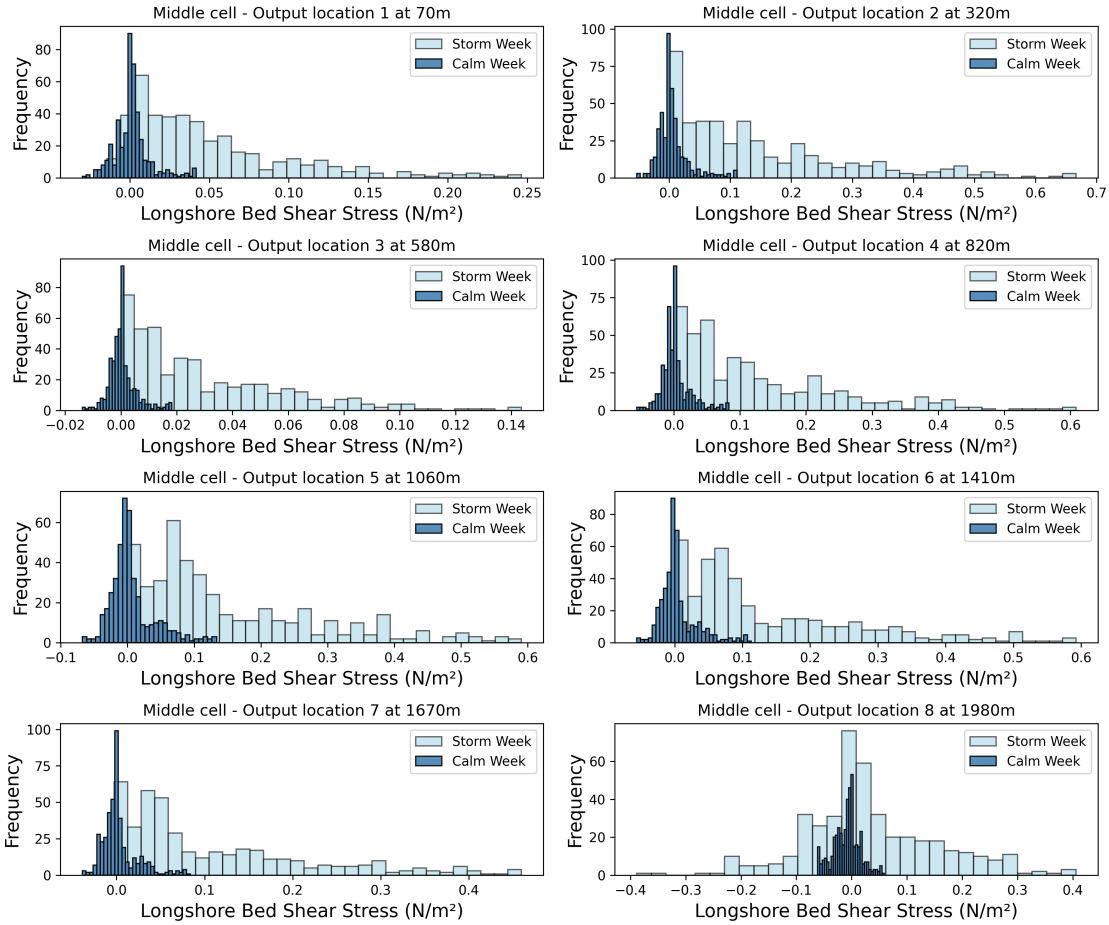

Figure G.1: Histograms of bed shear stress output during both high-energy and low-energy weeks, at each of the 8 modelled longshore output locations.

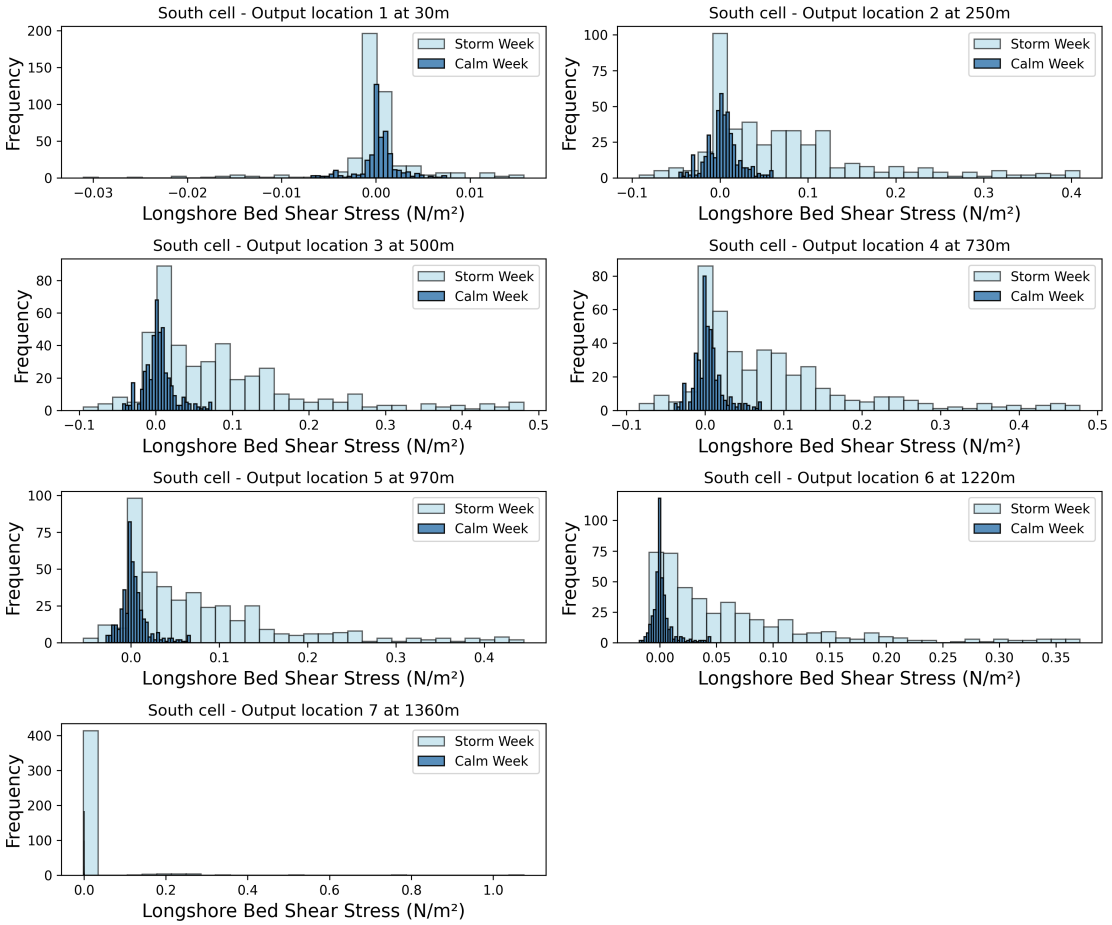

Figure G.2: Histograms of bed shear stress output during both high-energy and low-energy weeks, at each of the 7 modelled longshore output locations.